# Historical subtidal regime shifts echoed in an adjacent intertidal community

Julien Beaulieu*[1,2], Nicole S. Knight[3], Amelia V. Hesketh[4], Jake Lawlor[5], Maria Gheţa[6], Tianna Peller[7], Joseph B. Burant[8], Laura Super[3], Ellen K. Bledsoe[9], Kylla Benes[10], Jennifer A. Dijkstra[11], Jarrett E.K. Byrnes[12]

[1] Département des Sciences Biologiques, Université du Québec à Montréal
[2] Groupe de Recherche Interuniversitaire en Limnologie (GRIL)
[3] Department of Zoology, University of British Columbia
[4] School of Resource & Environmental Management, Simon Fraser University
[5] Department of Biology McGill University
[6] Institut des Sciences de la Mer (ISMER), Université du Québec à Rimouski
[7] Department of Ecology and Evolutionary Biology, University of Toronto
[8] Department of Animal Ecology, Netherlands Institute of Ecology
[9] School of Natural Resources and the Environment, University of Arizona
[10] Davidson Honors College, University of Montana & Shoals Marine Lab, University of New Hampshire
[11] Center for Coastal and Ocean Mapping, University of New Hampshire
[12] Department of Biology, University of Massachusetts Boston

Julien Beaulieu : 0000-0003-2597-8921 beaulieu.julien.2@uqam.ca
Nicole S. Knight: 0000-0001-9256-242X nknight@zoology.ubc.ca
Amelia V. Hesketh: 0000-0002-7344-8565 amelia_hesketh@sfu.ca
Jake Lawlor: 0000-0002-1499-5227 jake.lawlor@mail.mcgill.ca
Maria Gheţa: 0000-0002-7440-4476 mgheta98@gmail.com
Tianna Peller: 0000-0002-7131-2066 tianna.peller@utoronto.ca
Joseph B. Burant: 0000-0002-0713-3100 j.burant@nioo.knaw.nl
Laura Super: 0000-0002-5259-8708 leslaura@gmail.com
Ellen K. Bledsoe: 0000-0002-3629-7235 ebledsoe@arizona.edu
Kylla Benes: 0000-0003-4184-072X kylla.benes@umontana.edu
Jennifer A. Dijkstra: 0000-0003-4791-8305 jennifer.dijkstra@unh.edu
Jarrett E.K. Byrnes: 0000-0002-9791-9472 jarrett.byrnes@umb.edu

## Data availability statement

Data and codes can be found at:
https://github.com/Julien-Beaulieu/GOM_RegimeShift_timeSeries

## Conflict of interest disclosure

There are no competing interests to declare

**Key words:** Regime shift, cross-ecosystem linkage, intertidal, subtidal, benthic ecology, fisheries, climate changes, invasive species

# Abstract

Anthropogenic stressors can trigger regime shifts, causing ecosystems to reorganize into new states. Moreover, there is growing evidence of the importance of fluxes (e.g., energy, matter and nutrients) in linking adjacent systems, suggesting that regime shifts within one system may extend to neighboring systems through cross-ecosystem interactions. However, empirical evidence supporting this hypothesis is lacking. To address this gap, we analyzed over 40 years of community data from intertidal and subtidal ecosystems at Appledore Island in the Gulf of Maine, a region that has experienced multiple subtidal regime shifts. We identified three periods of rapid change in subtidal communities that are coherent with known regime shifts in the region. In the intertidal zone, we found that 58% of island-scale directional changes in community composition exhibited offset synchrony with subtidal regime shifts, meaning they started changing during subtidal regime shifts. Periods of rapid change in the abundance of key intertidal organisms also exhibited offset synchrony with subtidal regime shifts. We suggest that these offset synchronies may be the result of cross-ecosystem linkages through trophic interactions. Our results support the notion that regime shifts can propagate across ecosystem boundaries, demonstrating the importance of considering adjacent ecosystems as drivers of changes in any ecosystem of interest, and highlighting the need to consider the indirect effects of cross-ecosystem interactions for multiple ecological phenomena.

# Introduction

Regime shifts are abrupt and high amplitude shifts in the physical or ecological components of a system, which cause a transition to an alternative stable state that is difficult or virtually impossible to reverse (Beisner et al. 2003, Scheffer and Carpenter 2003, Lees et al. 2006). Regime shifts can be triggered by natural (e.g., hurricane) or anthropogenic (e.g., overharvesting) pressures (Genkai-Kato et al. 2012) and can have numerous cascading effects on biodiversity and ecosystem services. Regime shifts are challenging to reverse because they change the dominant positive feedbacks controlling the system in a way that reinforces the new state of the ecosystem even after the initial cause of the shift is removed (Scheffer and Carpenter 2003). Losses of ecosystem services caused by regime shifts can lead to substantial and persistent social and economic consequences, such as through the collapse of fisheries or resource harvesting industries (Scheffer et al. 2001, Scyphers et al. 2019, Janssen et al. 2021, Defeo et al. 2021, Kuzyk et al. 2026). However, the study of regime shifts often requires long-term datasets that are challenging to obtain, as these shifts may be difficult to distinguish from other types of changes, such as cyclic variations or reversible transitions (Biggs et al. 2009, Sundstrom et al. 2017).

Regime shifts in one ecosystem may affect adjacent ecosystems through cross-ecosystem interactions (Polis et al. 1997, Rocha et al. 2018, Rocha and Crepin 2023). Cross-ecosystem interactions occur primarily via two mechanisms: 1) the transport of matter and biologically available energy or nutrients between systems; and 2) mobile animals that cross systems boundaries and affect community structure or nutrient cycles (Krumhansl and Scheibling 2012, Subalusky et al. 2017, Brandt et al. 2024, Cereghetti et al. 2025), often through consumption or nutrient excretion (Scherer-Lorenzen et al., 2022). These cross-ecosystem interactions can influence the dynamics and structure of an ecosystem (e.g., nutrient dynamics and food web

95 structure) and shape their functions (e.g., pollination, Knight et al., 2005; metapopulation
96 dynamics, Montagano et al., 2019; and ecosystem metabolism, Gounand et al., 2018). Despite
97 the recognized importance of cross-ecosystem interactions in coupling the ecological dynamics
98 of adjacent ecosystems, few studies to date have examined how temporal shifts in species
99 composition (i.e., regime shifts) within one ecosystem may influence adjacent ecosystems
100 through such linkages (but see Rocha et al., 2018; Rocha & Crepin, 2023). Understanding these
101 dynamics is crucial, as cross-ecosystem interactions may initiate regime shifts in adjacent
102 ecosystems or amplify ecological disturbances by propagating regime shifts to coupled
103 ecosystems (Rocha et al. 2018; Rocha and Crepin 2023).

104 Cross-ecosystem interactions between intertidal and nearshore subtidal ecosystems are well-
105 documented. These adjacent ecosystems are connected by mobile predators such as fish,
106 lobsters and crabs that regularly forage across the intertidal-subtidal boundary (Rilov and
107 David 2006, Rilov and Schiel 2006, Silva et al. 2008, 2010, 2014, Christie et al. 2020).
108 Predators shape community structure in these ecosystems through top-down control (Pauly et
109 al. 1998, Williams et al. 2004, Peller et al. 2022), and have previously been implicated as key
110 players in regime shifts (Daskalov et al. 2007, Steneck et al. 2013).

111 At least three distinct subtidal regime shifts have been identified in the nearshore Gulf of Maine
112 during the past fifty years (Figure 1; Dijkstra et al., 2017; Jackson et al., 2001; Pershing et al.,
113 2015, 2016; Steneck et al., 2013). The first regime shift was driven by the overharvesting of
114 commercial predatory fish such as Atlantic cod (*Gadus morhua*) (Jackson et al. 2001, Myers
115 and Worm 2003) and occurred mainly around 1975–1980, but lasted until around 1990 in the
116 Gulf of Maine where a second decrease in stocks happened between 1980 and 1990 (Worm
117 and Myers 2002). This fisheries collapse released key benthic species from predation pressure,
118 including green sea urchins (*Strongylocentrotus droebachiensis*) (Jackson et al. 2001, Steneck

et al. 2013). Abundant sea urchins defoliated kelp beds, causing shifts to urchin barrens between 1975–1990 (Steneck et al. 2013). The second regime shift occurred between 1995–2000 when urchin populations collapsed due to overharvesting, increased predation, and disease outbreaks (Scheibling and Hennigar 1997, Steneck et al. 2013). Urchin declines allowed opportunistic species and non-native macroalgae to establish on the benthos, which facilitated larger invertebrate populations through habitat provisioning (Steneck et al. 2013). The third regime shift, likely driven by ongoing rapid ocean warming (Pershing et al. 2015), occurred around 2010 as non-native filamentous red algae proliferated (Newton et al. 2013, Dijkstra et al. 2017, O'Brien et al. 2018), affecting invertebrates and, indirectly, higher trophic levels (Dijkstra et al. 2017, O'Brien et al. 2018).

While changes in neighboring intertidal communities within the Gulf of Maine have not been explicitly defined, changes in populations and community compositions occurred across the same time period. When comparing shores from the 1970s to those in 2013–2014, Sorte et al. (2017) observed a decrease in Irish moss (*Chondrus crispus*) and blue mussels (*Mytilus edulis*) and an increase in the red alga *Mastocarpus stellatus* and crustose red algae. Petraitis & Dudgeon (2020) documented warming-associated declines in the recruitment of habitat-forming filter feeders (*M. edulis* and the barnacles *Semibalanus balanoides*), and ocean acidification-linked declines in the abundances of herbivorous gastropods and predatory whelks from 1996 to 2012. In addition to climate change, shifts in intertidal community composition may also be attributed to increases in harvesting, hurricane activity, and non-native species (Sorte et al. 2017).

Here, we use long-term data sets from the Gulf of Maine to examine whether shifts in intertidal communities correspond in time to subtidal regime shifts documented during a 42-year monitoring program. We do so by assessing periods and rates of change in both ecosystems

and how they align in time (Figure 3a). We hypothesized that subtidal regime shifts will have cascading effects on intertidal ecosystems, likely through altered trophic interactions propagating through linked food webs. We predict that if intertidal community composition is driven by cross-ecosystem interactions with subtidal communities, then changes in the intertidal community should lag behind those occurring in subtidal ecosystems in an "offset synchrony" pattern (Figure 3b). Alternatively, if intertidal community composition is largely independent of these cross-ecosystem interactions, then changes (not necessarily regime shifts) in intertidal assemblages should occur independently of subtidal transitions, if they occur at all.

# Methods

Our study focuses on Appledore Island in the Gulf of Maine (42.987°N, 70.609°W; Figure 2), where intertidal community composition has been monitored annually along permanent vertical transects since 1980, first as part of undergraduate field courses and later as part of a regular sampling program (Shoals Marine Laboratory 2018). To identify the subtidal regime shifts over the whole study period, we used NOAA bottom-trawl survey data from transects within 100 km from Appledore Island (Figure 2). We then identified periods of change in mobile and sessile intertidal communities in each of the five sites distributed around the island before relating the timing of periods of intertidal community changes to the subtidal regime shifts.

## NOAA Bottom Trawl Communities

To identify the timing of regime shifts in subtidal and pelagic ecosystems of the Gulf of Maine, we analyzed time-series data from sampled fishes and invertebrates as part of the Seasonal Bottom Trawl Surveys conducted by the National Oceanic and Atmospheric Administration

(Grosslein n.d., Johnston and Sosebee n.d., NOAA 2020). Initiated in 1963, these seasonal surveys follow a standard protocol to provide a harvesting-independent estimate of the abundances and biomasses of key fisheries species (Evans and Stauffer 2004). Each season, tows are conducted at more than 350 transects of different depths spanning the length of the northeastern US Atlantic coast from Cape Hatteras, North Carolina in the south (28.47°N) to the Canadian border in the north (44.52°N). In order to compare temporal changes in the intertidal community to those in the subtidal zone, we used only NOAA transects within 100 km of Appledore Island (42.987°N, 70.609°W) with complete survey data from 1980 onwards. With this approach, we selected six total transects: three inshore and three offshore (of a possible 56 total located within the Gulf of Maine; strata 01260, 01270, 01400, 03640, 03650, and 03660). The depth of the six transects selected were 366-549m, 549-732m, 0-27m, 110-183m, 183-366m, and 366-549m. We acknowledge that despite their proximity to Appledore Island, the communities described by the NOAA data may differ from those of the nearshore subtidal zone (e.g., more deep water species). We argue that these data are a more thorough indicator of the state of communities within the Gulf of Maine given their spatial scale and taxonomic diversity in order to characterize system-wide regime shifts (Jackson et al. 2001, Steneck et al. 2013, Pershing et al. 2015, Dijkstra et al. 2017). As a robustness check, we re-analyzed the data using only species sampled in nearshore surveys at 10m depth by the Kelp Ecosystem Ecology Network, and found the same results as analyzing the entire trawl data set with respect to timing of regime shifts (see Supplementary Material 3).

Data from the six NOAA transects were used to detect changes in subtidal community structure. We calculated the total number of individuals for each species captured in each transect at every sampling time. We similarly calculated the species-specific total biomass of all individuals caught in a given transect, season, and year. These biomass data were subsequently standardized by sampling effort by dividing the value by the number of samples

("tows") taken along each transect. Finally, we averaged the standardized effort values from all strata to arrive at season-specific time series for each species included in the dataset. Because data from summer and winter surveys were sparse relative to spring and autumn (summer and winter trawls have only been conducted since 1991 and 1992, respectively), we averaged spring and autumn records for calculating annual effort-standardized catch and biomass.

# Intertidal Communities

We divided Appledore Island into five regions that differ in wave exposure: Babb's Cove (BC); North-East Appledore (NE); North-West Appledore (NW); South-East Appledore (SE) and South-West Appledore (SW) (see Byrnes et al. (2024) for classification). A detailed description of the survey methods and timeline of sampling changes can be found in the open access data repository (Shoals Marine Laboratory 2018). Briefly, within each region, permanent transects were surveyed periodically from 1982–2022, for a total of 28 transects around the entire island. Within each transect, replicate 20 x 20 cm quadrats were placed every 0.3 m (1 ft) in elevation from the low to the high intertidal zone. Within quadrats, the presence and/or abundance of all observable species were documented. Mobile organisms were identified to species and counted within each quadrat. The percent cover of sessile organisms was estimated at the canopy and primary cover layers for all species with more than 3% cover. The percent cover used in this study is the sum of values for the two layers in each quadrat such that a species can have more than 100% cover. Organisms were identified to species or else the lowest possible taxonomic resolution possible (e.g., *Fucus* spp., amphipods). The number and length of transects and number of replicate quadrats within each transect surveyed varied among years. Each year, between one and 17 transects (8.3 per year on average), and between one and four replicate quadrats per tide height were sampled.

# Statistical analysis

## Subtidal regime shift identification

To identify the timing of subtidal regime shifts in the predator communities surrounding Appledore Island, we used ordination and multivariate generalized additive models (GAMs; Figure 3a). Fitted GAMs provided estimates of interannual community changes, and their derivatives indicated the rate and direction of those changes. Prior to analysis, we aggregated abundances to the genus level and excluded species recorded in fewer than 10 different years to reduce zero inflation (see supplementary material 1 for species retained in this analysis). Second, we performed a Principal Coordinate Analysis (PCoA) using Hellinger distance dissimilarity on the NOAA bottom trawl survey effort-corrected biomass data. The PCoA was calculated using the R package `*vegan*` (Oksanen et al. 2020). Next, we performed a time series analysis on ordination axes that explained 10% or more variability in community composition (the first two) using a Bayesian multivariate Gaussian Generalised Additive Model (GAM) with the three first ordination axes as dependent variables and year as predictor with a smoothing term. All time series models are listed in Table 1. The first three ordination axes were used because they all explained significant variation in community composition and had eigenvalues greater than one. The model was fitted with the `brms` package (Bürkner 2018) in R version 4.3.3 (CoreTeam 2020).

The identification of regime shifts is difficult as it requires demonstrating rapid and substantial changes in the community, in addition to the establishment of an alternative stable state (Scheffer and Carpenter 2003) and often an increase in variance and autocorrelation preceding the shift (Dakos et al. 2012, Guttal et al. 2013). In this study system, drastic changes in the subtidal community have been previously defined as regime shifts (Jackson et al. 2001,

237 Steneck et al. 2013, Pershing et al. 2015, Dijkstra et al. 2017). Consequently, we define subtidal
238 regime shifts as the periods of time when the rate of community change is at its highest while
239 transitioning from one extreme to another (i.e., the maximum of the first derivative of the curve)
240 (Figure 3a). To identify the timing of the subtidal regime shifts, we calculated the derivative
241 (i.e., rate of change) of 1000 draws of the posterior prediction of the time series for subtidal
242 community ordination axis one and two using forward difference. The regime shift interval
243 was identified as the period during which 95% of the derivatives of those 1000 draws were
244 maximal or minimal (Figure 1). A less conservative option would have been to define regime
245 shift time interval as the whole periods of change (i.e., derivative different from zero) and a
246 more conservative option would have been to take the time interval where the maximal during
247 which less than 95% (e.g. 80% or 60%) of the derivatives of those 1000 draws were maximal
248 or minimal. However, we chose the 95% credible interval of maximal or minimal slope because
249 it is standard in biology and it was a good balance between the less conservative option and the
250 more conservative options, although changing to the 80% credible interval of the maximal or
251 minimal slopes had no impact on the overall results (Supplementary Material 9).

252 **Timing of the changes in the intertidal community**

253 To identify periods of change in intertidal communities, we again used PCoA and GAMs to
254 estimate the magnitude of interannual community changes. First, we made one ordination for
255 sessile organisms and one ordination for mobile organisms using Hellinger dissimilarity for
256 each quadrat. Species present in less than 2.5% of the intertidal quadrats over the entire
257 sampling period were removed from those analyses to reduce zero-inflation. Next, we used two
258 separate multivariate hierarchical GAMs (HGAMs) for change analysis in sessile and mobile
259 intertidal communities on the ordination axis that explained minimum 10% of the variability
260 (first three axes). All time series models are listed in Table 1. We accounted for spatial
261 variability in these time series—both within and among transects—by including shore level as

a smoothing term and a random intercept for each transect and included transect correlation in the model. We used leave-one-out Informatio Criterion (LooIC) to select between models with different structures for time effects:

1) a shared temporal trend and similar smoothness between site referred to as the GS model (Pedersen et al. 2019):

$$y \sim 1 + s(year, bs = tp) + s(level, bs = tp) + t2(year, site, bs = c(tp, re), full = T) + (1|r|intertidal\ transect) \quad (1)$$

2) a shared trend and different smoothness between sites referred to as the GI model (Pedersen et al. 2019):

$$y \sim 1 + s(year, bs = tp) + s(year, by = site, bs = tp) + s(level, bs = tp) + s(site, bs = re) + (1|r|intertidal\ transect) \quad (2)$$

and 3) different trends and smoothness between sites referred to as the I model (Pedersen et al. 2019):

$$y \sim 1 + s(year, by = site, bs = tp) + s(level, bs = tp) + (1|r|intertidal\ transect) \quad (3)$$

Where the notation $(1|r|intertidal\ transect)$ specifies correlated random intercepts, $s(\ )$ are thin plate regression splines and $t2(\ )$ tensor product smooth. For all the following analyses, the model with different trends and smoothness between sites (equation 3) was selected (Table 1).

Because some taxa were numerically dominant and/or participate in key trophic interactions linking intertidal and subtidal communities, we generated additional time series for eleven focal taxa: Amphipoda; Isopoda; *Mytilus edulis*; *Semibalanus balanoides*; *Nucella lapillus*; *Littorina spp.*; *Carcinus maenas*; *Mastocarpus stellatus*; *Fucus* spp.; *Chondrus crispus*; and

*Ascophyllum nodosum*. We used the same GAM formulation to generate focal taxa time series data, accounting for spatial heterogeneity (equation 3). We modeled mobile species with count data using the zero-inflated negative binomial distribution or zero-inflated Poisson distribution because overdispersion caused convergence issues (Table 1). We modelled percent cover of sessile invertebrates using the zero-inflated beta distribution, and the percent cover of algae were modeled with gamma hurdle distribution. Zero-inflated and hurdle terms were fitted with the same formula (equation 3). All priors were non-informative and weakly regularizing (see supplementary material 7).

## Comparison of Subtidal and Intertidal Periods of Change

To test whether regime shifts from the subtidal zone propagated to the intertidal zone, we identified periods of changes in subtidal and intertidal communities as changes in temporal trend direction (second derivative different from zero) of the previously described time series models. A useful framework to assess whether or not a time series influences another is Granger causality (Granger 1969). However, this approach requires high data frequency and linear causal relationships (Maziarz 2015), which are lacking here. While many studies use visual assessment, we instead opted for a quantitative approach to account for uncertainties in temporal trends and reduce bias. We compared the timing of changes in temporal trends in intertidal community composition over time with the timing of subtidal community changes. We assumed that if intertidal communities are influenced by trophic interactions with subtidal predators, subtidal regime shifts will lead to corresponding intertidal shifts beginning when the rate of subtidal change is at its maximum. (Figures 2a–b). Changes in the temporal trend direction (forming an “elbow” shape) can be quantified using the second derivative, with a second derivative significantly different than zero implying a shift in trend direction. A non-zero second derivative of the intertidal community during a subtidal regime shift therefore indicates that intertidal community composition begins to change at the same time as the

subtidal regime shift occurs, implying cross-ecosystem interactions. We therefore expect that intertidal community change will not be perfectly synchronous with subtidal regime shifts, but delayed. This pattern—hereafter referred to as offset synchrony—indicates a potential propagation of the subtidal regime shift to the intertidal system and corresponds to the concept of Granger causality, wherein changes in one ecosystem precede and potentially influence another ecosystem. Offset synchrony is also coherent with our hypothesis of regime shift propagation through altered trophic interactions between the subtidal and intertidal zones, as changes in abundance due to trophic interactions inherently includes a lag in time (Wangersky 1978).

To identify shifts in trend direction, we calculated the second derivative for each intertidal time series using the central difference method across 1000 posterior predictive draws. This included site by species combinations where a significant interaction between the two factors was detected. Changes in the second derivative that were completely asynchronous with a subtidal regime shift were attributed to variables unrelated to the subtidal regime shift. Finally, as the intertidal and subtidal community compositions were quantified using Hellinger dissimilarity, the magnitude of the changes in community composition over time can therefore be compared by looking directly at the magnitude of changes over time.

# Results

## Subtidal regime shift identification

Subtidal community composition around Appledore Island (i.e., pelagic and benthic fishes and invertebrates from the NOAA trawl survey) was nonstationary over the 40-year period, as demonstrated by constant change on the first or the second ordination axes (Figure 4). Rates of community change were also variable through time, with the first derivative (slope) reaching a

maximum around the year 2000 on the first ordination axis, and around 1990 and 2010 on the second axis (Figure 4, Supplementary Material 2). For the remainder of this study, we considered these periods of particularly fast changes in community composition in 1990, 2000, and 2010 as the first, second, and third subtidal regime shifts (see Supplementary Figures S1 and S4). Driven by the first regime shift (~1990), the subtidal predator community changed on the second ordination axis from an assemblage characterized by a higher abundance of large predatory and benthic invertivore fish (e.g., *Gadus morua, Pollachius virens,* and *Cyclopterus lumpus*) to one characterized by invertebrates (e.g., crabs, shrimps, squid; Figure 4, Tables S1 and S2). This trend was reversed ~20 years later during the third regime shift (~2010), when predatory fish again became more abundant. The second regime shift (~2000) drove a change from a community characterized by a higher abundance of large vertebrate and invertebrate predators (e.g., *Lumpenus spp, Scomber scombrus, Brosme brosme, Cancer* spp. crabs and *Lithodes maja*), to a community characterized by a high abundance of invertebrates (e.g., *Bathypolypus arcticus, Maurolicus weitzmani*, *Sepiolidae*, *Lycenchelys verrilli*, *Lebbeus polaris*, *Pontophilus norvegicus* and *Spirontocaris liljeborgii*) and barndoor skate (*Dipturus laevis*; Figure 4 and S1).

## Comparison of Intertidal and Subtidal Regime Shifts and Changes in Intertidal Communities

### Mobile invertebrate intertidal community

The composition of the intertidal mobile invertebrate community changed through time across all sites (Figure 5) on the first and third ordination axis. We identified ten changes in the second derivative of the mobile intertidal community, four of which displayed offset synchrony with the three subtidal regime shifts (Figure 5, Supplementary Material 6). Moreover, all six intertidal mobile invertebrate genera that we analyzed exhibited changes corresponding to

359 offset synchrony with the subtidal regime shifts (Figure 6, Supplementary Material 6,
360 repository table).

361 Spatial position (i.e., intertidal height and site) explained more variation in intertidal
362 communities of mobile organisms than the temporal trends we observed. Higher intertidal
363 communities were characterized by low abundances of mobile organisms; lower intertidal
364 communities exhibited high abundances of *Nucella*, *Amphipoda* and *Littorina* (Figure S3).
365 Spatial position also influenced the trajectory of intertidal change at SE Appledore, which
366 showed a more delayed response to subtidal changes than did other sites (Figure 6).

367 The magnitude of island-wide shifts in species composition, measured in Hellinger distance,
368 were less pronounced in the intertidal community than in the subtidal community over the study
369 period. Intertidal community changes ranged between -0.1 to 0.1 on the first axis and -0.2 and
370 0.2 on the second axis, approximately five to ten times smaller than changes in the subtidal
371 community (-1 to 1 on both axes) (Figures 3 and 4).

372 **Sessile intertidal community**

373 We identified two changes in the sessile intertidal community, both along the first ordination
374 axis only (Figure 7). Island-wide shifts in the intertidal sessile community composition showed
375 offset synchrony with subtidal regime shifts along the first ordination axis in 1990, but not in
376 2000 nor 2010 (Figure 7, Supplementary Material 6). Of the five focal sessile organisms
377 analyzed, four displayed some level of offset synchrony with subtidal regime shifts (*S.*
378 *balanoides, C. crispus, M. stellatus*, and *Fucus* spp.), especially *S. balanoides* and *C. crispus*
379 (Figure 6, Supplementary Material 6). Similar to the intertidal mobile invertebrate community,
380 the sessile community was mainly influenced by intertidal height and site position.

381 **Long-term community changes in the intertidal zone**

Overall, 58% (7/12) of the periods of changes in both sessile and mobile intertidal communities (i.e., number of times the second derivative differed from zero) corresponded to offset synchrony with subtidal regime shifts (Figures 4 and 6, Supplementary Material 6, repository table). However, both sessile and mobile intertidal communities also tended to change starting around 2005 until the end of the study period that were asynchronous with the identified subtidal regime shifts (Figures 4 and 6), although these changes were not significant (second derivative overlapping with zero, Figure S5). Similar patterns were observed for many focal taxa that decreased in abundance post-2005 in some sites: *C. crispus*; *M. edulis*; *N. lapillus*; and amphipods, although their abundance started decreasing at the beginning of the study (1980). At the same time, there was an increase in *Fucus sp.* presence. These changes lasted until the end of the study period, although the mobile invertebrate community began to stabilize towards 2020 (Figure 5, Supplementary Material 6). There were also variable changes in abundance over time for *C. crispus, Fucus* spp., and *Littorina* spp. around 1995 that did not overlap with any subtidal regime shifts, but these changes were short-lived, and a subsequent abundance change in 2000 occurred in offset synchrony with the second subtidal regime shift (Supplementary Material 6).

# Discussion

Regime shifts are often examined in isolation within individual habitats, limiting our understanding of how a shift in one habitat may influence shifts in others. In our analyses of a 42-year dataset of subtidal and intertidal ecosystems in the Gulf of Maine, we found that 58% of the changes in intertidal communities (at the island and community-wide scale) displayed offset synchrony with subtidal regime shifts. This pattern, which was consistent across three distinct regime shifts and among key intertidal species, suggests that cross-ecosystem

interactions might be able to propagate regime shifts between intertidal and subtidal communities The remaining 42% of directional changes in intertidal community composition were mainly long-term (~20 years) starting around 2005 and correspond to expected consequences of climate change on intertidal communities rather than linkages to the subtidal community (Passarelli et al. 2017; Petraitis and Dudgeon 2020; Lawlor et al. 2026).

# Subtidal regime shifts identification

We identified three periods of rapid change in the subtidal community composition since 1980 in the Appledore Island area. These changes correspond with previous benthic and pelagic documented regime shifts (Jackson et al. 2001; Steneck et al. 2013; Pershing et al. 2015; Dijkstra et al. 2017). The first regime shift, detected around 1990, is attributed to the collapse of larger fish due to overharvesting (Jackson et al. 2001; Myers and Worm 2003). The second regime shift, detected around 2000, aligns well with the collapse of urchins and the rise of invasive macroalgae as the ecosystem reorganized (Steneck et al. 2013; Dijkstra et al. 2017). The third subtidal regime shift, detected around 2010, appears to coincide with the introduction and proliferation of exotic filamentous red algae (Dijkstra et al. 2017) and warming oceans (Pershing et al. 2015; Greene 2016; Bianchi et al. 2023). While we used trawl data to characterize regime shifts, these Gulf-wide shifts were likely felt in multiple parts of the system including the nearshore subtidal zone.Our analysis of the subtidal community when selecting only species commonly present in the nearshore subtidal zone of Appledore Island shows similar patterns as the analysis of the full dataset (Supplementary Material 3).

By using multivariate approaches for whole-community analyses, we found that the subtidal community composition has experienced continuous change over the last 40 years. Some components of the community had periods of relative stability, but consistent structural

changes over this period suggest stressors occurred at a greater frequency than the ability of the community to stabilize. The absence of a stable state points towards the need to promote ecosystem resilience in the Gulf of Maine in the face of ongoing changes in climate (Caddy and Seijo 2005). Within dynamic communities there is growing evidence of the importance of ecosystem-based (Curtin and Prellezo 2010) and adaptive management approaches (Williams 2011) for bolstering ecosystem resilience to external perturbations (DeYoung et al. 2008; Pace et al. 2015) and prevent new regime shifts as anthropogenic stressors erode ecosystem resilience (DeYoung et al. 2008).

## Regime shift propagation and changes in intertidal communities

We identified periods of change in the intertidal community that occurred in offset synchrony with the changes to the subtidal community, supporting the hypothesis that the effects of regime shifts can propagate between ecosystems. However, all three periods of change in the subtidal community were followed by changes in intertidal community composition (i.e., offset synchrony), which may reflect changes in top-down trophic pressure from the subtidal to the intertidal zone. Moreover, we have defined the temporal duration of regime shifts conservatively here and may be underestimating the prevalence of offset synchrony if intertidal responses to cross-ecosystem interactions (e.g., top-down effects of subtidal predators) are significantly delayed relative to the timing of subtidal regime shifts.

Intertidal shifts were smaller in magnitude than subtidal regime shifts, possibly owing to stabilizing interactions, which can dampen the effects of subtidal regime shifts as they cross ecosystem boundaries (Gladstone-Gallagher et al. 2023), or higher spatial heterogeneity in the intertidal zone, which can promote stability by increasing overall richness and providing a range of refugia (Oliver et al. 2015). Whether these changes in the intertidal zone constitute

452 regime shifts or not is beyond the scope of this study. Formal identification of regime shifts
453 requires showing fast and major changes (as here) in addition to reaching an alternative stable
454 state (Scheffer and Carpenter 2003). While we observed substantial shifts in intertidal
455 community composition, the reversibility of the changes is impossible to determine with the
456 data available.

457 **Potential mechanism for regime shifts propagation from the subtidal to the**
458 **intertidal zone**

459 We identified offset synchrony between the intertidal and the subtidal communities for all three
460 subtidal regime shifts at both the whole island and community scale, although the sites and
461 species impacted differed. While our data does not address specific interactions that would
462 cause the shifts *per se*, based on the natural history of the system and cross-correlations in
463 species abundances, we hypothesize that the propagation of subtidal regime shifts to the
464 intertidal ecosystem occurs primarily through changes in cross-ecosystem top-down regulation
465 (Supplementary Material 8). We identified 60 subtidal consumer species present around
466 Appledore Island that feed on taxa identified in the intertidal zone (Fig. S92). Of those 60
467 consumers, 39 were identified to be impacted by one or two subtidal regime shifts based on the
468 ordinations and subtidal time series (Fig. S92). Of those 39 species' biomass, 31 were
469 negatively cross-correlated with the abundance of some of their intertidal prey (suggesting top-
470 down regulation) and impacted by the same regime shift at one or more sites. Yet, among those
471 31 species potentially linking the subtidal to the intertidal ecosystem, six were detected in the
472 nearshore subtidal zone during a visual survey between 2014 and 2018, and their predation on
473 intertidal organisms could have cascaded through intertidal food webs and altered grazing
474 dynamics (Lubchenco 1978, 1980, Ellis et al. 2007). For example, *Cancer borealis* is a known
475 top-down regulator of intertidal communities at Appledore Island (Ellis et al. 2007), but the

476 impact of the five other species (*Homarus americanus, Pollachius virens, Pseudopleuronectes*
477 *americanus, Tautogolabrus adspersus* and *Urophycis regia*) on intertidal communities is
478 untested, partly because intertidal surveys are being done at low tide when these predators
479 cannot access immersed intertidal prey. However, as subtidal communities vary substantially
480 with depth, the offshore NOAA bottom trawl surveys, which focus effort on deeper-water
481 species, may not capture all nearshore species that contribute to trophic linkages by foraging
482 in the intertidal zone.

483 Another potential linkage mechanism between the intertidal and the subtidal is changes in
484 propagule pressure or migration from the subtidal to the intertidal zone, which can impact
485 intertidal communities (Menge et al. 2003, Hedge et al. 2014, Pearman et al. 2020), and could
486 produce a similar offset synchrony patterns. Some species showing offset synchrony are
487 exclusively intertidal such as *Littorina obtustata* and *Littorinasaxitalis*, but other species
488 showing offset synchrony have life stages (*Semibalanus balanoides, Littorina littorea, Mytilus*
489 *edulis* and *C. maenas*) or potential source populations (Amphipoda or Isopoda) inhabiting the
490 subtidal or pelagic zones. It is therefore also possible that Gulf-wide regime shifts impact
491 intertidal communities by altering predation pressure on or the feeding condition of non-
492 intertidal life stages or metapopulation dynamics (Hedge et al. 2014; Pearman et al. 2020).

493 We acknowledge that the cross-ecosystem linkage mechanisms in this article remain
494 speculative, although the food webs of the intertidal and subtidal are known to be highly
495 interconnected in the Gulf of Maine. We also acknowledge that some intertidal community
496 change could result from effects that are confounded with subtidal changes, qualities inherent
497 to any time series analysis. However, our finding of offset synchrony in intertidal communities
498 across all three subtidal regime shifts, combined with our knowledge of the ecological
499 relationships between subtidal and intertidal species, provides compelling circumstantial

evidence that subtidal regime shifts are influencing adjacent intertidal ecosystems. Our findings suggest that further investigations of the impacts of regime shifts on adjacent ecosystems, particularly the mechanisms by which those impacts propagate, are worthy of investigation.

### Independent changes in the intertidal communities

Many (42%) of the changes in direction of the intertidal community composition at the island- and community-wide scales did not correspond to offset synchrony with subtidal regime shifts. These longer-term tendencies are coherent with the expected consequences of climate change, as we have seen an increase in warm-affinity species and a decrease in cold-affinity species on Appledore Island (Lawlor et al. 2026). Here, we found a general tendency for change starting around 2005 that lasted until the end of the study period in sessile and mobile communities. These changes include a decreased abundance of many key intertidal taxa (*C. crispus*, *M. edulis*, Amphipoda, and *Nucella sp.*), all of which are likely negatively impacted by increasing temperatures, either in their adult stage (Khan et al. 2018), as planktonic larvae (Petraitis and Dudgeon 2020), or indirectly through increased susceptibility to parasites (Lavaniegos and Ohman 1998, Mouritsen et al. 2005). Other abiotic factors including acidity and salinity may contribute to declines in *Nucella* and Amphipoda (Passarelli et al. 2017, Petraitis and Dudgeon 2020). The reduction in *M. edulis* may also be attributable to the increased abundance of predatory *C. borealis* (Ellis et al. 2007), from 2005 to the end of the study period.

## Conclusion

The propagation of regime shifts has been theorized (Rocha et al. 2018, Rocha and Crepin 2023) but empirical evidence has been lacking. Our results offer some support for cross-ecosystem interactions between subtidal and intertidal systems, wherein all major community changes in the subtidal zone were followed by corresponding changes in the intertidal zone,

and abundance of subtidal consumers was negatively cross-correlated with the abundance of their intertidal prey. Propagation of regime shifts from subtidal to intertidal ecosystems is plausible due to top-down control from subtidal predators feeding in the intertidal zone at high tide (Rilov and David R 2006, Rilov and Schiel 2006, Silva et al. 2008, 2010, 2014, Christie et al. 2020). Importantly, through our analysis we were able to distinguish between changes in intertidal communities that are likely attributable to subtidal regime shifts, and changes that are likely attributable to other causes, particularly climate change. This result demonstrates the broad importance of considering community regime shifts in adjacent ecosystems as putative drivers of change in any ecosystem of interest and the importance of considering cross-ecosystem interactions to understand ecosystem functioning.

# Acknowledgements

We thank the Derry lab (UQAM) for feedback. JB was funded by NSERC Discovery Grant 2022-03706 (Alison Derry). This publication originated from a Living Data Project working group funded by the Canadian Institute of Ecology and Evolution and a Natural Sciences and Engineering Research Council CREATE grant. In addition, Jarrett E. K. Byrnes, Jennifer A. Dijkstra, and Kylla Benes were supported to curate and explore long-term data from the Shoals Marine Lab by the Regional Association for Research in the Gulf of Maine. This is publication number 219 of the Shoals Marine Laboratory.

# Conflict of interest

The authors declare no conflict of interest.

# Author contribution

All authors played a role in Conceptualization (supporting), Writing - Review & Editing (supporting). JEKB, JBB and EKB participated in Project Administration. JEKB also played a role in Formal Analysis (supporting), and Funding Acquisition. JEKB, JAD and KB had a role in Supervision. JB did conceptualization (lead), formal analysis (lead), visualization (lead), writing - original draft (lead).

# References


Beisner, B. E., Haydon, D. T., & Cuddington, K. (2003). Alternative stable states in ecology. *Frontiers in Ecology and the Environment*, *1*(7), 376–382. https://doi.org/10.1890/1540-9295(2003)001[0376:ASSIE]2.0.CO;2

Bianchi, T. S., Brown, C. J., Snelgrove, P. V. R., Stanley, R. R. E., Cote, D., & Morris, C. (2023). Benthic Invertebrates on the Move: A Tale of Ocean Warming and Sediment Carbon Storage. *Limnology and Oceanography Bulletin*, *32*(1), 1–5. https://doi.org/10.1002/lob.10544

Biggs, R., Carpenter, S. R., & Brock, W. A. (2009). *Turning back from the brink: Detecting an impending regime shift in time to avert it*. www.pnas.org/cgi/content/full/

Brandt, J. E., Wesner, J. S., Ruggerone, G. T., Jardine, T. D., Eagles-Smith, C. A., Ruso, G. E., Stricker, C. A., Voss, K. A., & Walters, D. M. (2024). Continental-scale nutrient and contaminant delivery by Pacific salmon. *Nature*, *634*(8035), 875–882. https://doi.org/10.1038/s41586-024-07980-2

Bürkner, P. C. (2018). Advanced Bayesian multilevel modeling with the R package brms. *R Journal*, *10*(1), 395–411. https://doi.org/10.32614/rj-2018-017

Byrnes, J. E. K., Brown, A., Sheridan, K., Peller, T., Lawlor, J., Beaulieu, J., Muñoz, J., Hesketh, A., Pereira, A., Knight, N. S., Super, L., Bledsoe, E. K., Burant, J. B., Dijkstra, J. A., & Benes, K. (2024). Notes from the past show how local variability can stymie urchins and the rise of the reds in the Gulf of Maine. *Ecosphere*, *15*(4). https://doi.org/10.1002/ecs2.4800

Caddy, J. F., & Seijo, J. C. (2005). This is more difficult than we thought! The responsibility of scientists, managers and stakeholders to mitigate the unsustainability of marine fisheries. *Philosophical Transactions of the Royal Society B: Biological Sciences*, *360*(1453), 59–75. https://doi.org/10.1098/rstb.2004.1567

Cereghetti, E., Peller, T., Kaeser, S., Gounand, I., & Altermatt, F. (2025). Seasonal dynamics of detritus flows and decomposition across ecosystem boundaries. *Current Biology*, *35*(9), 2139-2145.e3. https://doi.org/10.1016/j.cub.2025.03.019

Christie, H., Kraufvelin, P., Kraufvelin, L., Niemi, N., & Rinde, E. (2020). Disappearing Blue Mussels – Can Mesopredators Be Blamed? *Frontiers in Marine Science*, *7*(July), 1–8. https://doi.org/10.3389/fmars.2020.00550

CoreTeam, R. (2020). *R: A language and environment for statistical computing*. R Foundation for Statistical Computing. https://www.r-project.org

Curtin, R., & Prellezo, R. (2010). Understanding marine ecosystem based management: A literature review. *Marine Policy*, *34*(5), 821–830. https://doi.org/10.1016/j.marpol.2010.01.003

Dakos, V., Van Nes, E. H., D'Odorico, P., & Scheffer, M. (2012). Robustness of variance and autocorrelation as indicators of critical slowing down. *Ecology*, *93*(2), 264–271. https://doi.org/10.1890/11-0889.1

Daskalov, G. M., Grishin, A. N., Rodionov, S., & Mihneva, V. (2007). Trophic cascades triggered by overfishing reveal possible mechanisms of ecosystem regime shifts. *Proceedings of the National Academy of Sciences of the United States of America*, *104*(25), 10518–10523. https://doi.org/10.1073/pnas.0701100104

Defeo, O., McLachlan, A., Armitage, D., Elliott, M., & Pittman, J. (2021). Sandy beach social–ecological systems at risk: regime shifts, collapses, and governance challenges. In *Frontiers*

*in Ecology and the Environment* (Vol. 19, Number 10, pp. 564–573). John Wiley and Sons Inc. https://doi.org/10.1002/fee.2406

DeYoung, B., Barange, M., Beaugrand, G., Harris, R., Perry, R. I., Scheffer, M., & Werner, F. (2008). Regime shifts in marine ecosystems: detection, prediction and management. *Trends in Ecology and Evolution*, *23*(7), 402–409. https://doi.org/10.1016/j.tree.2008.03.008

Dijkstra, J. A., Harris, L. G., Mello, K., Litterer, A., Wells, C., & Ware, C. (2017). Invasive seaweeds transform habitat structure and increase biodiversity of associated species. *Journal of Ecology*, *105*(6), 1668–1678. https://doi.org/10.1111/1365-2745.12775

Ellis, J. C., Shulman, M. J., Wood, M., Witman, J. D., & Lozyniak, S. (2007). Regulation of intertidal food webs by avian predators on new England rocky shores. *Ecology*, *88*(4), 853–863. https://doi.org/10.1890/06-0593

Evans, D. L., & Stauffer, G. (2004). *NOAA Protocols for Groundfish Bottom Trawl Surveys of the Nation's Fishery Resources*. http://spo.nmfs.noaa.gov/tm/

Genkai-Kato, M., Vadeboncoeur, Y., Liboriussen, L., & Jeppesen, E. (2012). Benthic–planktonic coupling, regime shifts, and whole-lake primary production in shallow lakes. *Ecology*, *93*(3), 619–631. https://doi.org/10.1890/10-2126.1

Gladstone-Gallagher, R. V., Thrush, S. F., Low, J. M. L., Pilditch, C. A., Ellis, J. I., & Hewitt, J. E. (2023). Toward a network perspective in coastal ecosystem management. In *Journal of Environmental Management* (Vol. 346). Academic Press. https://doi.org/10.1016/j.jenvman.2023.119007

Gounand, I., Little, C. J., Harvey, E., & Altermatt, F. (2018). Cross-ecosystem carbon flows connecting ecosystems worldwide. *Nature Communications*, *9*(1), 4825. https://doi.org/10.1038/s41467-018-07238-2

Granger, C. W. J. (1969). Investigating Causal Relations by Econometric Models. *Econometrica*, *37*(3), 424–438.

Greene, C. H. (2016). North America's Iconic marine species at risk due to unprecedented ocean warming. *Oceanography*, *29*(3), 14–17. https://doi.org/10.5670/oceanog.2016.67

Grosslein, M. D. (n.d.). *Bottom Trawl Survey Methods of the Northeast Fisheries Center Wooos Hole. Mass. USA*.

Guttal, V., Jayaprakash, C., & Tabbaa, O. P. (2013). Robustness of early warning signals of regime shifts in time-delayed ecological models. *Theoretical Ecology*, *6*(3), 271–283. https://doi.org/10.1007/s12080-013-0194-4

Jackson, J. B. C., Kirby, M. X., Berger, W. H., Bjorndal, K. A., Botsford, L. W., Bourque, B. J., Bradbury, R. H., Cooke, R., Erlandson, J., Estes, J. A., Hughes, T. P., Kidwell, S., Lange, C. B., Lenihan, H. S., Pandolfi, J. M., Peterson, C. H., Steneck, R. S., Tegner, M. J., & Warner, R. R. (2001). Historical overfishing and the recent collapse of coastal ecosystems. *Science*, *293*(5530), 629–637. https://doi.org/10.1126/science.1059199

Janssen, A. B. G., Hilt, S., Kosten, S., de Klein, J. J. M., Paerl, H. W., & Van de Waal, D. B. (2021). Shifting states, shifting services: Linking regime shifts to changes in ecosystem services of shallow lakes. In *Freshwater Biology* (Vol. 66, Number 1, pp. 1–12). Blackwell Publishing Ltd. https://doi.org/10.1111/fwb.13582

Johnston, R., & Sosebee, K. (n.d.). *History of the United States Bottom Trawl Surveys, NAFO Subareas 4-7*.

637 Khan, A. H., Levac, E., van Guelphen, L., Pohle, G., & Chmura, G. L. (2018). The effect of global
638 climate change on the future distribution of economically important macroalgae (seaweeds)
639 in the northwest Atlantic. *Facets*, *3*(1), 275–286. https://doi.org/10.1139/facets-2017-0091
640 Knight, T. M., McCoy, M. W., Chase, J. M., McCoy, K. A., & Holt, R. D. (2005). Trophic
641 cascades across ecosystems. *Nature*, *437*(7060), 880–883.
642 https://doi.org/10.1038/nature03962
643 Krumhansl, K. A., & Scheibling, R. E. (2012). Production and fate of kelp detritus. In *Marine*
644 *Ecology Progress Series* (Vol. 467, pp. 281–302). https://doi.org/10.3354/meps09940
645 Kuzyk, Z., Leblanc, M., Ehn, J., Crawford A., ..., & O'Connor, M. I. (2026). Losing
646 Shikaapaashkw: Hydropower dams, compounded by climate change, caused eelgrass social-
647 ecological system collapse. *Nature Communication*.
648 Lavaniegos, B. E., & Ohman, M. D. (1998). Hyperiid Amphipods as indicators of climate changes
649 in the california current. *Proceedings of the Fourth International Crustacean Congress*.
650 Lawlor, J., Hesketh, A., Beaulieu, J., Knight, N., Peller, T., Super, L., Pereira, A., Bledsoe, E.,
651 Burant, J., Dijkstra, J., Benes, K., & Byrnes, J. (2026). *Global Patterns Predict Local*
652 *Biodiversity Shifts in a Climate Change Hotspot*. https://doi.org/10.32942/X20H2J
653 Lees, K., Pitois, S., Scott, C., Frid, C., & MacKinson, S. (2006). Characterizing regime shifts in
654 the marine environment. In *Fish and Fisheries* (Vol. 7, Number 2, pp. 104–127).
655 https://doi.org/10.1111/j.1467-2979.2006.00215.x
656 Lubchenco, J. (1978). Plant Species Diversity in a Marine Intertidal Community: Importance of
657 Herbivore Food Preference and Algal Competitive Abilities. *The American Naturalist*,
658 *112*(983), 23–39. https://doi.org/10.1086/283250
659 Lubchenco, J. (1980). Algal Zonation in the New England Rocky Intertidal Community: An
660 Experimental Analysis. In *Source: Ecology* (Vol. 61, Number 2).
661 Maziarz, M. (2015). A review of the Granger-causality fallacy. *Journal of Philosophical*
662 *Economics*, *Volume VII*(Articles). https://doi.org/10.46298/jpe.10676
663 Montagano, L., Leroux, S. J., Giroux, M. A., & Lecomte, N. (2019). The strength of ecological
664 subsidies across ecosystems: a latitudinal gradient of direct and indirect impacts on food
665 webs. *Ecology Letters*, *22*(2), 265–274. https://doi.org/10.1111/ele.13185
666 Mouritsen, K. N., Tompkins, D. M., & Poulin, R. (2005). Climate warming may cause a parasite-
667 induced collapse in coastal amphipod populations. *Oecologia*, *146*(3), 476–483.
668 https://doi.org/10.1007/s00442-005-0223-0
669 Myers, R. A., & Worm, B. (2003). Rapid worldwide depletion of predatory fish communities.
670 *Nature*, *423*(6937), 280–283. https://doi.org/10.1038/nature01610
671 Newton, C., Bracken, M. E. S., McConville, M., Rodrigue, K., & Thornber, C. S. (2013). Invasion
672 of the Red Seaweed Heterosiphonia japonica Spans Biogeographic Provinces in the Western
673 North Atlantic Ocean. *PLoS ONE*, *8*(4). https://doi.org/10.1371/journal.pone.0062261
674 NOAA. (2020, March 2). *Resource Survey Report : Bottom Trawl Survey, Cape Hatteras – Gulf of*
675 *Maine*.
676 O'Brien, B. S., Mello, K., Litterer, A., & Dijkstra, J. A. (2018). Seaweed structure shapes trophic
677 interactions: A case study using a mid-trophic level fish species. *Journal of Experimental*
678 *Marine Biology and Ecology*, *506*(April), 1–8. https://doi.org/10.1016/j.jembe.2018.05.003
679 Oksanen, J., Blanchet, F. G., Friendly, M., Kindt, R., Legendre, P., Mcglinn, D., Minchin, P. R.,
680 Hara, R. B. O., Simpson, G. L., Solymos, P., Stevens, M. H. H., Szoecs, E., & Wagner, H.

(2020). *vegan: community ecology package. R Package Version 2.5-6.* 2395–2396. https://cran.r-project.org/pack- age=vegan.

Oliver, T. H., Heard, M. S., Isaac, N. J. B., Roy, D. B., Procter, D., Eigenbrod, F., Freckleton, R., Hector, A., Orme, C. D. L., Petchey, O. L., Proença, V., Raffaelli, D., Suttle, K. B., Mace, G. M., Martín-López, B., Woodcock, B. A., & Bullock, J. M. (2015). Biodiversity and Resilience of Ecosystem Functions. *Trends in Ecology and Evolution*, *30*(11), 673–684. https://doi.org/10.1016/j.tree.2015.08.009

Pace, M. L., Carpenter, S. R., & Cole, J. J. (2015). With and without warning: Managing ecosystems in a changing world. In *Frontiers in Ecology and the Environment* (Vol. 13, Number 9, pp. 460–467). Ecological Society of America. https://doi.org/10.1890/150003

Passarelli, M. C., Riba, I., Cesar, A., Serrano-Bernando, F., & DelValls, T. A. (2017). Assessing the influence of ocean acidification to marine amphipods: A comparative study. *Science of the Total Environment*, *595*, 759–768. https://doi.org/10.1016/j.scitotenv.2017.04.004

Pauly, D., Christensen, V., Dalsgaard, J., Froese, R., & Torres, F. (1998). Fishing down marine food webs. *Science*, *279*(5352), 860–863. https://doi.org/10.1126/science.279.5352.860

Pedersen, E. J., Miller, D. L., Simpson, G. L., & Ross, N. (2019). Hierarchical generalized additive models in ecology: An introduction with mgcv. *PeerJ*, *2019*(5). https://doi.org/10.7717/peerj.6876

Peller, T., Marleau, J. N., & Guichard, F. (2022). Traits affecting nutrient recycling by mobile consumers can explain coexistence and spatially heterogeneous trophic regulation across a meta-ecosystem. *Ecology Letters*, *25*(2), 440–452. https://doi.org/10.1111/ele.13941

Pershing, A. J., Alexander, M. A., Hernandez, C. M., Kerr, L. A., Le Bris, A., Mills, K. E., Nye, J. A., Record, N. R., Scannell, H. A., Scott, J. D., Sherwood, G. D., & Thomas, A. C. (2016). Response to Comments on "Slow adaptation in the face of rapid warming leads to collapse of the Gulf of Maine cod fishery." *Science*, *352*(6284), 423–423. https://doi.org/10.1126/science.aae0463

Pershing, A. J., Mills, K. E., Record, N. R., Stamieszkin, K., Wurtzell, K. V., Byron, C. J., Fitzpatrick, D., Golet, W. J., & Koob, E. (2015). Evaluating trophic cascades as drivers of regime shifts in different ocean ecosystems. *Philosophical Transactions of the Royal Society B: Biological Sciences*, *370*(1659), 1–9. https://doi.org/10.1098/rstb.2013.0265

Petraitis, P. S., & Dudgeon, S. R. (2020). Declines over the last two decades of five intertidal invertebrate species in the western North Atlantic. *Communications Biology*, *3*(1), 1–7. https://doi.org/10.1038/s42003-020-01326-0

Polis, G. A., Anderson, W. B., & Holt, R. D. (1997). Toward an integration of landscape and food web ecology: The dynamics of spatially subsidized food webs. *Annual Review of Ecology and Systematics*, *28*(1997), 289–316. https://doi.org/10.1146/annurev.ecolsys.28.1.289

Rilov, G., & David R, S. (2006). Seascape-dependent subtidal – intertidal trophic linkages. *Ecology*, *87*(3), 731–744.

Rilov, G., & Schiel, D. (2006). Trophic linkages across seascapes: subtidal predators limit effective mussel recruitment in rocky intertidal communities. *Marine Ecology Progress Series*, *327*(1991), 83–93. https://doi.org/10.3354/meps327083

Rocha, J. C., & Crepin, A.-S. (2023). *Structural Controllability and Management of Cascading Regime Shifts*.

724 Rocha, J. C., Peterson, G., Bodin, Ö., & Levin, S. (2018). Cascading regime shifts within and
725 across scales. *Science*, *362*(6421), 1379–1383. https://doi.org/10.1126/science.aat7850
726 Scheffer, M., Carpenter, S., Foley, J. A., Folke, C., & Walker, B. (2001). Catastrophic shifts in
727 ecosystems. *Nature*, *413*(6856), 591–596. https://doi.org/10.1038/35098000
728 Scheffer, M., & Carpenter, S. R. (2003). Catastrophic regime shifts in ecosystems: Linking theory
729 to observation. In *Trends in Ecology and Evolution* (Vol. 18, Number 12, pp. 648–656).
730 Elsevier Ltd. https://doi.org/10.1016/j.tree.2003.09.002
731 Scheibling, R., & Hennigar, A. (1997). Recurrent outbreaks of disease in sea urchins
732 Strongylocentrotus droebachiensis in Nova Scotia:evidence for a link with large-scale
733 meteorologic and oceanographic events. *Marine Ecology Progress Series*, *152*(128), 155–
734 165. https://doi.org/10.3354/meps152155
735 Scyphers, S. B., Steven Picou, J., & Grabowski, J. H. (2019). Chronic social disruption following
736 a systemic fishery failure. *Proceedings of the National Academy of Sciences of the United*
737 *States of America*, *116*(46), 22912–22914. https://doi.org/10.1073/pnas.1913914116
738 Shoals Marine Laboratory. (2018). *Shoals Marine Laboratory Long-term Rocky Interdidal*
739 *Monitoring program*. (August).
740 Silva, A. C. F., Boaventura, D. M., Thompson, R. C., & Hawkins, S. J. (2014). Spatial and
741 temporal patterns of subtidal and intertidal crabs excursions. *Journal of Sea Research*, *85*,
742 343–348. https://doi.org/10.1016/j.seares.2013.06.006
743 Silva, A. C. F., Hawkins, S. J., Boaventura, D. M., & Thompson, R. C. (2008). Predation by small
744 mobile aquatic predators regulates populations of the intertidal limpet Patella vulgata (L.).
745 *Journal of Experimental Marine Biology and Ecology*, *367*(2), 259–265.
746 https://doi.org/10.1016/j.jembe.2008.10.010
747 Silva, A., Hawkins, S., Boaventura, D., Brewster, E., & Thompson, R. (2010). Use of the intertidal
748 zone by mobile predators: influence of wave exposure, tidal phase and elevation on
749 abundance and diet. *Marine Ecology Progress Series*, *406*, 197–210.
750 https://doi.org/10.3354/meps08543
751 Sorte, C. J. B., Davidson, V. E., Franklin, M. C., Benes, K. M., Doellman, M. M., Etter, R. J.,
752 Hannigan, R. E., Lubchenco, J., & Menge, B. A. (2017). Long-term declines in an intertidal
753 foundation species parallel shifts in community composition. *Global Change Biology*, *23*(1),
754 341–352. https://doi.org/10.1111/gcb.13425
755 Steneck, R. S., Leland, A., McNaught, D. C., & Vavrinec, J. (2013). Ecosystem flips, locks, and
756 feedbacks: The lasting effects of fisheries on Maine's kelp forest ecosystem. *Bulletin of*
757 *Marine Science*, *89*(1), 31–55. https://doi.org/10.5343/bms.2011.1148
758 Subalusky, A. L., Dutton, C. L., Rosi, E. J., & Post, D. M. (2017). Annual mass drownings of the
759 Serengeti wildebeest migration influence nutrient cycling and storage in the Mara River.
760 *Proceedings of the National Academy of Sciences of the United States of America*, *114*(29),
761 7647–7652. https://doi.org/10.1073/pnas.1614778114
762 Sundstrom, S. M., Eason, T., Nelson, R. J., Angeler, D. G., Barichievy, C., Garmestani, A. S.,
763 Graham, N. A. J., Granholm, D., Gunderson, L., Knutson, M., Nash, K. L., Spanbauer, T.,
764 Stow, C. A., & Allen, C. R. (2017). Detecting spatial regimes in ecosystems. *Ecology Letters*,
765 *20*(1), 19–32. https://doi.org/10.1111/ele.12709
766 Wangersky, P. J. (1978). Lotka-Volterra Population Models. In *Source: Annual Review of Ecology*
767 *and Systematics* (Vol. 9). https://about.jstor.org/terms

Williams, B. K. (2011). Adaptive management of natural resources-framework and issues. *Journal of Environmental Management*, *92*(5), 1346–1353. https://doi.org/10.1016/j.jenvman.2010.10.041

Williams, T. M., Estes, J. A., Doak, D. F., & Springer, A. M. (2004). Killer Apetite: Assessing the role of Predators in Ecological Communitied. *Ecology*, *85*(12), 3373–3384. https://doi.org/10.1890/03-0696

Worm, B., & Myers, R. A. (2002). Top-Down Versus Bottom-Up Control in Oceanic Food Webs: a Meta-Analysis of Cod-Shrimp Interactions in the North Atlantic. *Ecology*, (December).

# Tables

**Table 1:** Models ran and their performance. The GS model is a model with a shared trend and similar smoothness between sites (equation 1), the GI model has a shared trend and different smoothness between sites (equation 2), and the I model has different trends and smoothness between sites (equation 3). The family column is the modeling family used for each variable.

| Variable | Model type | looIC | Bayes $R^2$ | Family |
|---|---|---|---|---|
| Subtidal predators community | - | 30.5 | 0.83 | Gaussian |
| Sessile community | GS | 28084.9 | 0.55 | Gaussian |
| **Sessile community** | **GI** | **18803.5** | **0.55** | **Gaussian** |
| Sessile community | I | 18826.0 | 0.55 | Gaussian |
| Mobile community | GS | 19593.5 | 0.16 | Gaussian |
| **Mobile community** | **GI** | **19553.8** | **0.17** | **Gaussian** |
| Mobile community | I | 19659.9 | 0.16 | Gaussian |
| Ascophyllum | I | 12594.4 | 0.52 | Hurdle Gamma |
| Chondrus | I | 20301.6 | 0.50 | Hurdle Gamma |
| C. maenas | I | 3632.0 | 0.13 | Zero-Inflated Poisson |
| Fucus | I | 48214.2 | 0.31 | Hurdle Gamma |

| | | | | |
|---|---|---|---|---|
| Littorina | I | 114252.1 | 0.11 | Zero-Inflated Negative Binominal |
| Mastocarpus | I | 17553.3 | 0.36 | Hurdle Gamma |
| Mytilus | I | 9067.3 | 0.38 | Zero-Inflated Beta |
| Nucella | I | 16017.7 | 0.30 | Zero-Inflated Negative Binominal |
| Semibalanus | I | 8689.5 | 0.39 | Zero-Inflated Beta |
| Amphipoda | I | 77154.3 | 0.16 | Zero-Inflated Poisson |
| Isopoda | I | 11816.8 | 0.42 | Zero-Inflated Poisson |

# Figure captions

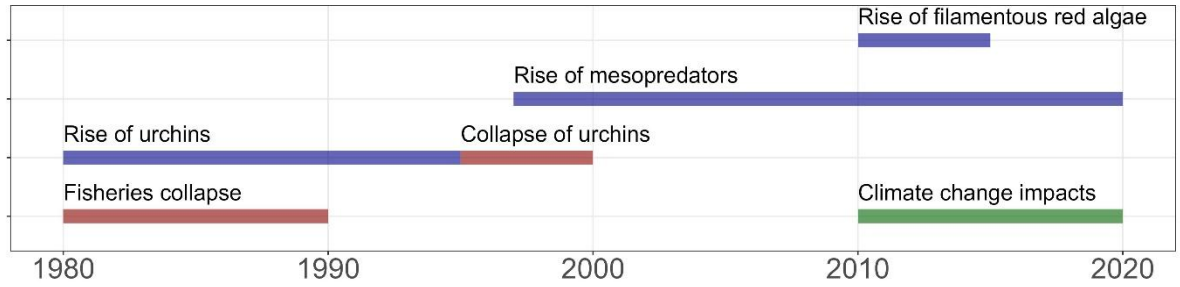


**Figure 1.** Timeline of subtidal regime shifts within the Gulf of Maine since 1980 based on Dijkstra et al. (2017); Pershing et al. (2015); Petraitis & Dudgeon (2020); Steneck & Wahle (2013).

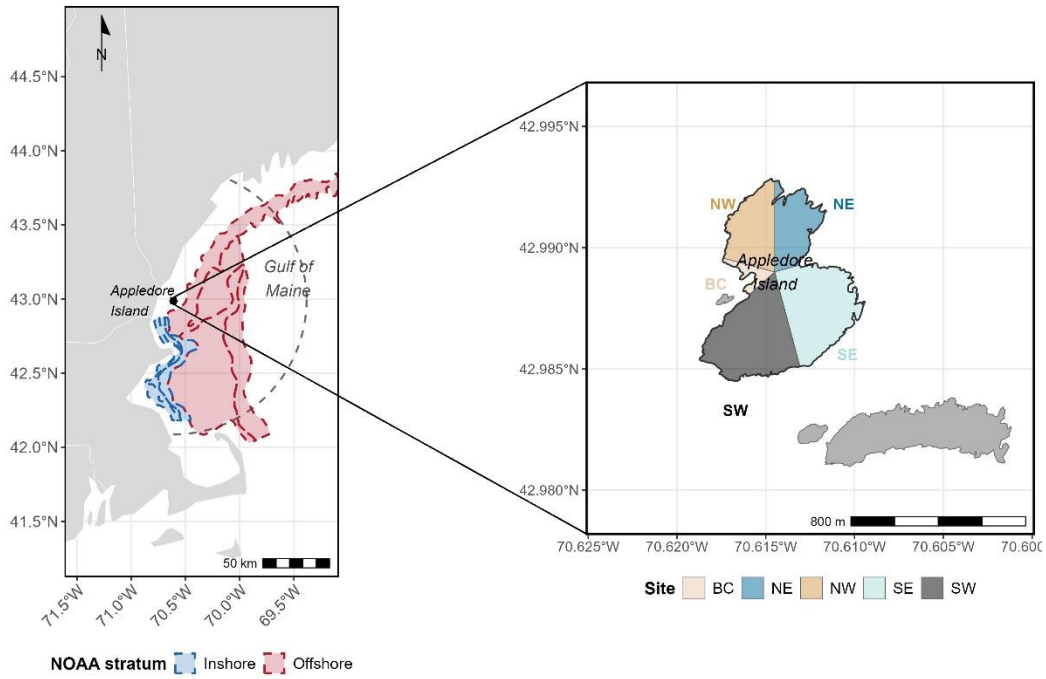


789

790

791 **Figure 2.** Map of the study system. The grey dashed line in the larger scale map is the 100 Km
792 radius from Appledore Island. NOAA stratum are the surfaces covered by the NOAA bottom
793 trawl survey data we used for subtidal regime shifts timing identification.

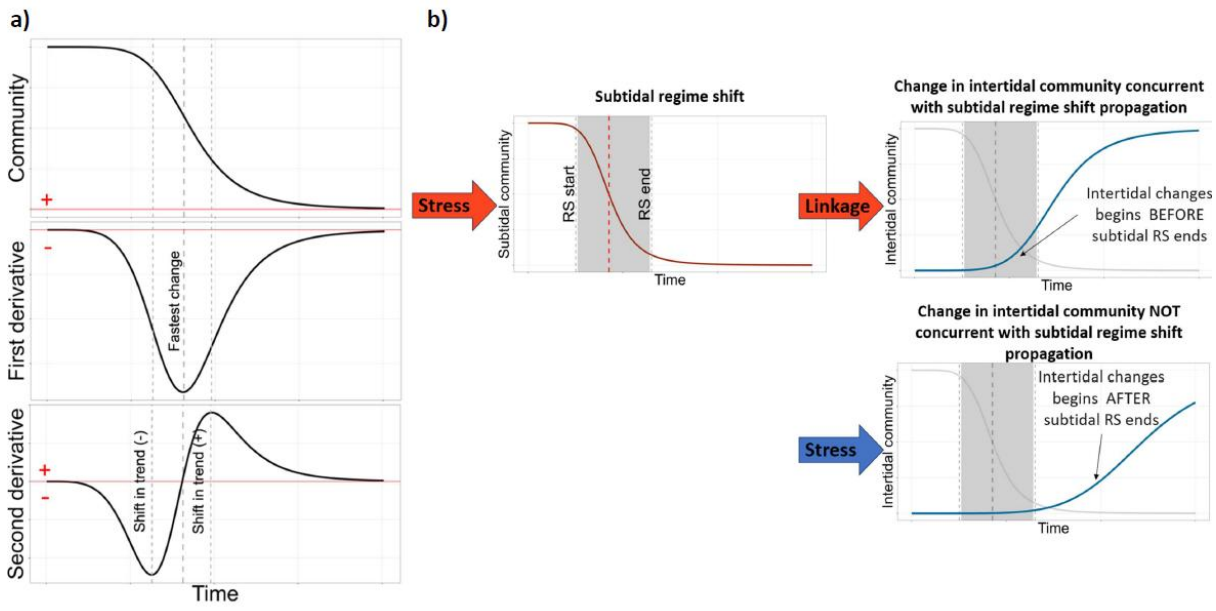


794

795 **Figure 3**. Illustrated hypotheses and timing of regime shifts within the Gulf of Maine. a) a
796 hypothetical temporal trend with the corresponding first and second derivatives. b) conceptual
797 figure of the hypothesis of where the subtidal regime shifts impact the intertidal community
798 and the alternative hypothesis where the changes in intertidal community are the result of the
799 direct effects of a stressor on the intertidal.

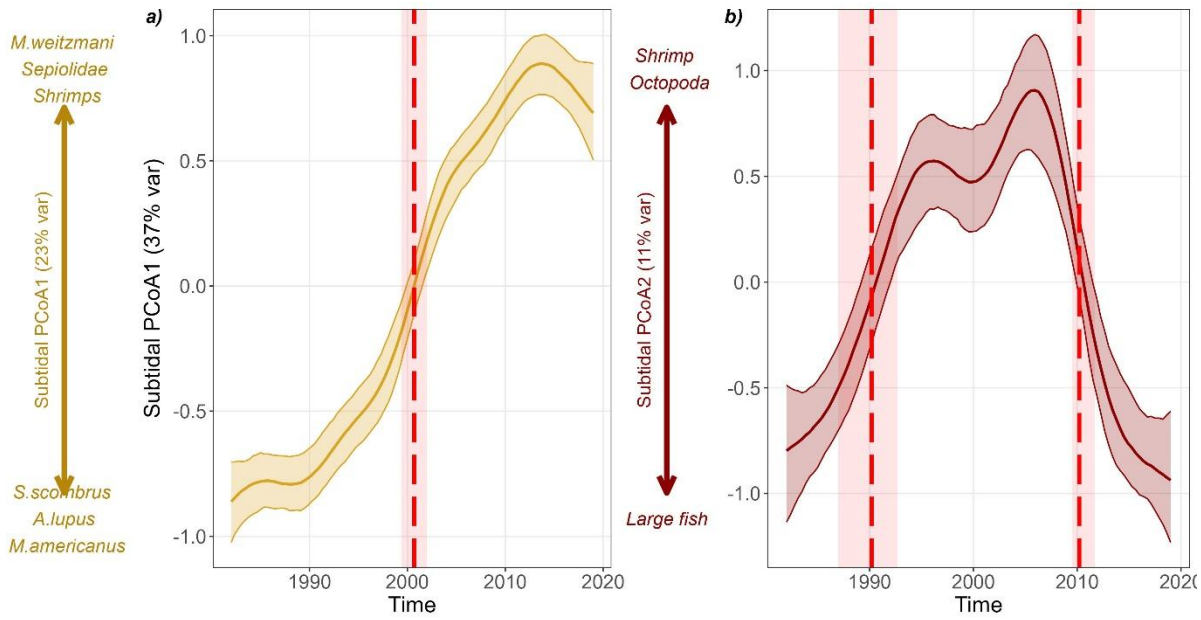


**Figure 4**. Changes in the subtidal predator community through time, as shown through ordination axes. The first ordination axis is in (a), and the second ordination axis is in (b). The shaded area represents the 95% credible interval of the centered posterior predicted trends (without the intercept). The red dashed lines represent the moments when the rate of change was particularly fast (regime shifts) and the red shaded area around this line represents its 95% credible interval.

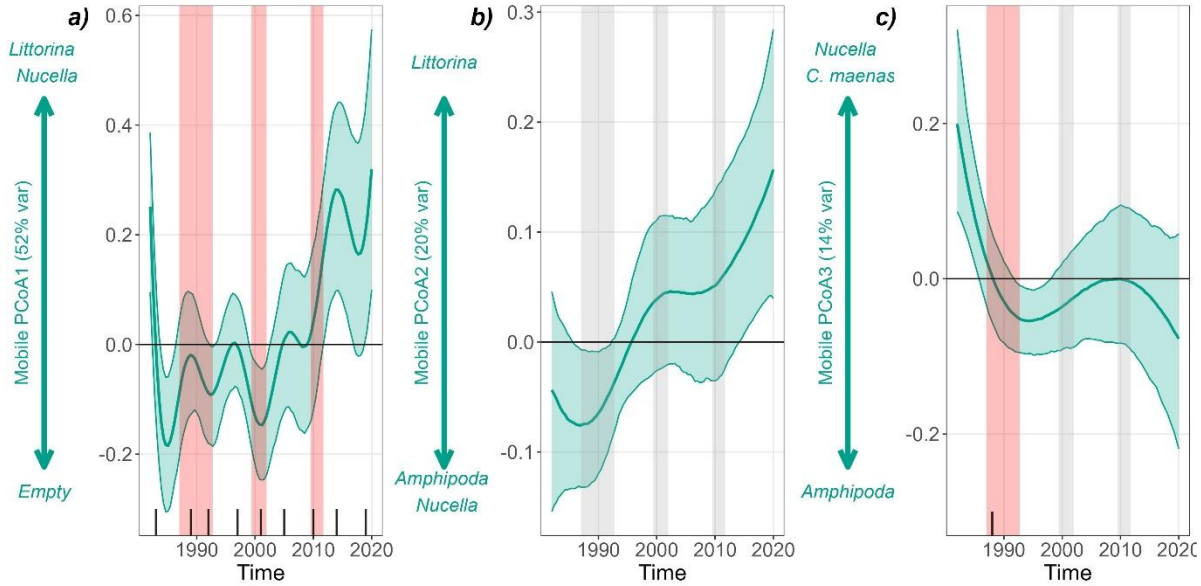


**Figure 5**. Island-wide changes in the intertidal mobile community through time, as shown through ordination axes. In a) island-scale trend in ordination axis 1, in b) island-wide trend in ordination axis 2, and in c) island-wide trend in ordination axis 3. The blue shaded area represents the 95% credible interval of the centered posterior predicted trends (without the intercept). The red and grey shaded areas represent the 95% CI of the subtidal regime shifts. This area is red when we detected offset synchrony and grey if we did not. The small grey lines

at the bottom are times where there were significant changes in direction (second derivative different from zero). The site specific trends are in supplementary material 4.

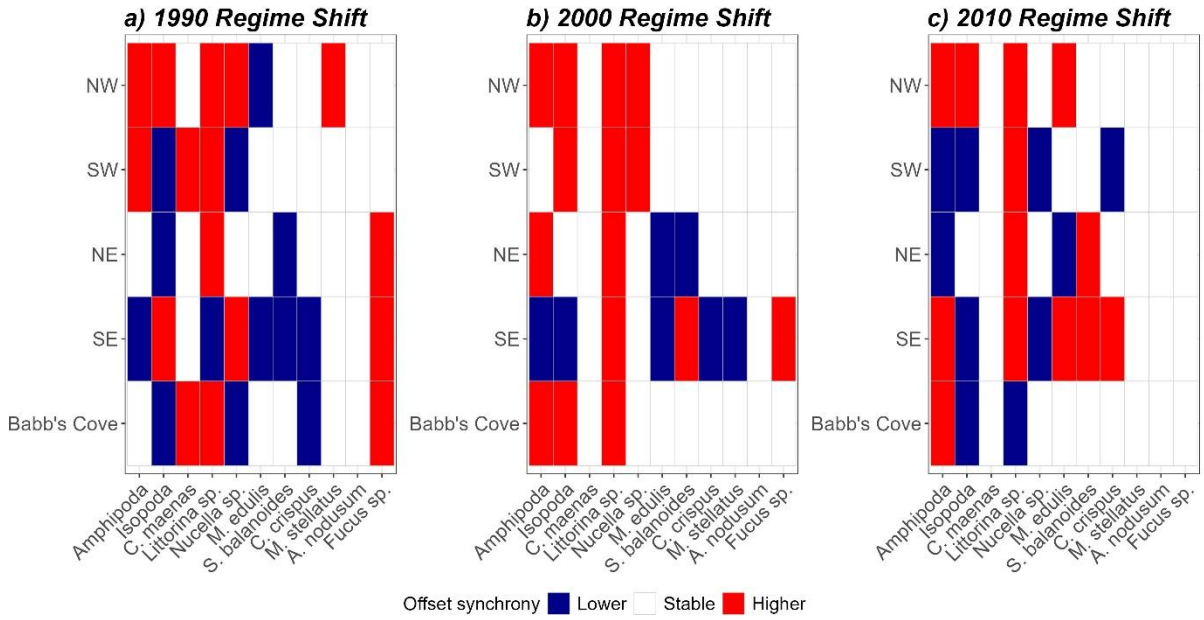


**Figure 6.** Heatmap of the offset synchrony of intertidal species changes in abundance for each subtidal regime shift. The sites are on the y-axis and the focal groups in the x-axis. Red represents a shift toward a higher abundance, blue represents a shift toward a lower abundance, and white represents the absence of shift. We considered a shift in direction as significant when the 95% credible interval of the second derivative differed from zero during the time period of a subtidal regime shift. Temporal trends for each focal taxa are in supplementary material 5.

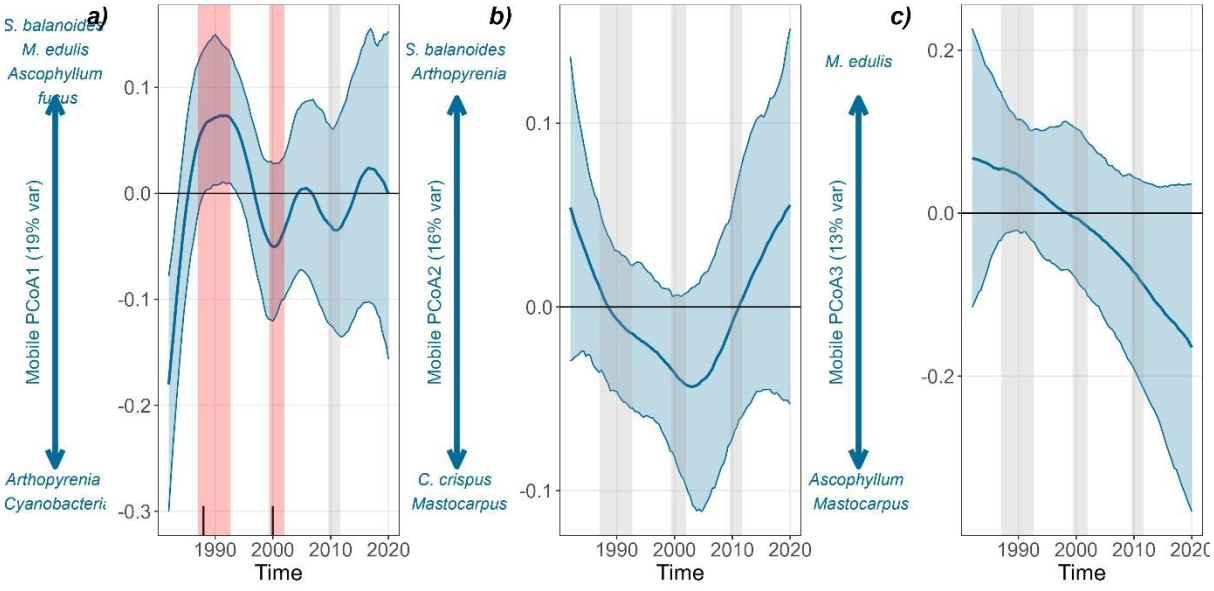


**Figure 7.** Island-wide changes in the intertidal sessile community through time, as shown through ordination axes. In a) island-scale trend in ordination axis 1, in b) island-wide trend in PCoA axis 2, and in c) island-wide trend in ordination axis 3. The blue shaded area represents

827 the 95% credible interval of the centered posterior predicted trends (without the intercept). The
828 red and grey shaded areas represent the 95% CI of the subtidal regime shifts. This area is red
829 when we detected offset synchrony and grey if we did not. The small grey lines at the bottom
830 are times where there were significant changes in direction (second derivative different from
831 zero). The site-specific trends are in supplementary material 4.

# Table of Contents

Supplementary Material 1: Ordinations (PCoA) Figures ..... 2
Subtidal community composition ..... 2
Intertidal sessile organism community composition ..... 4
Intertidal mobile organism community ..... 5
Supplementary Material 2: Subtidal changes in community: first derivative. ..... 6
Supplementary Material 3: Subtidal regime shifts when using only species detected in the near shore subtidal ..... 7
Supplementary Material 4: Site specific temporal trends in intertidal community composition 9
Supplementary Material 5: Focal species temporal trends. ..... 13
Supplementary Material 6: Intertidal community composition second derivative to estimate the effect of subtidal regime shift on intertidal key species abundance. ..... 26
Supplementary Material 7: Intertidal community composition and species specific trends' first derivative to assess a general shift starting in 2005. ..... 40
Supplementary Material 8: Priors used for time series fit ..... 56
Supplementary Material VIII: Potential top-down pressure from the subtidal to the intertidal 61

# Supplementary Material 1: Ordinations (PCoA) Figures

## Subtidal community composition

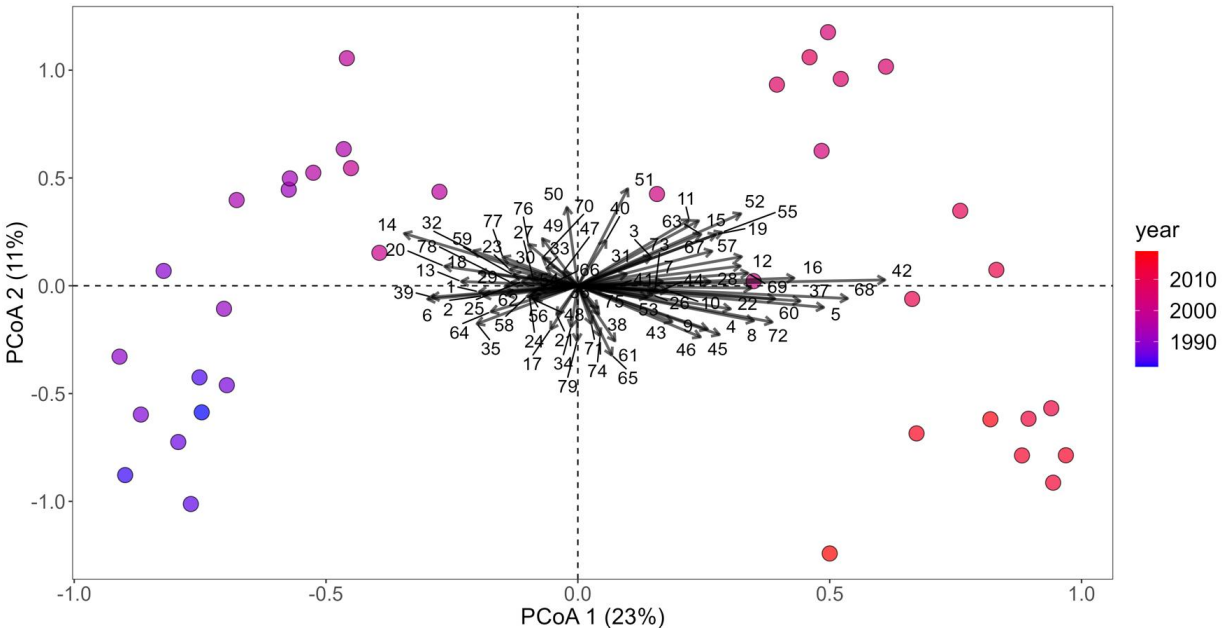


**Figure SM1**: Ordination of the subtidal consumer community. The data are from the bottom trawl surveys from the National Oceanic and Atmospheric Administration (NOAA) in 100 km around Appledore Island. Abundances were Hellinger transformed and Euclidean distance was used. Numbers correspond to taxa names defined in Table SM1 (below).

**Table SM1**: List of taxa and numerical ID attributed for subtidal consumers community analysis.

| Taxa | Numerical ID | Taxa | Numerical ID |
|---|---|---|---|
| amblyraja_radiata | 1 | malacoraja_senta | 41 |
| anarhichas_lupus | 2 | maurolicus_weitzmani | 42 |
| | | melanogrammus_aeglefinus | 43 |
| aspidophoroides_monopterygius | 4 | melanostigma_atlanticum | 44 |
| bathypolypus_arcticus | 5 | merluccius_bilinearis | 45 |

| | | | |
|---|---|---|---|
| brosme_brosme | 6 | myctophidae | 46 |
| chionoecetes_opilio | 7 | myoxocephalus_octodecemspinosus | 47 |
| chlorophthalmus_agassizi | 8 | myxine_glutinosa | 48 |
| citharichthys_arctifrons | 9 | octopoda | 49 |
| clupea_harengus | 10 | pandalus_borealis | 50 |
| crangon_septemspinosa | 11 | pandalus_montagui | 51 |
| crustacea_shrimp | 12 | pandalus_propinquus | 52 |
| cryptacanthodes_maculatus | 13 | paralepidae | 53 |
| cyclopterus_lumpus | 14 | paralichthys_oblongus | 54 |
| dichelopandalus_leptocerus | 15 | pasiphaea_multidentata | 55 |
| dipturus_laevis | 16 | peprilus_triacanthus | 56 |
| enchelyopus_cimbrius | 17 | petromyzon_marinus | 57 |
| gadus_morhua | 18 | placopecten_magellanicus | 58 |
| gasterosteus_aculeatus | 19 | pollachius_virens | 59 |
| geryon_quinquedens | 20 | pontophilus_norvegicus | 60 |
| glyptocephalus_cynoglossus | 21 | prionotus_carolinus | 61 |
| helicolenus_dactylopterus | 22 | pseudopleuronectes_americanus | 62 |
| hemitripterus_americanus | 23 | reinhardtius_hippoglossoides | 63 |
| hippoglossoides_platessoides | 24 | scomber_scombrus | 64 |
| hippoglossus_hippoglossus | 25 | scomberesox_saurus | 65 |
| homarus_americanus | 26 | scophthalmus_aquosus | 66 |
| illex_illecebrosus | 27 | sebastes_fasciatus | 67 |
| lebbeus_polaris | 28 | sepiolidae | 68 |
| leucoraja_erinacea | 29 | spirontocaris_liljeborgii | 69 |
| leucoraja_ocellata | 30 | squalus_acanthias | 70 |
| limanda_ferruginea | 31 | stenotomus_chrysops | 71 |
| lithodes_maja | 32 | stoloteuthis_leucoptera | 72 |

| | | | |
|---|---|---|---|
| loligo_pealeii | 33 | tautogolabrus_adspersus | 73 |
| lophius_americanus | 34 | triglops_murrayi | 74 |
| lumpenus_lumpretaeformis | 35 | sum_alosa | 75 |
| lumpenus_maculatus | 36 | sum_ammodytes | 76 |
| lycenchelys_verrilli | 37 | sum_argentina | 77 |
| macrouridae | 38 | sum_cancer | 78 |
| macrozoarces_americanus | 39 | sum_urophycis | 79 |
| majidae | 40 | | |

## Intertidal sessile organism community composition

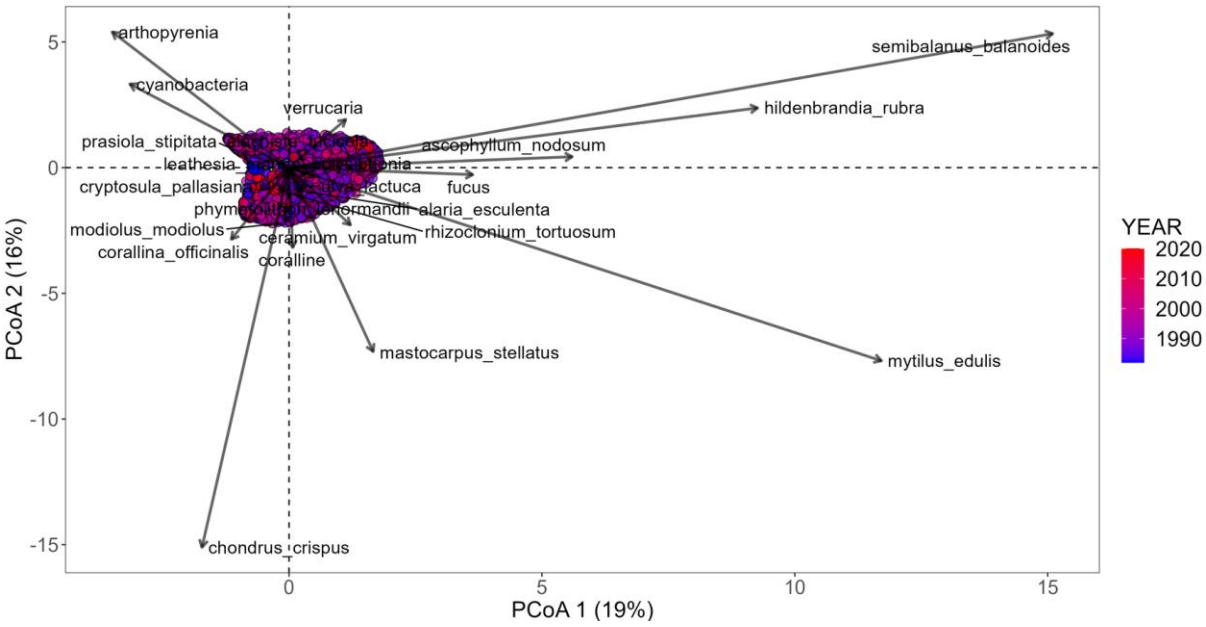


**Figure SM2**: Ordination of the intertidal sessile organism community. Abundances were Hellinger transformed and Euclidean distance was used. Each quadrats for each timepoint was plotted individually.

# Intertidal mobile organism community

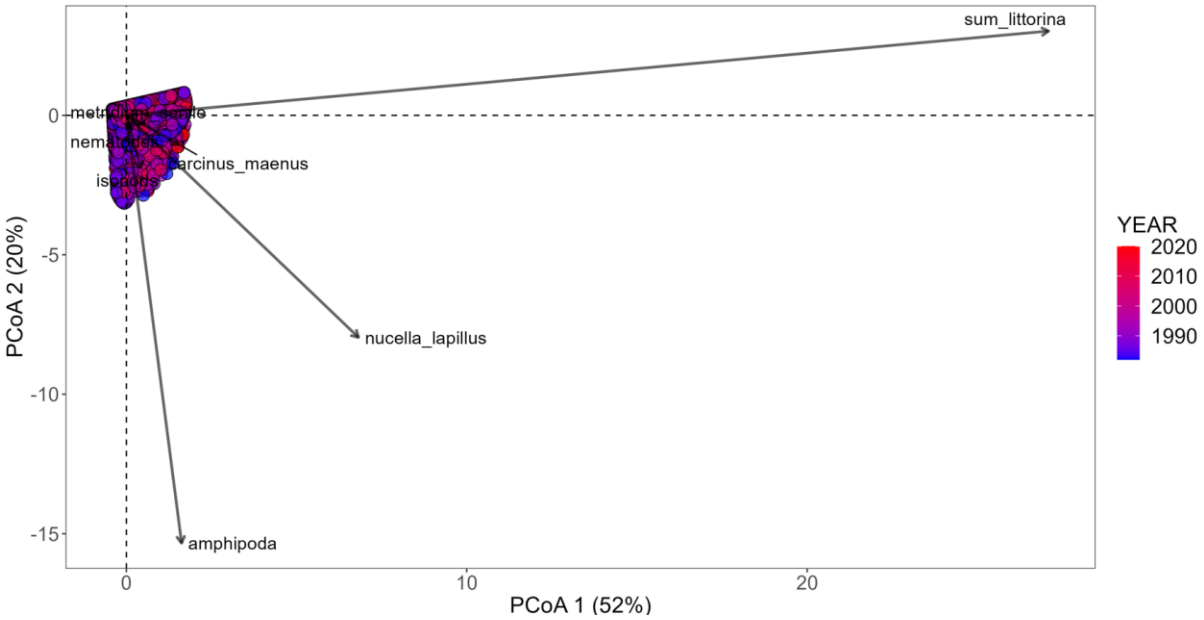


**Figure SM3**: Ordination of the intertidal sessile organism community. Abundances were Hellinger transformed and Euclidean distance was used. Each quadrats for each timepoint was plotted individually.

# Supplementary Material 2: Subtidal changes in community: first derivative.

For **SM4 to SM91** the shaded areas around the trend lines represents the 95% credible interval of the second derivative, and the red shaded area represents the time of each regime shift.

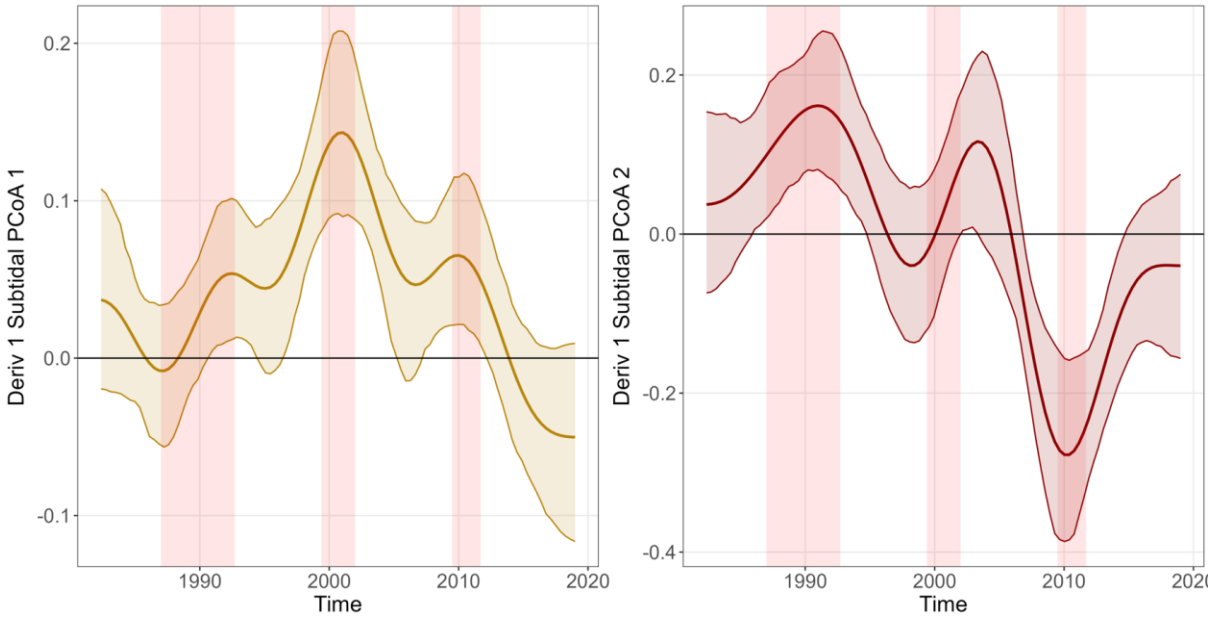


**Figure SM4**. First derivative of the temporal trend in subtidal consumers community composition. The first derivative was calculated by forward difference with 1000 draws. The shaded area represents the 95% credible interval of the first derivative, and the red shaded area represents the time of each regime shift.

# Supplementary Material 3: Subtidal regime shifts when using only species detected in the near shore subtidal

To assess if the near shore subtidal likely changed at the same time as the larger subtidal communities described by the NOAA data, we identified regime shifts but we selected only the subtidal species also detected in the near shore subtidal between 2014 and 2018. Subtidal regime shifts were then identified the exact same way as with the full subtidal community and the results were quite similar, although the second regime shift was moved from 2000 to 2005. However the credible interval was very large, going from 1992 to 2018.

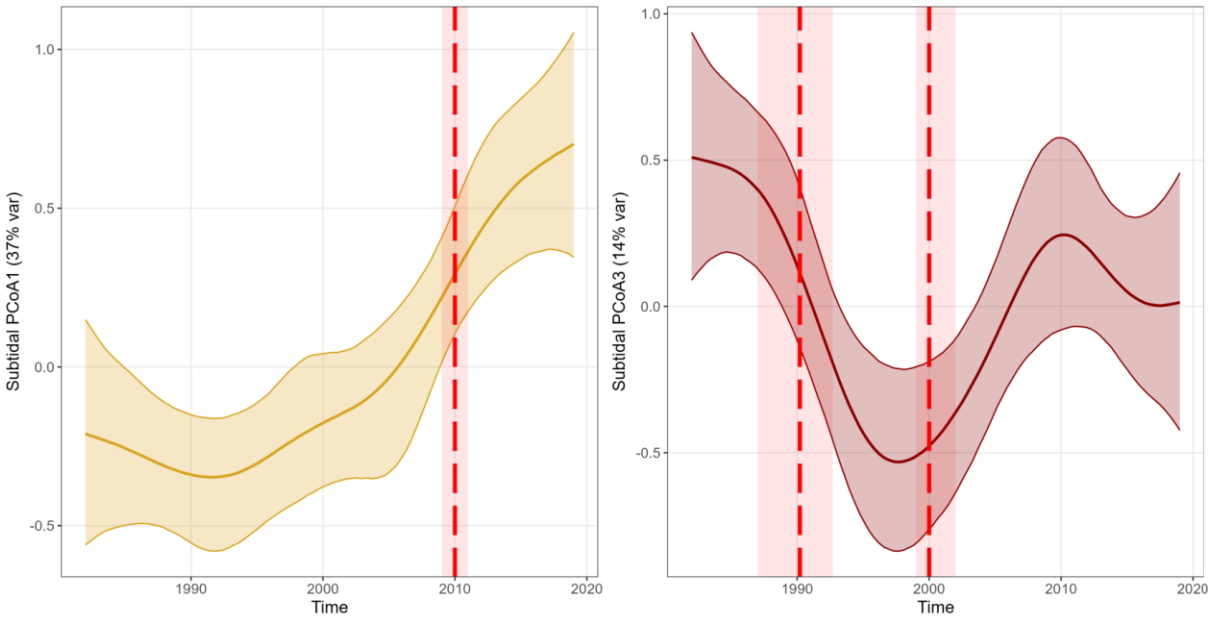


**Figure SM5.** Changes in the subtidal predator community through time when using only the species detected in the near shore subtidal surveys. In a) the first ordination axis, and in b) the third ordination axis. The shaded area represents the 95% credible interval of the centered posterior predicted trends (without the intercept). The red dashed lines represent the moments where the rate of change was particularly fast (regime shifts) and the red shaded area around this line represents its 95% credible interval. These regime shifts are those calculated using the whole subtidal NOAA data.

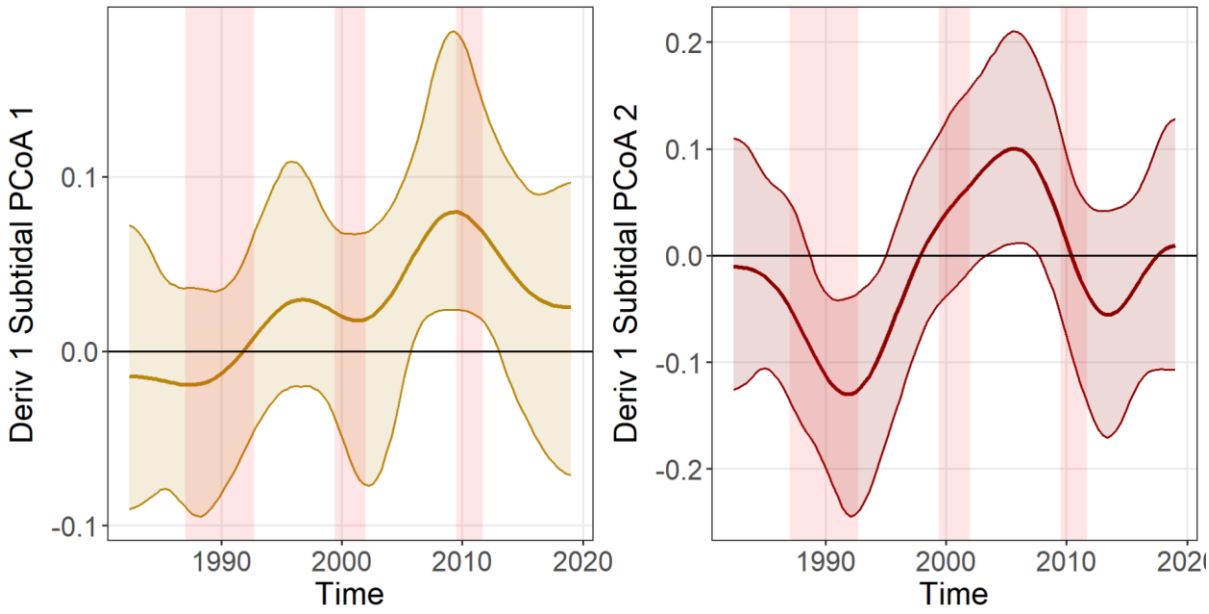


**Figure SM6**. First derivative of the temporal trend in subtidal consumers community composition when using only the species detected in the near shore subtidal surveys. The first derivative was calculated by forward difference with 1000 draws. The shaded area represents the 95% credible interval of the first derivative, and the red shaded area represents the time of each regime shift.These regime shifts are those calculated using the whole subtidal NOAA data.

# Supplementary Material 4: Site specific temporal trends in intertidal community composition

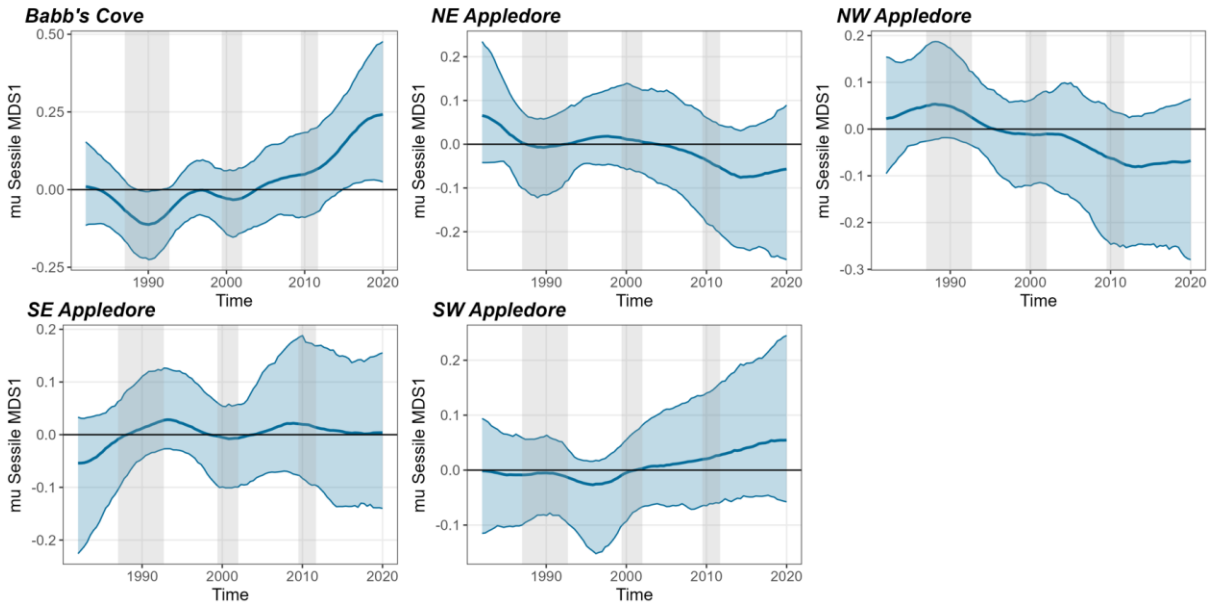


**Figure SM5**. Temporal trend in sessile organism community at the site scale for the first ordination axis. The blue shaded area represents the 95% credible interval of the second derivative, and the red shaded area represents the time of each regime shift. The grey and red shaded areas represent the time of each subtidal regime shift. A red shaded area means that the second derivative is different from zero at that site for that specific regime shift. A grey shaded area means that the second derivative overlaps with zero at that site for that specific regime shift.

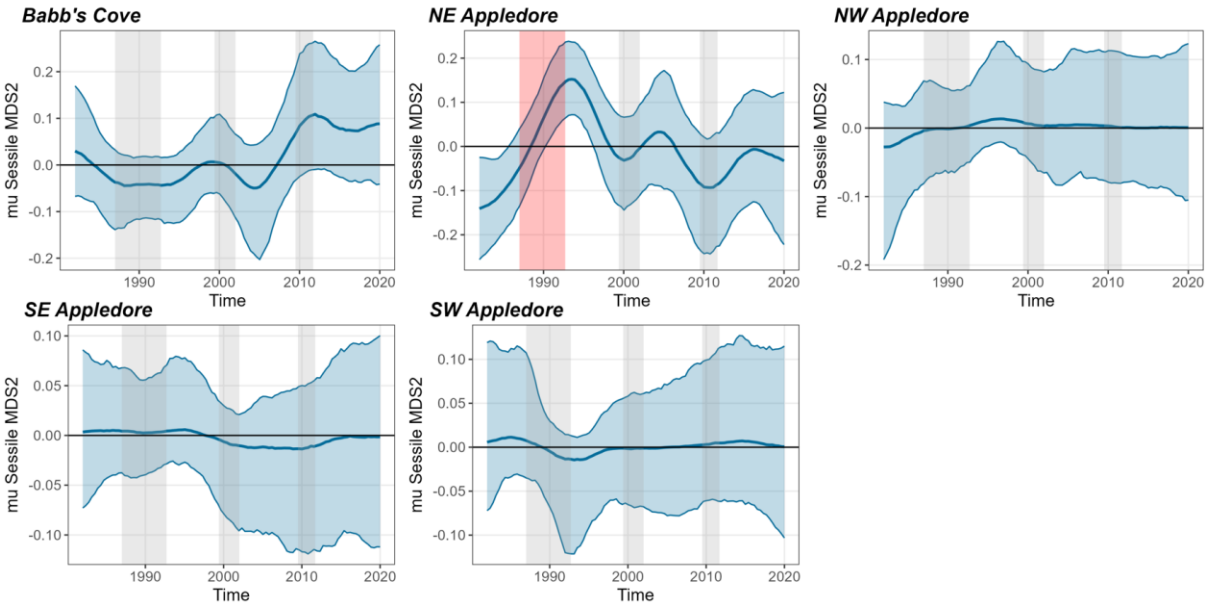


**Figure SM6**. Temporal trend in sessile organism community at the site scale for the second ordination axis. The blue shaded area represents the 95% credible interval of the second derivative, and the red shaded area represents the time of each regime shift. The grey and red shaded areas represent the time of each subtidal regime shift. A red shaded area means that the second derivative is different from zero at that site for that specific regime shift. A grey shaded area means that the second derivative overlaps with zero at that site for that specific regime shift.

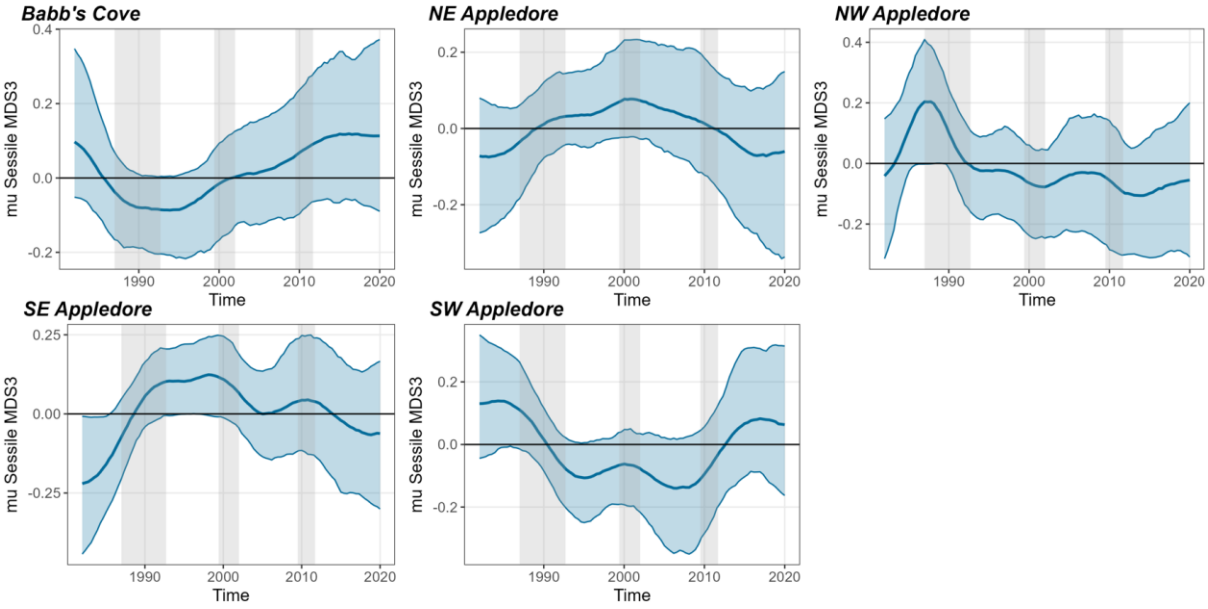


**Figure SM7**. Temporal trend in sessile organism community at the site scale for the third ordination axis. The second derivative was calculated by central difference with 1000 draws. The blue shaded area represents the 95% credible interval of the second derivative, and the red shaded area represents the time of each regime shift. The grey and red shaded areas represent the time of each subtidal regime shift. A red shaded area means that the second

derivative is different from zero at that site for that specific regime shift. A grey shaded area means that the second derivative overlaps with zero at that site for that specific regime shift.

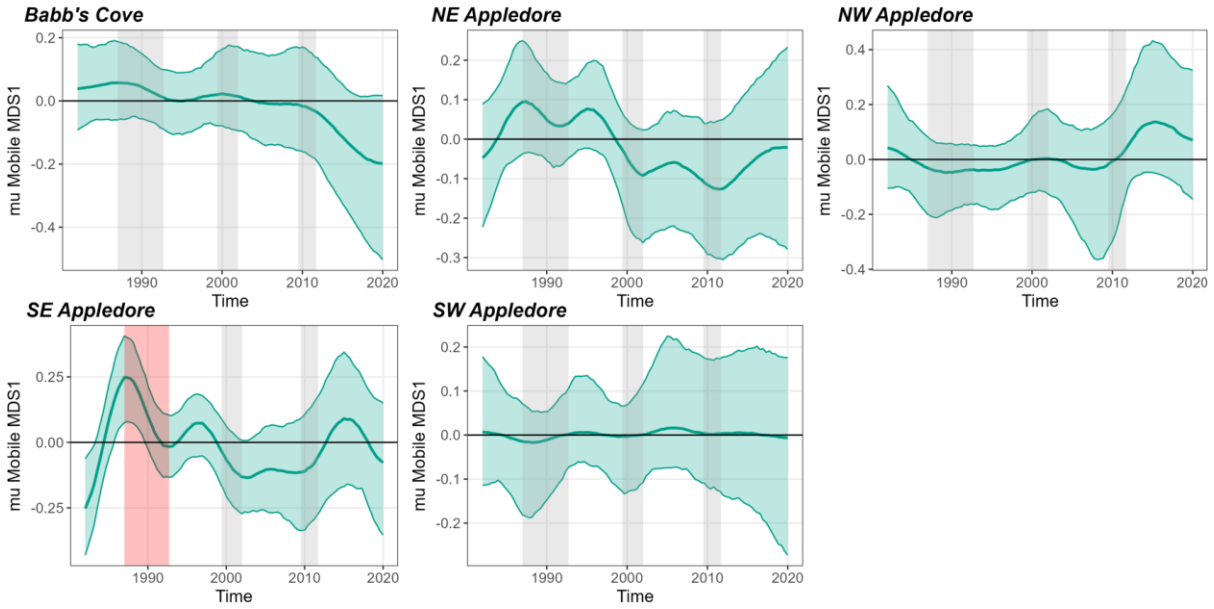


**Figure SM8**. Temporal trend in mobile organism community at the site scale for the first ordination axis. The second derivative was calculated by central difference with 1000 draws. The blue shaded area represents the 95% credible interval of the second derivative, and the red shaded area represents the time of each regime shift. The grey and red shaded areas represent the time of each subtidal regime shift. A red shaded area means that the second derivative is different from zero at that site for that specific regime shift. A grey shaded area means that the second derivative overlaps with zero at that site for that specific regime shift.

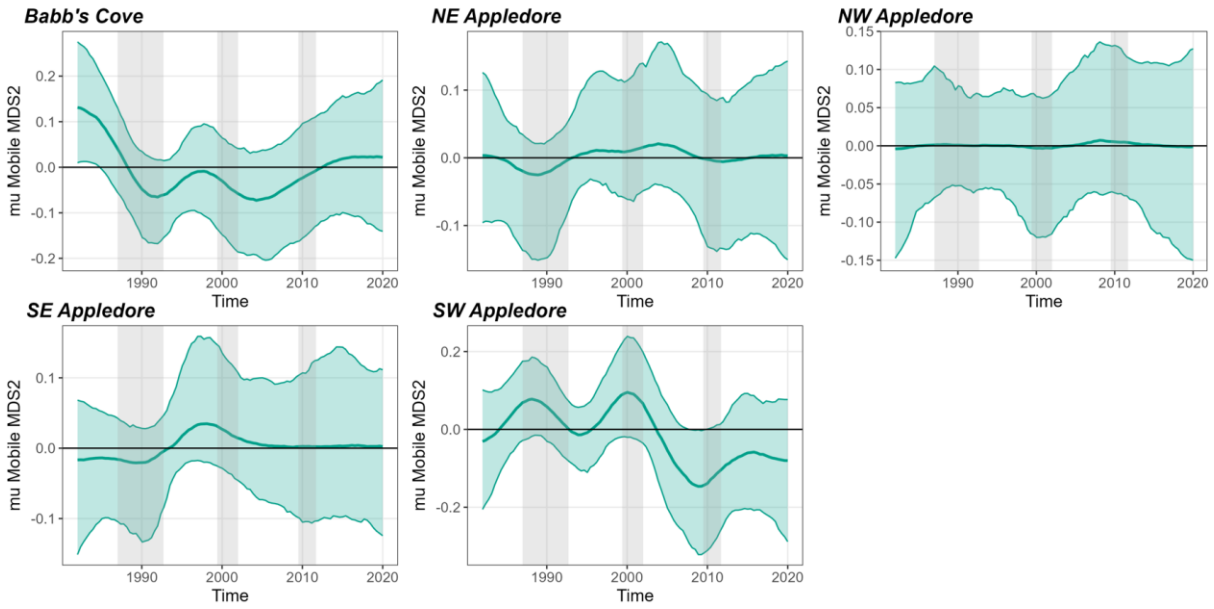


**Figure SM9**. Temporal trend in mobile organism community at the site scale for the second ordination axis. The second derivative was calculated by central difference with 1000 draws. The blue shaded area represents the 95% credible interval of the second derivative, and the

red shaded area represents the time of each regime shift. The grey and red shaded areas represent the time of each subtidal regime shift. A red shaded area means that the second derivative is different from zero at that site for that specific regime shift. A grey shaded area means that the second derivative overlaps with zero at that site for that specific regime shift.

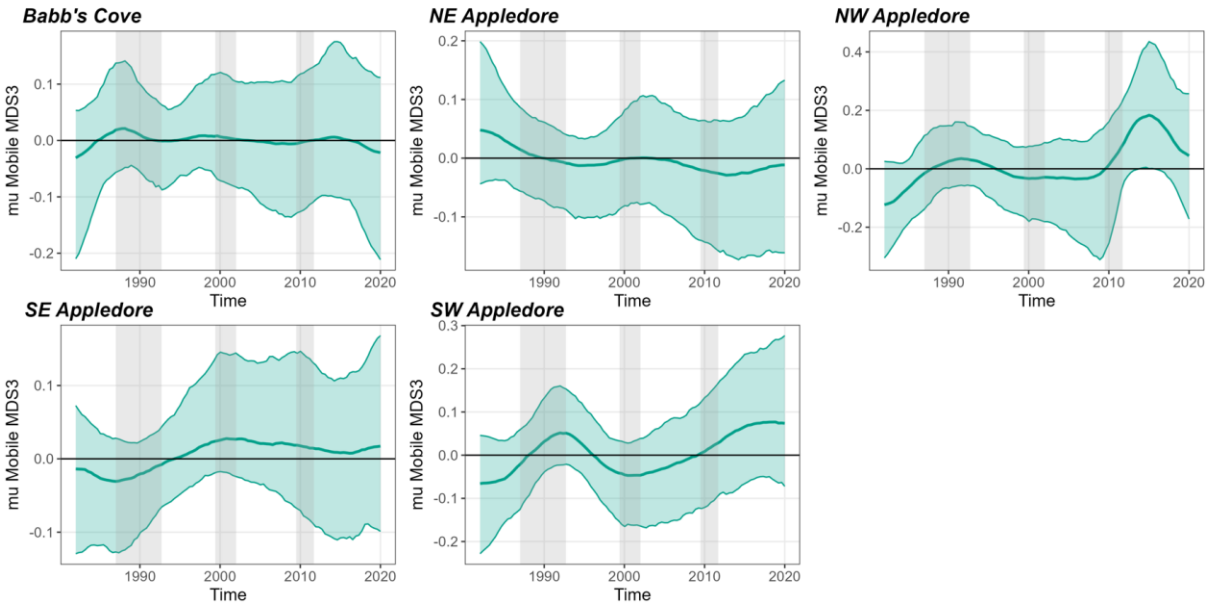


**Figure SM10**. Temporal trend in mobile organism community at the site scale for the third ordination axis. The second derivative was calculated by central difference with 1000 draws. The blue shaded area represents the 95% credible interval of the second derivative, and the red shaded area represents the time of each regime shift. The grey and red shaded areas represent the time of each subtidal regime shift. A red shaded area means that the second derivative is different from zero at that site for that specific regime shift. A grey shaded area means that the second derivative overlaps with zero at that site for that specific regime shift.

# Supplementary Material 5: Focal species temporal trends.

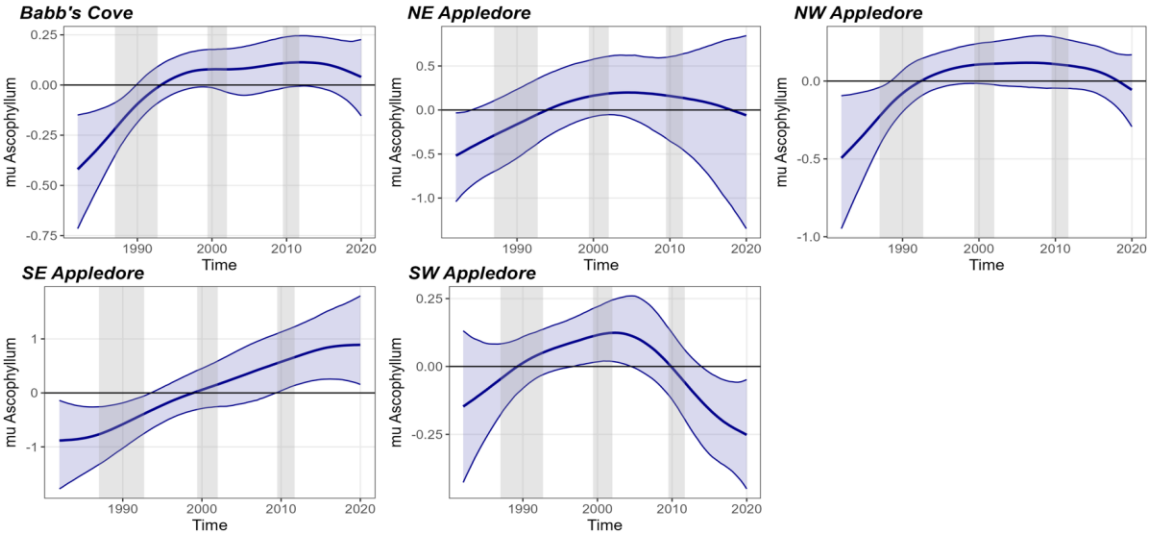


**Figure SM11.** Temporal trends in *Ascophyllum* abundance. This is the centered marginal prediction of the time effect for each site. The blue shaded area represents the 95% credible intervals. The grey and red shaded areas represent the time of each subtidal regime shift. A red shaded area means that the second derivative is different from zero at that site for that specific regime shift. A grey shaded area means that the second derivative overlaps with zero at that site for that specific regime shift.

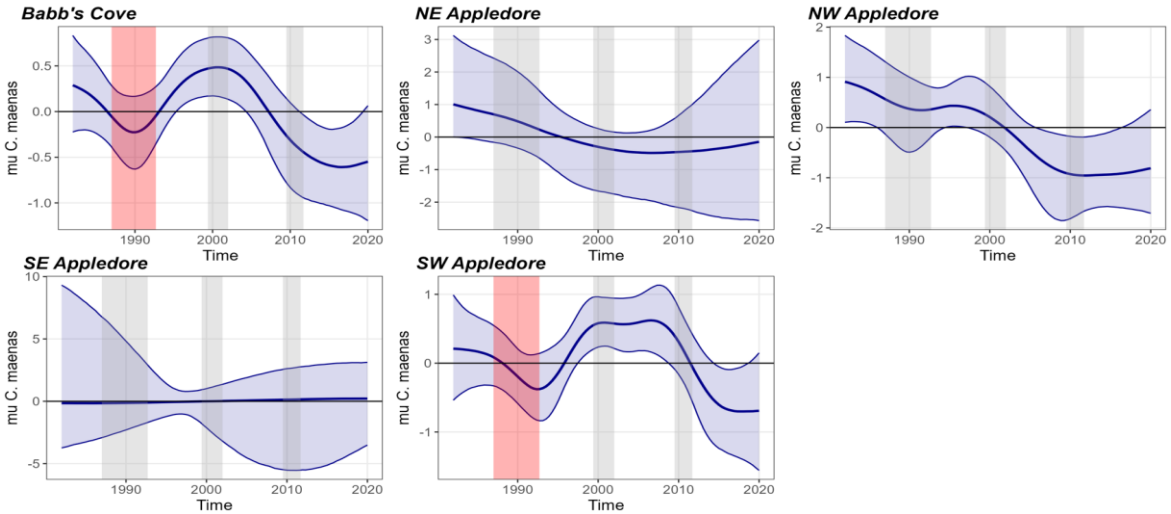


**Figure SM12.** Temporal trends in *C. maenas* abundance. This is the centered marginal prediction of the time effect for each site. The blue shaded area represents the 95% credible intervals. The grey and red shaded areas represent the time of each subtidal regime shift. A red shaded area means that the second derivative is different from zero at that site for that

specific regime shift. A grey shaded area means that the second derivative overlaps with zero at that site for that specific regime shift.

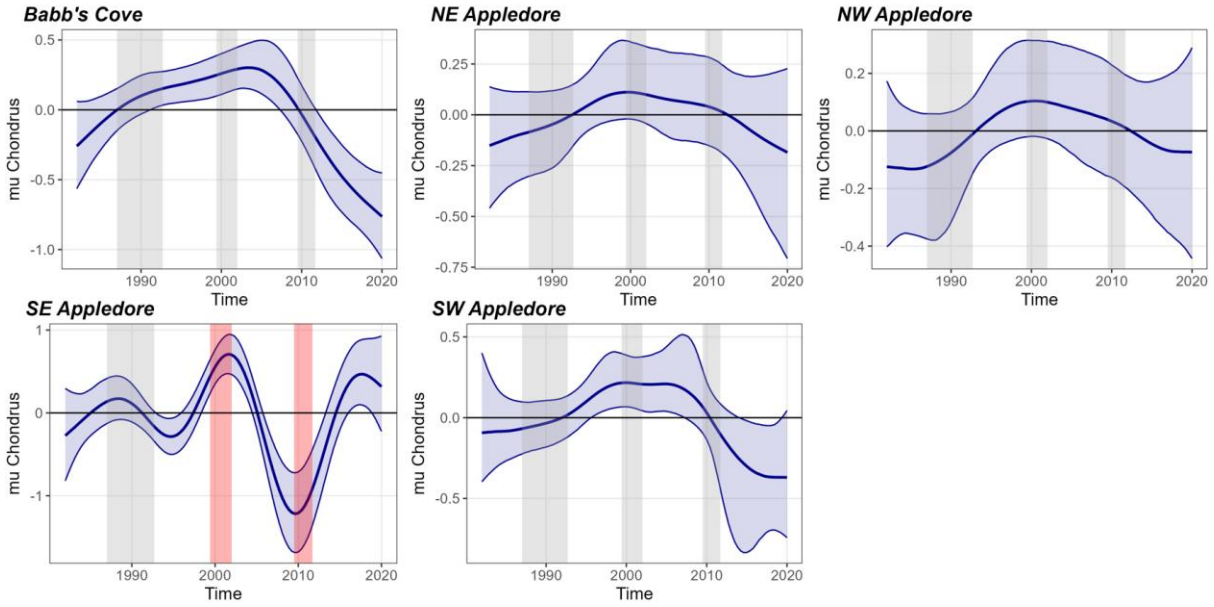


**Figure SM13.** Temporal trends in *Chondrus* abundance. This is the centered marginal prediction of the time effect for each site. The blue shaded area represents the 95% credible intervals. The grey and red shaded areas represent the time of each subtidal regime shift. A red shaded area means that the second derivative is different from zero at that site for that specific regime shift. A grey shaded area means that the second derivative overlaps with zero at that site for that specific regime shift.

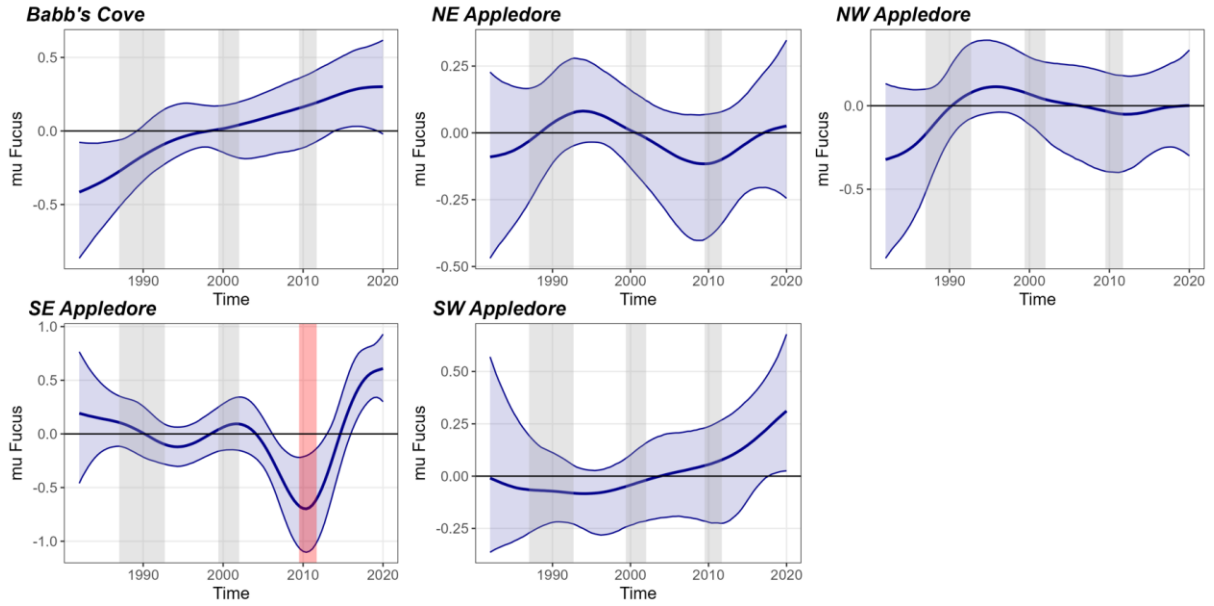


**Figure SM14.** Temporal trends in *Fucus* abundance. This is the centered marginal prediction of the time effect for each site. The blue shaded area represents the 95% credible intervals. The grey and red shaded areas represent the time of each subtidal regime shift. A

red shaded area means that the second derivative is different from zero at that site for that specific regime shift. A grey shaded area means that the second derivative overlaps with zero at that site for that specific regime shift.

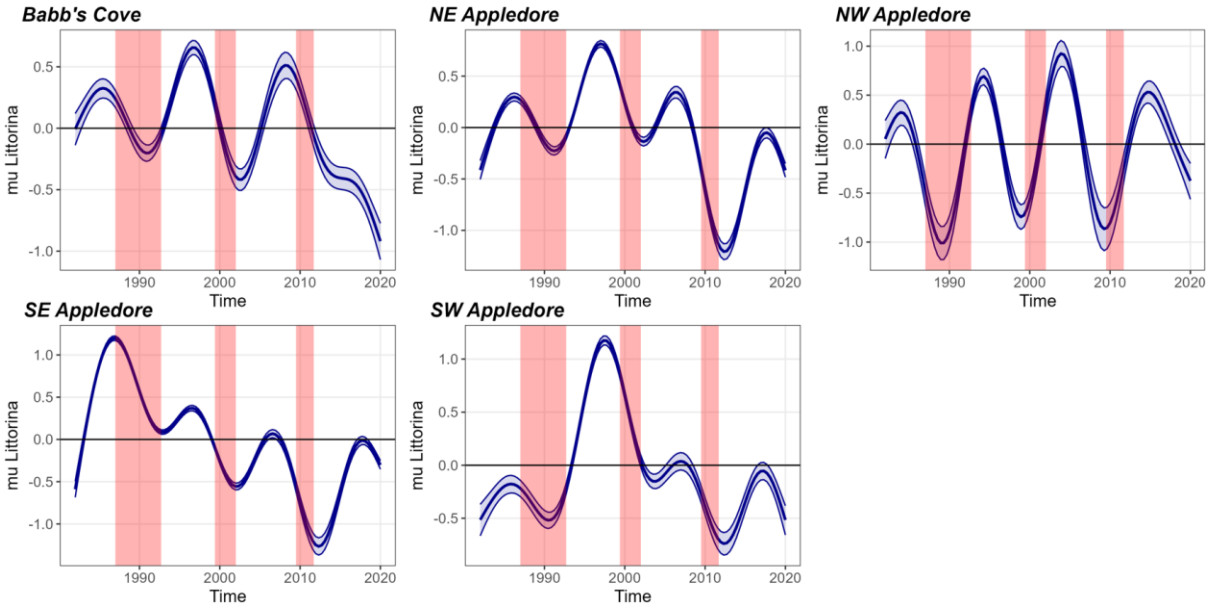


**Figure SM15.** Temporal trends in *Littorina* abundance. This is the centered marginal prediction of the time effect for each site. The blue shaded area represents the 95% credible intervals. The grey and red shaded areas represent the time of each subtidal regime shift. A red shaded area means that the second derivative is different from zero at that site for that specific regime shift. A grey shaded area means that the second derivative overlaps with zero at that site for that specific regime shift.

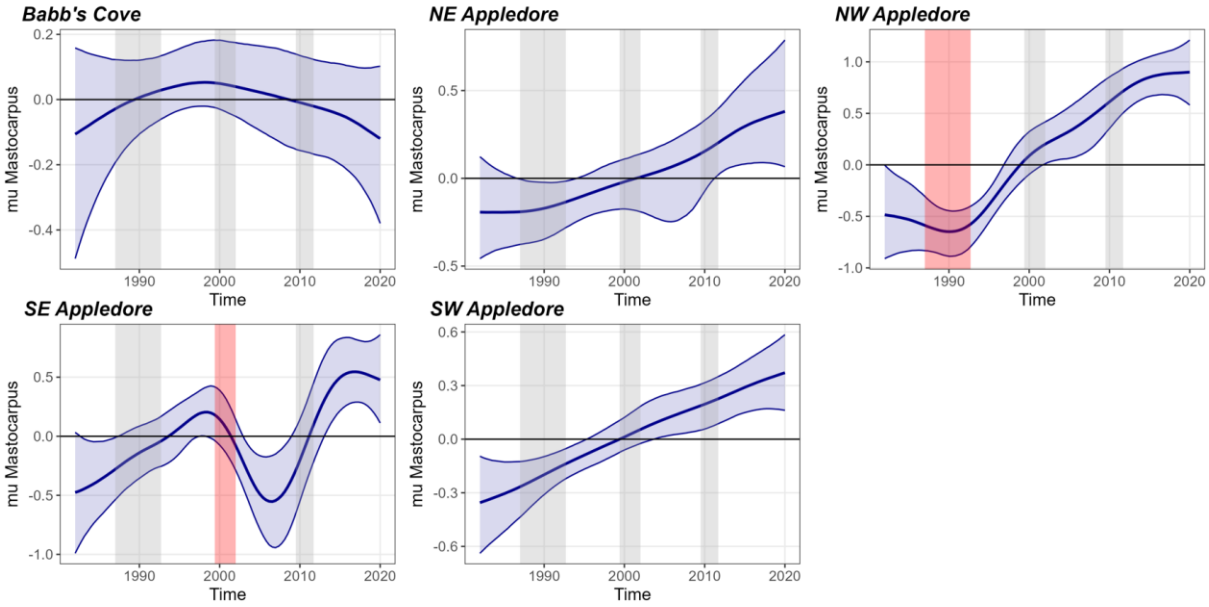


**Figure SM16.** Temporal trends in *Mastocarpus* abundance. This is the centered marginal prediction of the time effect for each site. The blue shaded area represents the 95% credible

intervals. The grey and red shaded areas represent the time of each subtidal regime shift. A red shaded area means that the second derivative is different from zero at that site for that specific regime shift. A grey shaded area means that the second derivative overlaps with zero at that site for that specific regime shift.

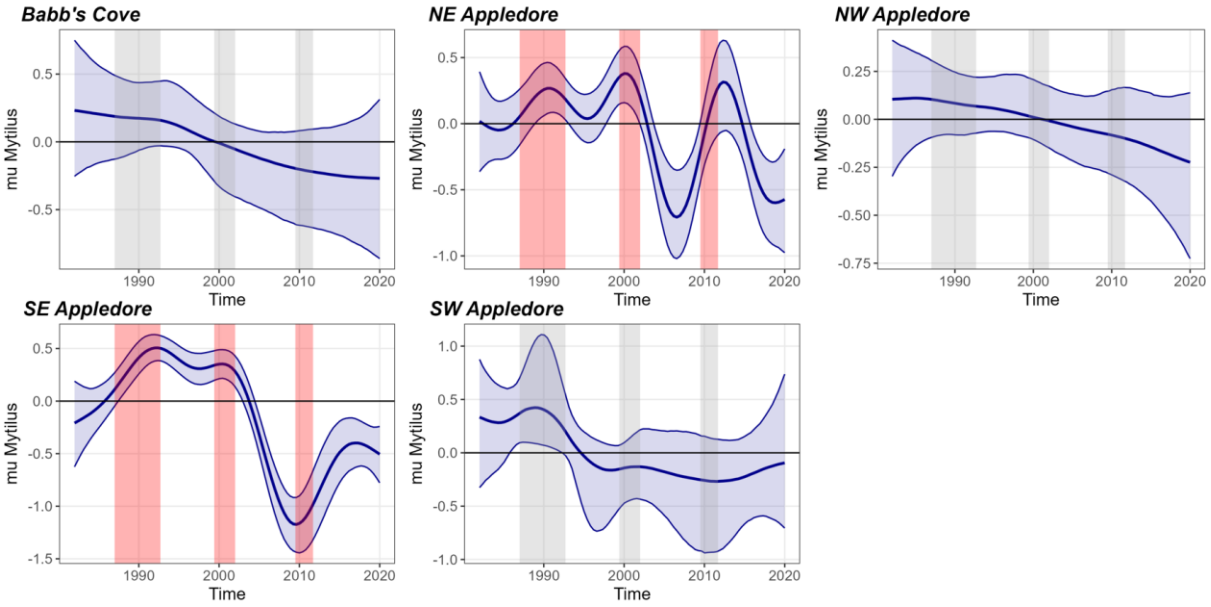


**Figure SM17.** Temporal trends in *Mytilus* abundance. This is the centered marginal prediction of the time effect for each site. The blue shaded area represents the 95% credible intervals. The grey and red shaded areas represent the time of each subtidal regime shift. A red shaded area means that the second derivative is different from zero at that site for that specific regime shift. A grey shaded area means that the second derivative overlaps with zero at that site for that specific regime shift.

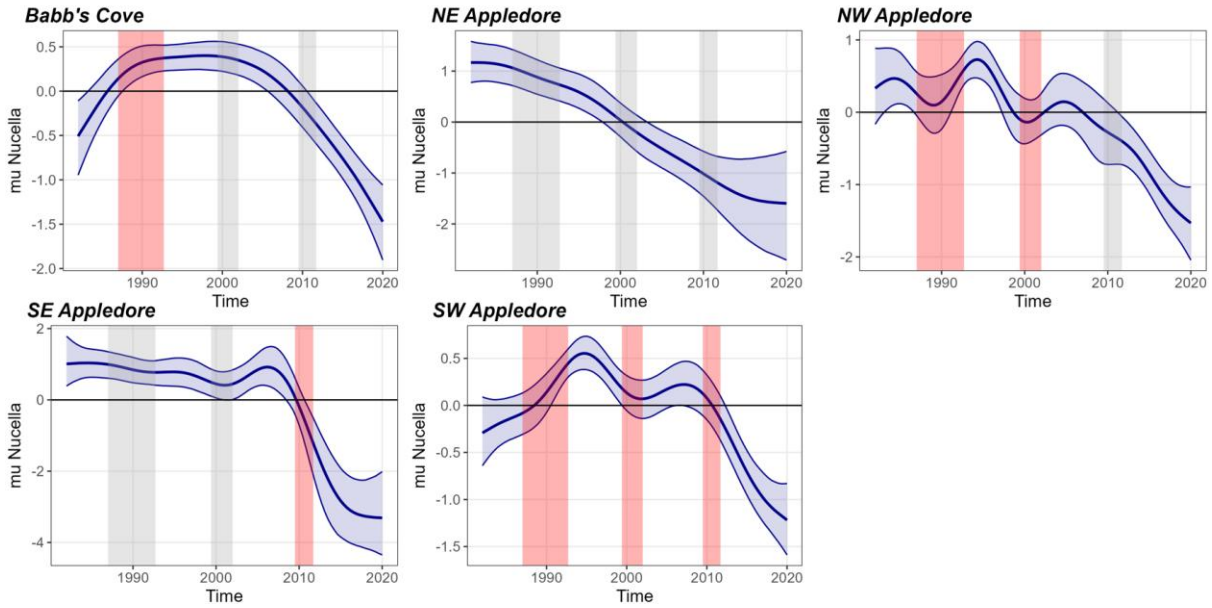


**Figure SM18.** Temporal trends in *Nucella* abundance. This is the centered marginal prediction of the time effect for each site. The blue shaded area represents the 95% credible intervals. The grey and red shaded areas represent the time of each subtidal regime shift. A red shaded area means that the second derivative is different from zero at that site for that specific regime shift. A grey shaded area means that the second derivative overlaps with zero at that site for that specific regime shift.

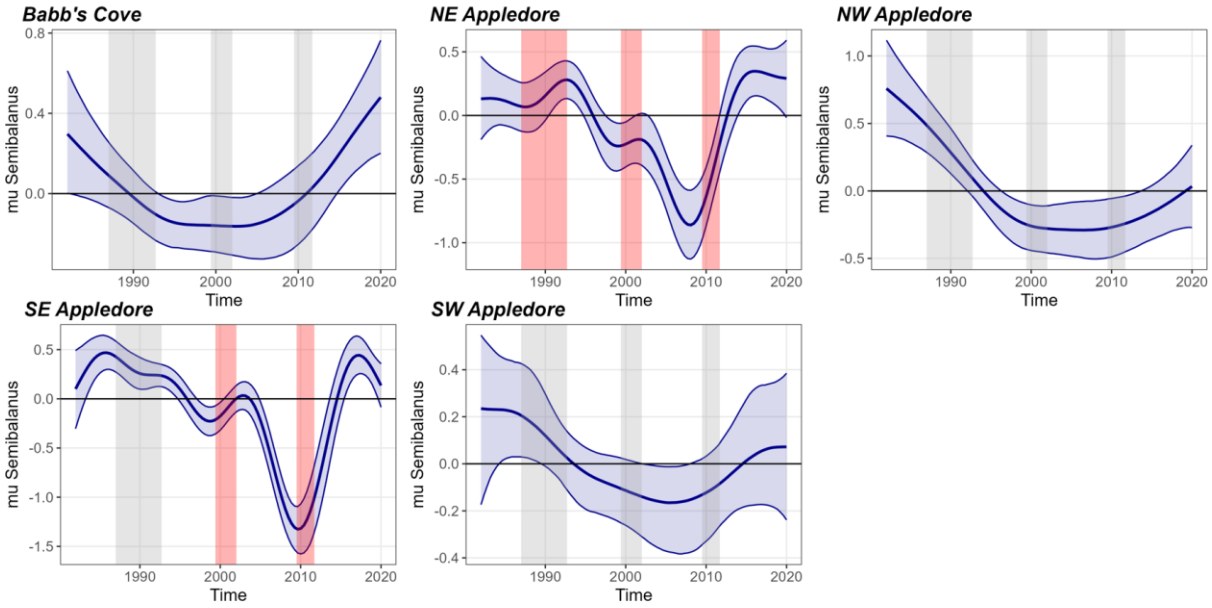


**Figure SM19.** Temporal trends in *Semibalanus* abundance. This is the centered marginal prediction of the time effect for each site. The blue shaded area represents the 95% credible intervals. The grey and red shaded areas represent the time of each subtidal regime shift. A

red shaded area means that the second derivative is different from zero at that site for that specific regime shift. A grey shaded area means that the second derivative overlaps with zero at that site for that specific regime shift.

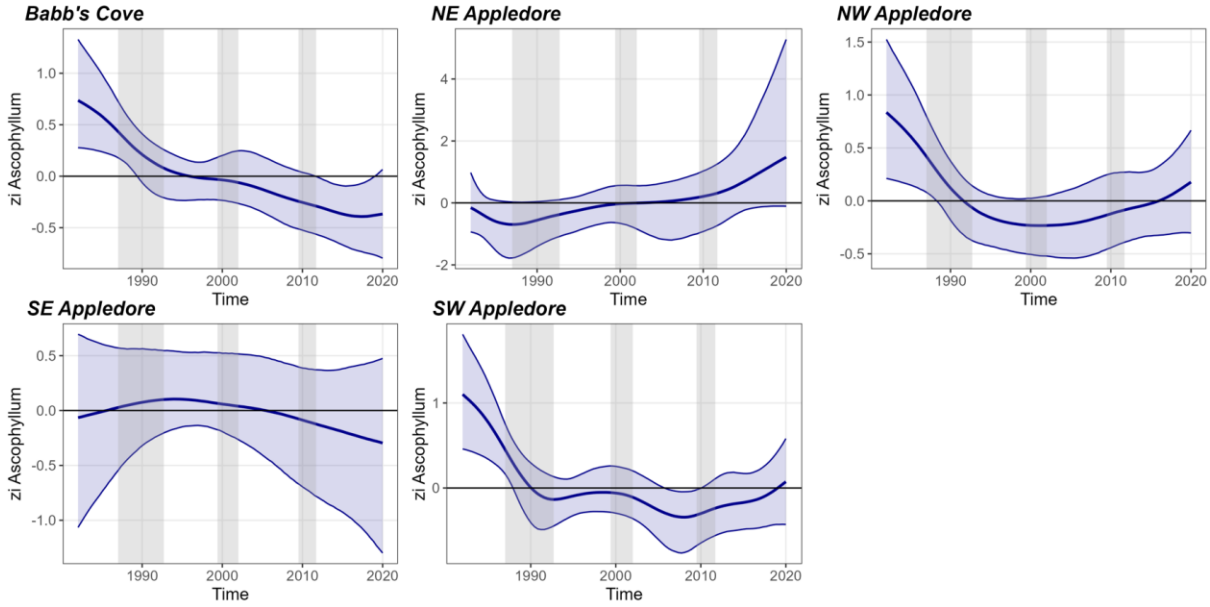


**Figure SM20.** Temporal trends in *Ascophyllum* abundance. This is the centered marginal prediction of the time effect for each site. The blue shaded area represents the 95% credible intervals. The grey and red shaded areas represent the time of each subtidal regime shift. A red shaded area means that the second derivative is different from zero at that site for that specific regime shift. A grey shaded area means that the second derivative overlaps with zero at that site for that specific regime shift.

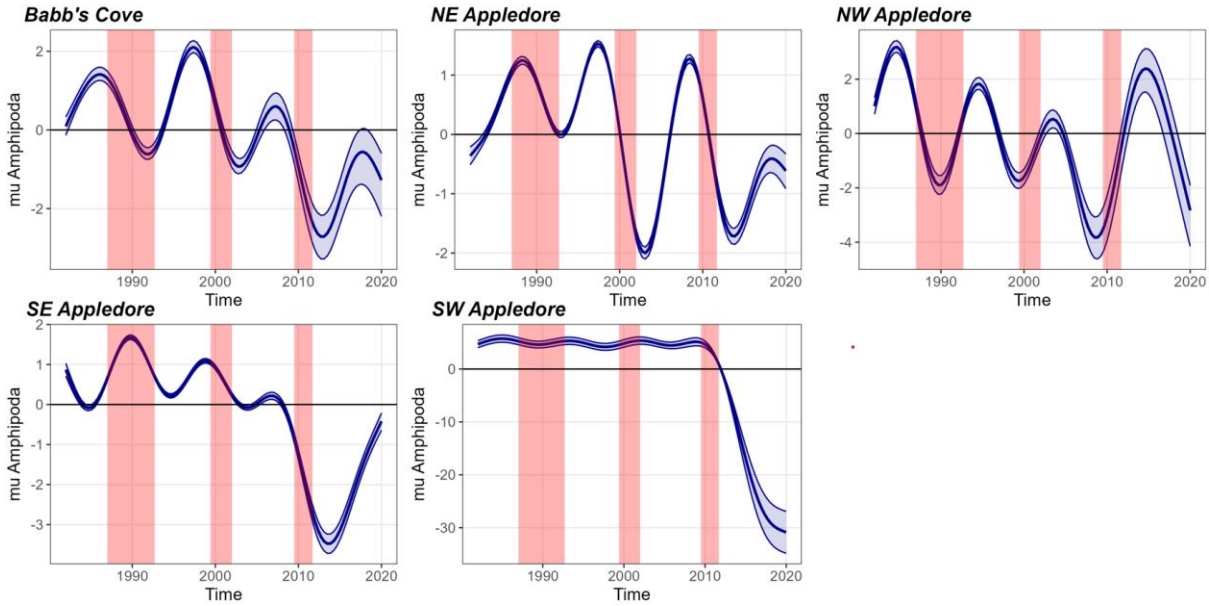


**Figure SM21.** Temporal trends in *Amphipoda* abundance. This is the centered marginal prediction of the time effect for each site. The blue shaded area represents the 95% credible intervals. The grey and red shaded areas represent the time of each subtidal regime shift. A red shaded area means that the second derivative is different from zero at that site for that specific regime shift. A grey shaded area means that the second derivative overlaps with zero at that site for that specific regime shift.

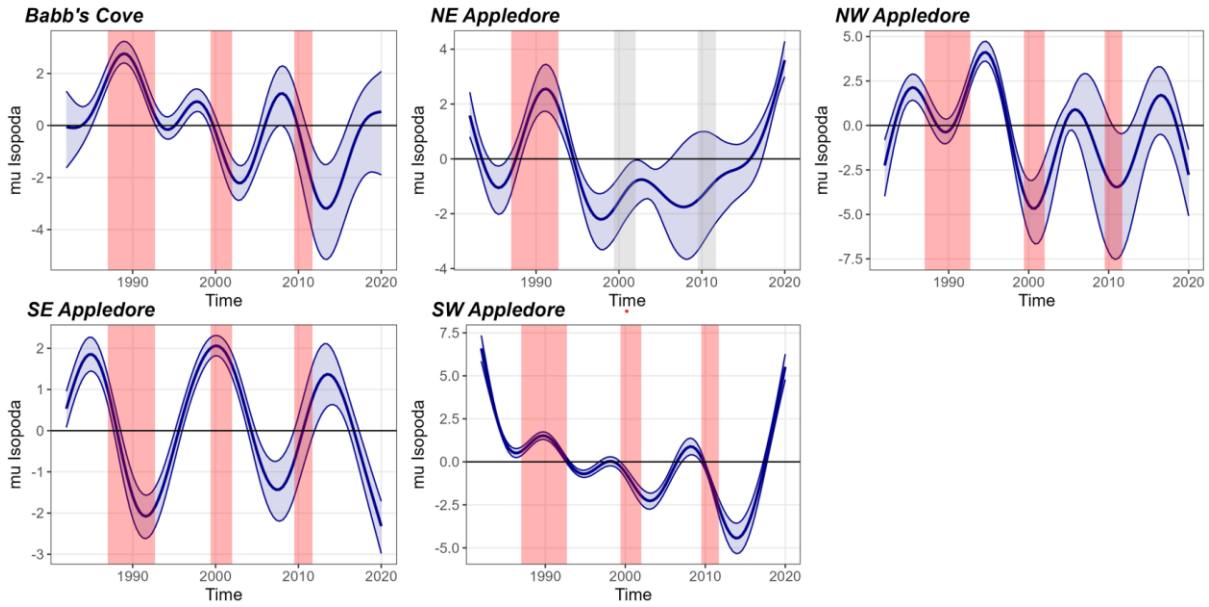


**Figure SM22.** Temporal trends in *Isopoda* abundance. This is the centered marginal prediction of the time effect for each site. The blue shaded area represents the 95% credible intervals. The grey and red shaded areas represent the time of each subtidal regime shift. A red shaded area means that the second derivative is different from zero at that site for that specific regime shift. A grey shaded area means that the second derivative overlaps with zero at that site for that specific regime shift.

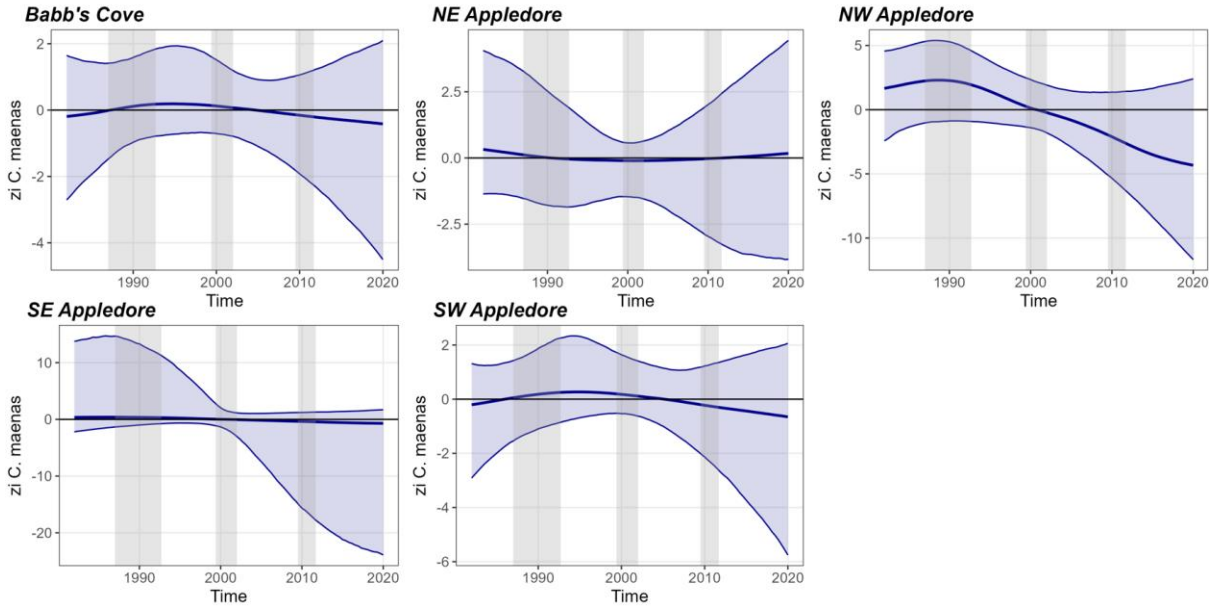


**Figure SM23.** Temporal trends in *C. maenas* presence. The presence is given by the zero inflated part of the model. This is the centered marginal prediction of the time effect for each site. The blue shaded area represents the 95% credible intervals. The grey and red shaded areas represent the time of each subtidal regime shift. A red shaded area means that the second derivative is different from zero at that site for that specific regime shift. A grey shaded area means that the second derivative overlaps with zero at that site for that specific regime shift.

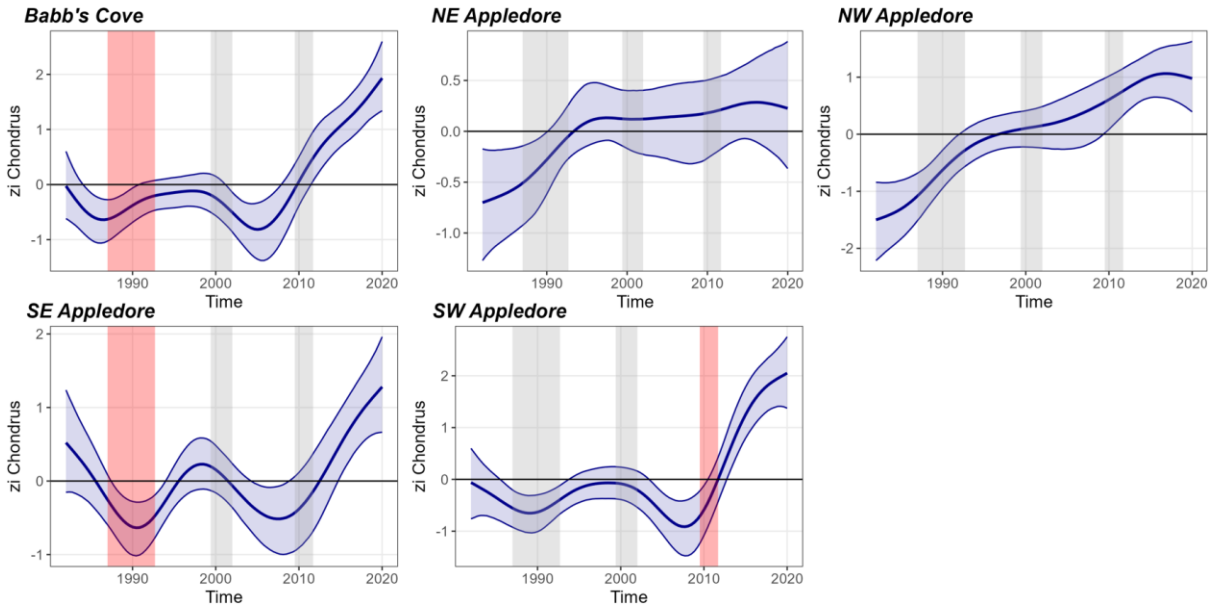


**Figure SM24.** Temporal trends in *Chondrus* presence. The presence is given by the zero inflated part of the model. This is the centered marginal prediction of the time effect for each site. The blue shaded area represents the 95% credible intervals. The grey and red shaded areas represent the time of each subtidal regime shift. A red shaded area means that the second derivative is different from zero at that site for that specific regime shift. A grey

shaded area means that the second derivative overlaps with zero at that site for that specific regime shift.

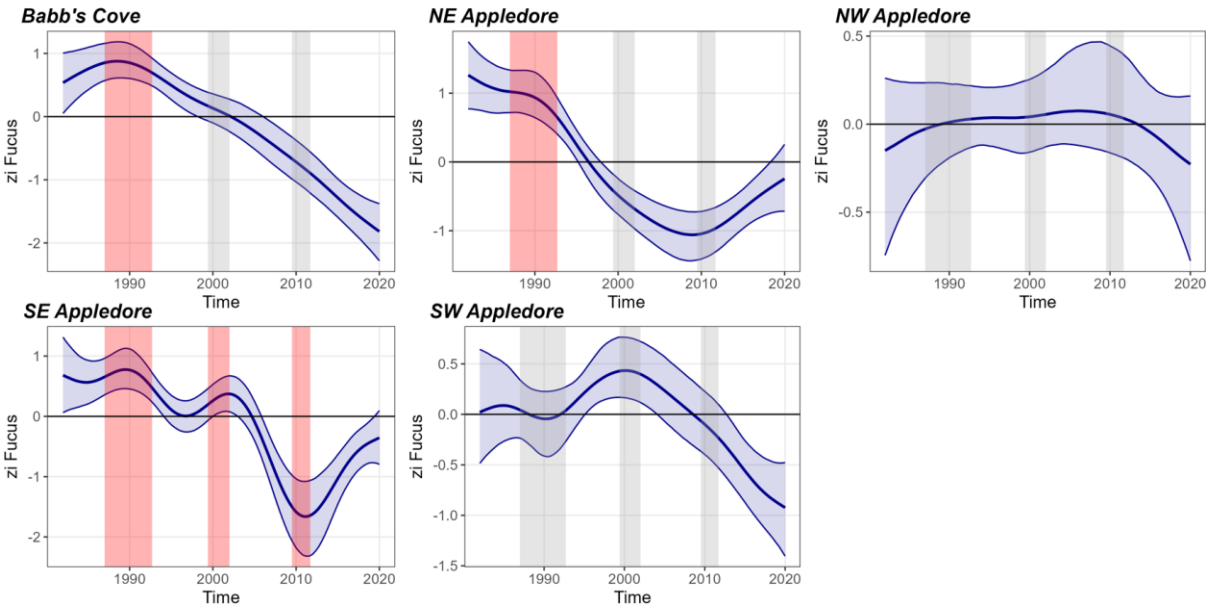


**Figure SM25.** Temporal trends in *Fucus* presence. The presence is given by the zero inflated part of the model. This is the centered marginal prediction of the time effect for each site. The blue shaded area represents the 95% credible intervals. The grey and red shaded areas represent the time of each subtidal regime shift. A red shaded area means that the second derivative is different from zero at that site for that specific regime shift. A grey shaded area means that the second derivative overlaps with zero at that site for that specific regime shift.

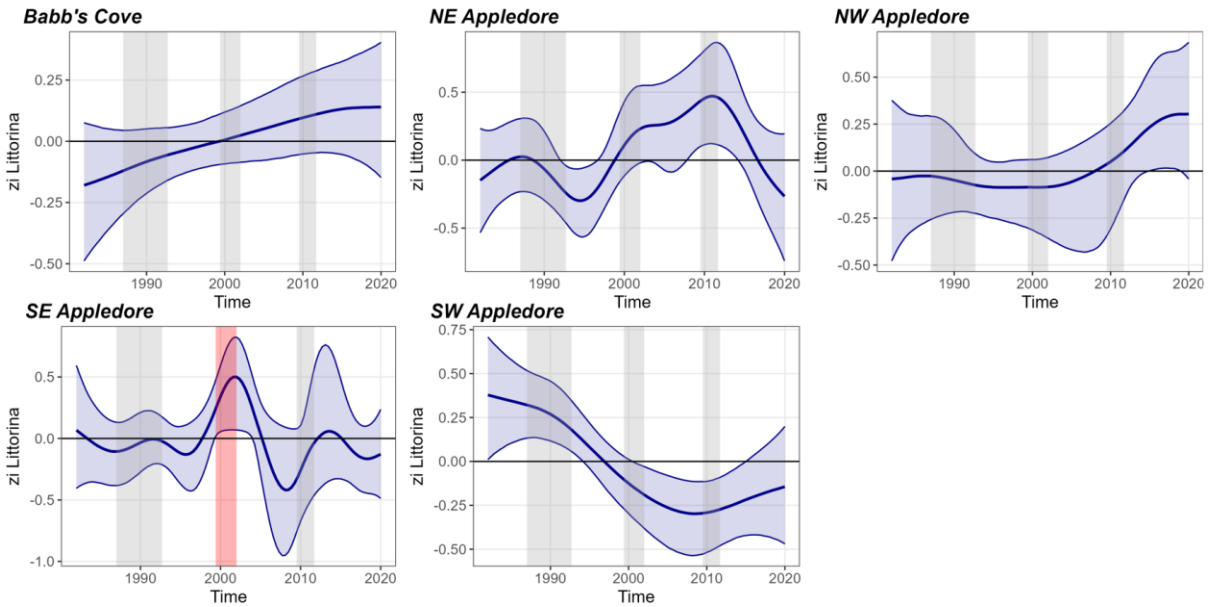


**Figure SM26.** Temporal trends in *Littorina* presence. The presence is given by the zero inflated part of the model. This is the centered marginal prediction of the time effect for each site. The blue shaded area represents the 95% credible intervals. The grey and red shaded

areas represent the time of each subtidal regime shift. A red shaded area means that the second derivative is different from zero at that site for that specific regime shift. A grey shaded area means that the second derivative overlaps with zero at that site for that specific regime shift.

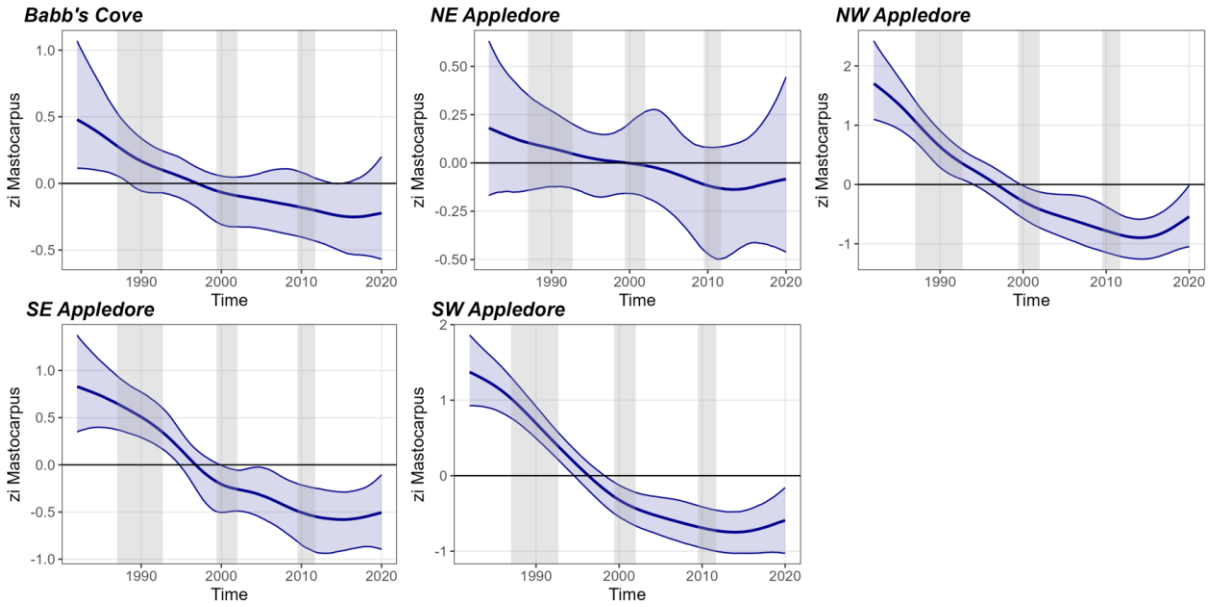


**Figure SM27.** Temporal trends in *Mastocarpus* presence. The presence is given by the zero inflated part of the model. This is the centered marginal prediction of the time effect for each site. The blue shaded area represents the 95% credible intervals. The grey and red shaded areas represent the time of each subtidal regime shift. A red shaded area means that the second derivative is different from zero at that site for that specific regime shift. A grey shaded area means that the second derivative overlaps with zero at that site for that specific regime shift.

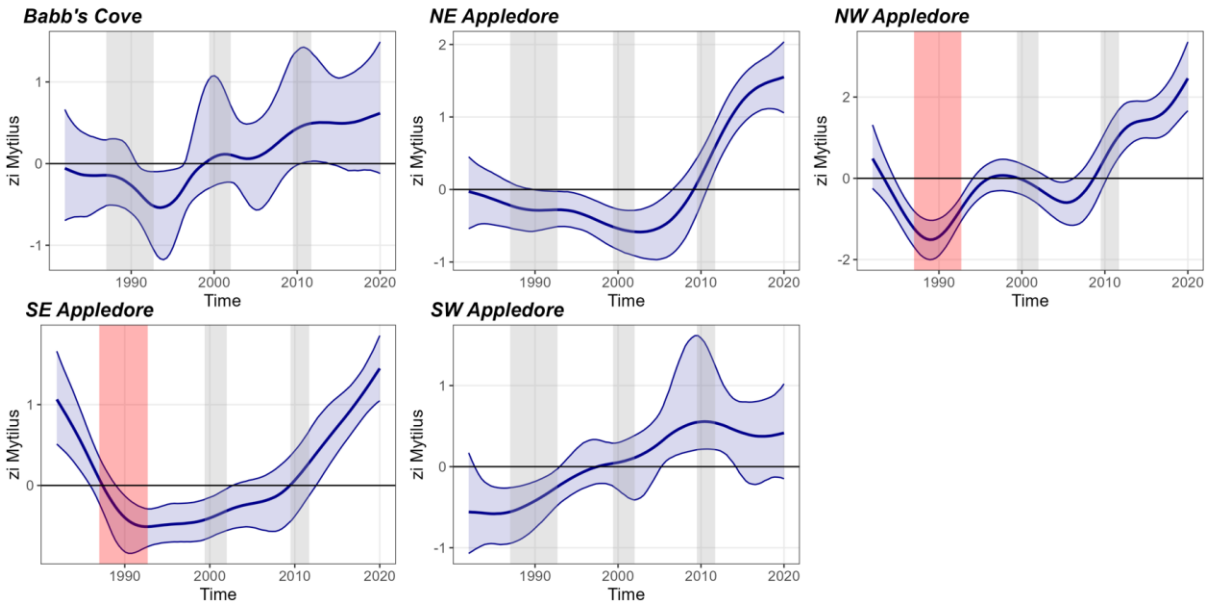

**Figure SM28** Temporal trends in *Mytilus* presence. The presence is given by the zero inflated part of the model. This is the centered marginal prediction of the time effect for each site. The blue shaded area represents the 95% credible intervals. The grey and red shaded areas represent the time of each subtidal regime shift. A red shaded area means that the second derivative is different from zero at that site for that specific regime shift. A grey shaded area means that the second derivative overlaps with zero at that site for that specific regime shift.

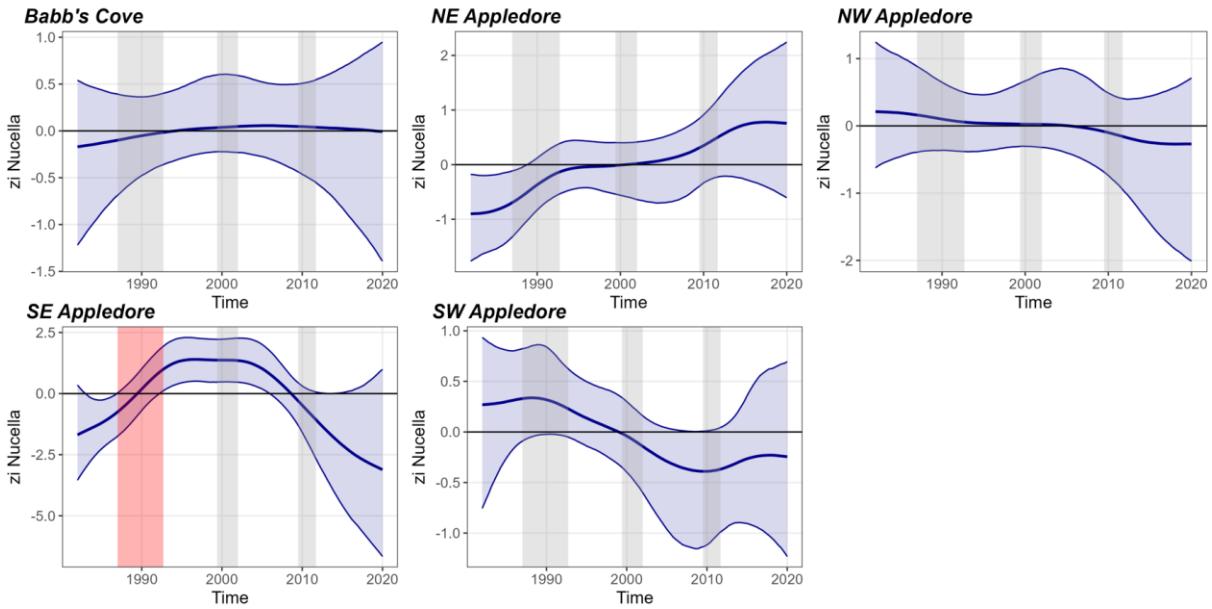


**Figure SM29.** Temporal trends in *Nucella* presence. The presence is given by the zero inflated part of the model. This is the centered marginal prediction of the time effect for each site. The blue shaded area represents the 95% credible intervals. The grey and red shaded areas represent the time of each subtidal regime shift. A red shaded area means that the second derivative is different from zero at that site for that specific regime shift. A grey shaded area means that the second derivative overlaps with zero at that site for that specific regime shift.

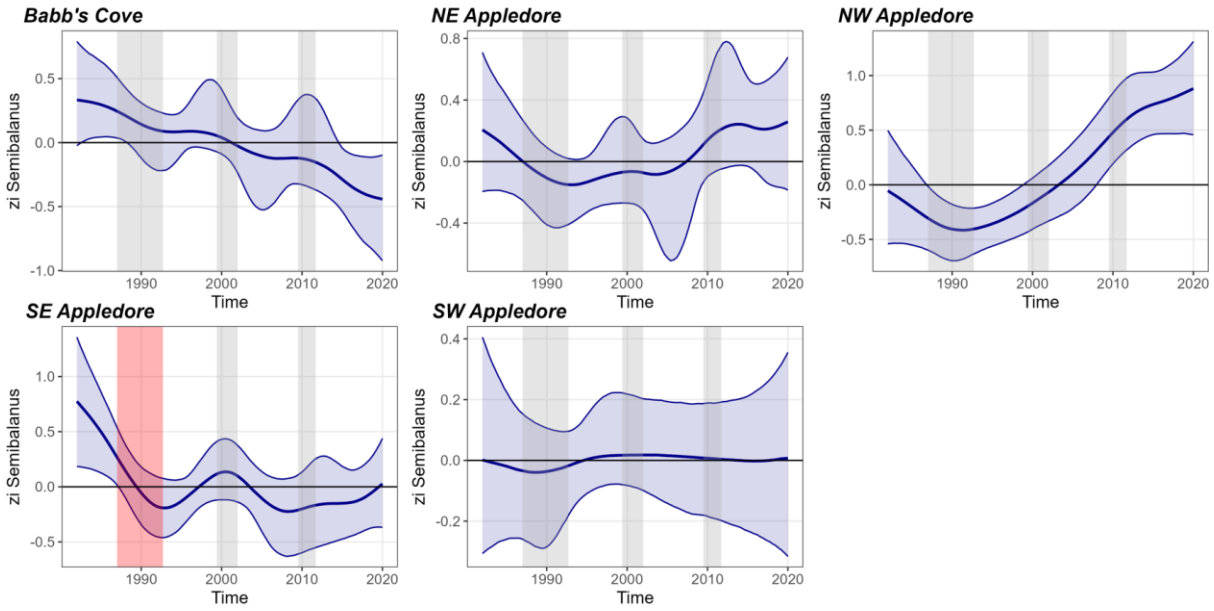


**Figure SM30.** Temporal trends in *Semibalanus* presence. The presence is given by the zero inflated part of the model. This is the centered marginal prediction of the time effect for each site. The blue shaded area represents the 95% credible intervals. The grey and red shaded areas represent the time of each subtidal regime shift. A red shaded area means that the second derivative is different from zero at that site for that specific regime shift. A grey shaded area means that the second derivative overlaps with zero at that site for that specific regime shift.

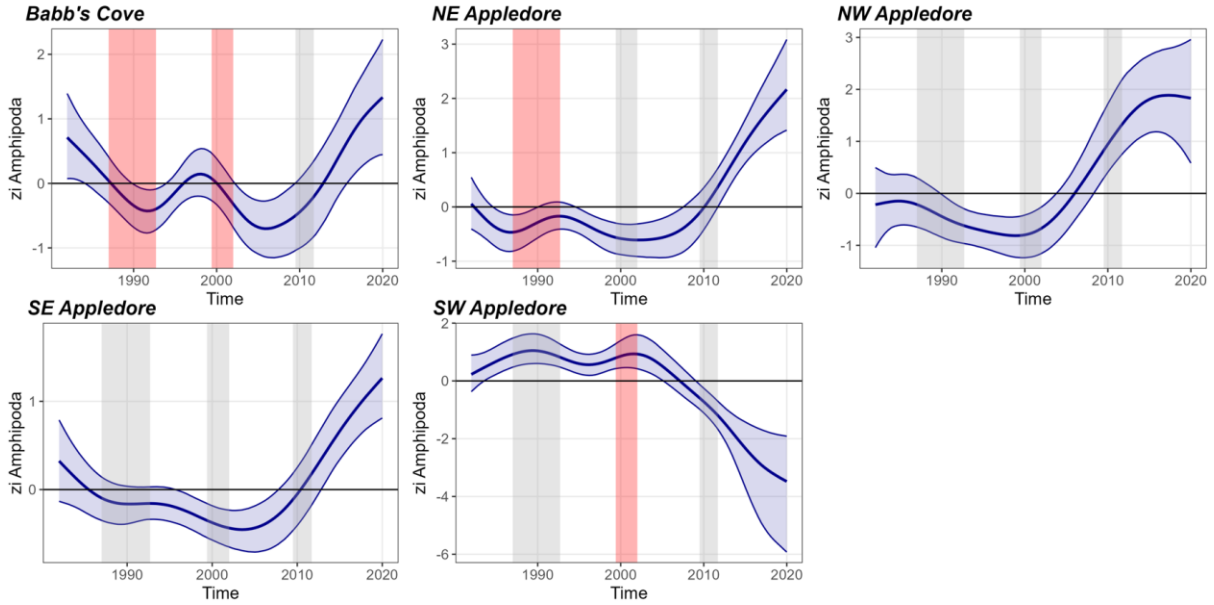


**Figure SM31.** Temporal trends in *Amphipoda* presence. The presence is given by the zero inflated part of the model. This is the centered marginal prediction of the time effect for each site. The blue shaded area represents the 95% credible intervals. The grey and red shaded areas represent the time of each subtidal regime shift. A red shaded area means that the second derivative is different from zero at that site for that specific regime shift. A grey shaded area means that the second derivative overlaps with zero at that site for that specific regime shift.

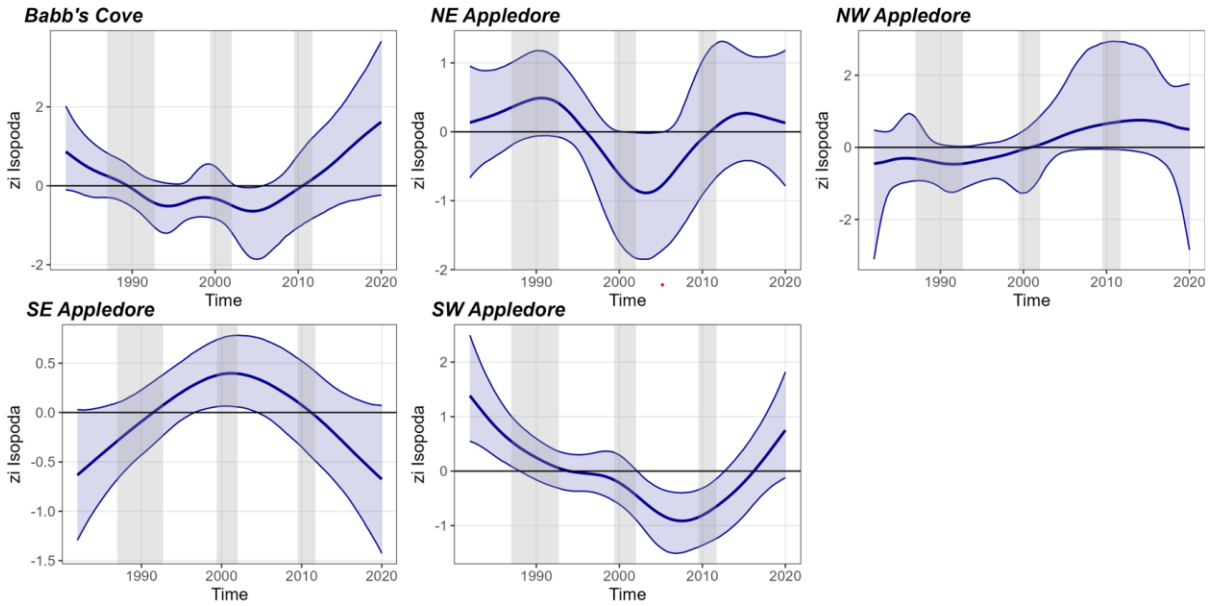


**Figure SM32.** Temporal trends in *Isopoda* presence. The presence is given by the zero inflated part of the model. This is the centered marginal prediction of the time effect for each site. The blue shaded area represents the 95% credible intervals. The grey and red shaded areas represent the time of each subtidal regime shift. A red shaded area means that the second derivative is different from zero at that site for that specific regime shift. A grey shaded area means that the second derivative overlaps with zero at that site for that specific regime shift.

# Supplementary Material 6: Intertidal community composition second derivative to estimate the effect of subtidal regime shift on intertidal key species abundance.

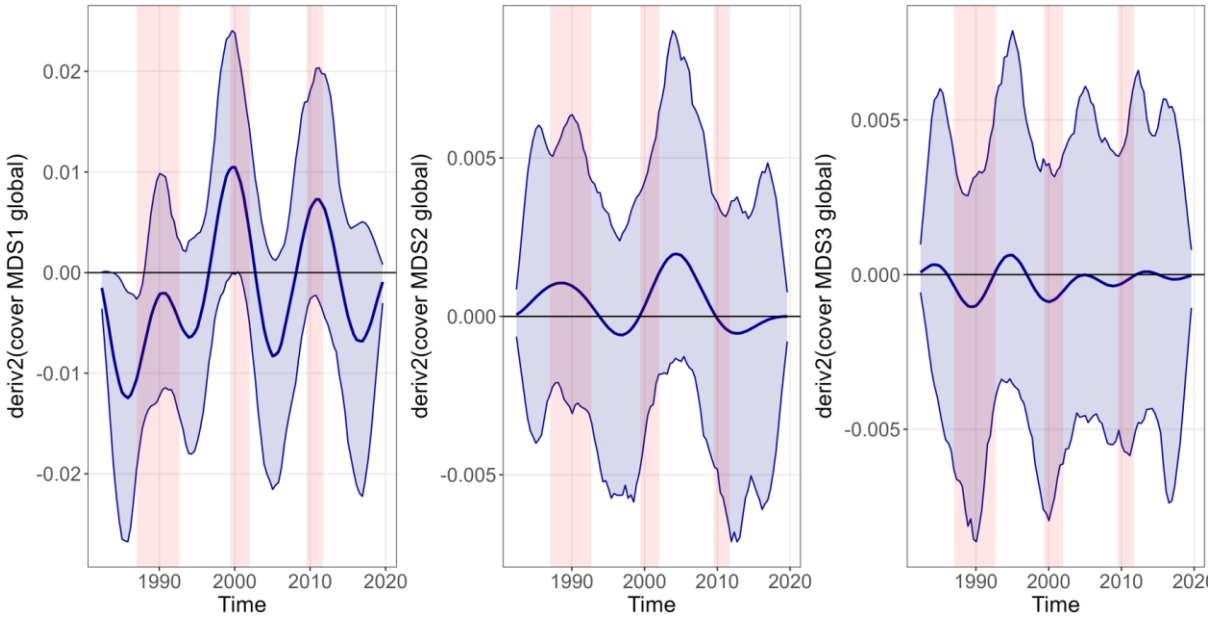


**Figure SM34**. Second derivative of the temporal trend in sessile organism community at the island scale. The second derivative was calculated by central difference with 1000 draws. The blue shaded area represents the 95% credible interval of the second derivative, and the red shaded area represents the time of each regime shift.

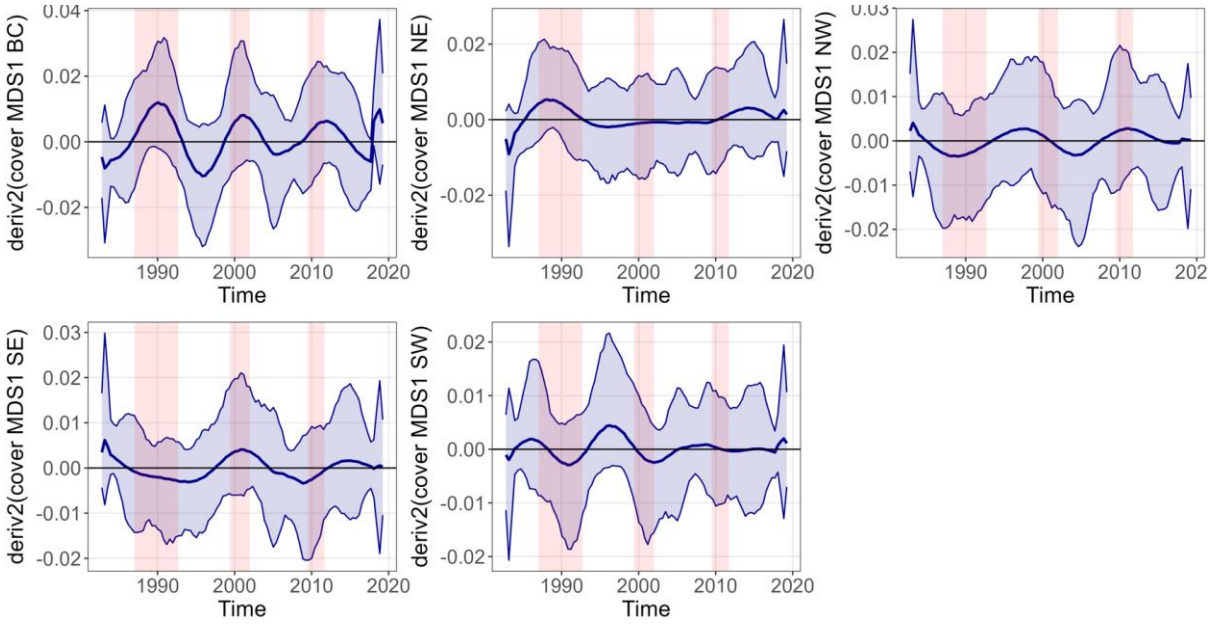

**Figure SM35**. Second derivative of the temporal trend in sessile organism community at the site scale for the first ordination axis. The second derivative was calculated by central difference with 1000 draws. The blue shaded area represents the 95% credible interval of the second derivative, and the red shaded area represents the time of each regime shift.

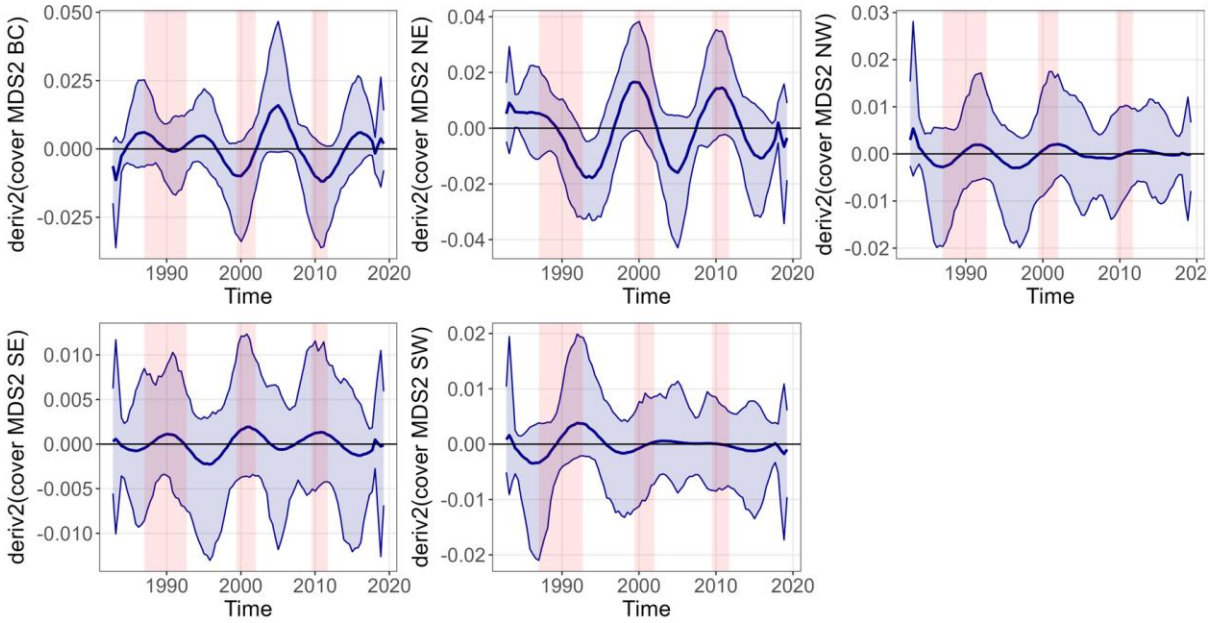


**Figure SM36**. Second derivative of the temporal trend in sessile organism community at the site scale for the second ordination axis. The second derivative was calculated by central difference with 1000 draws. The blue shaded area represents the 95% credible interval of the second derivative, and the red shaded area represents the time of each regime shift.

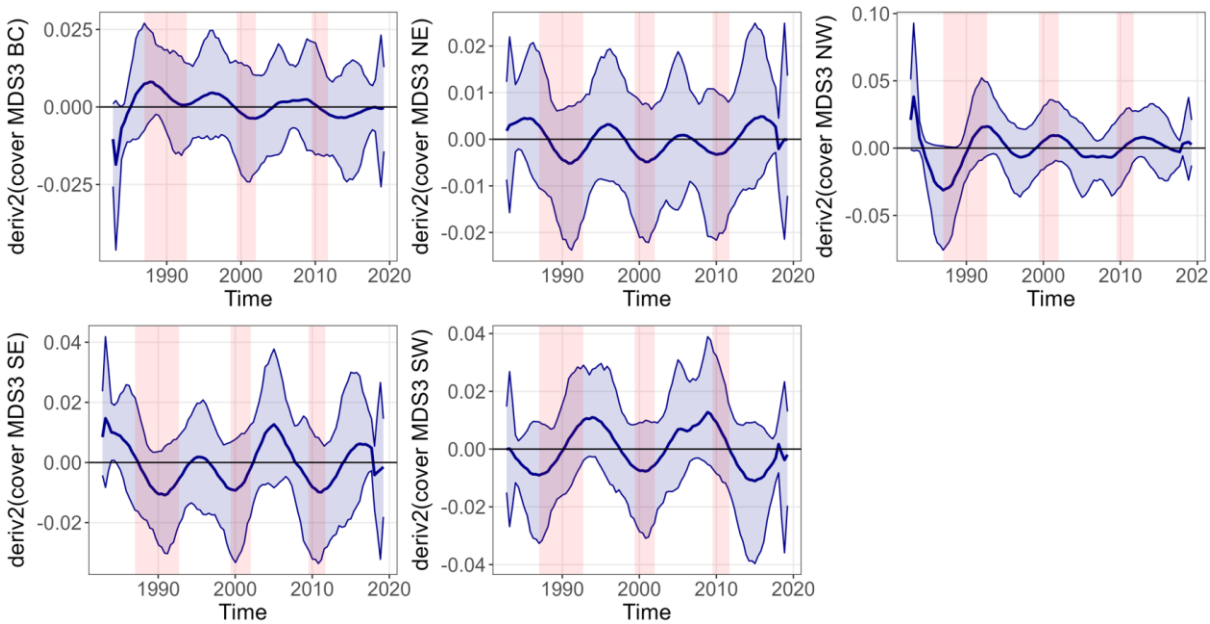


**Figure SM37**. Second derivative of the temporal trend in sessile organism community at the site scale for the third ordination axis. The second derivative was calculated by central

difference with 1000 draws. The blue shaded area represents the 95% credible interval of the second derivative, and the red shaded area represents the time of each regime shift.

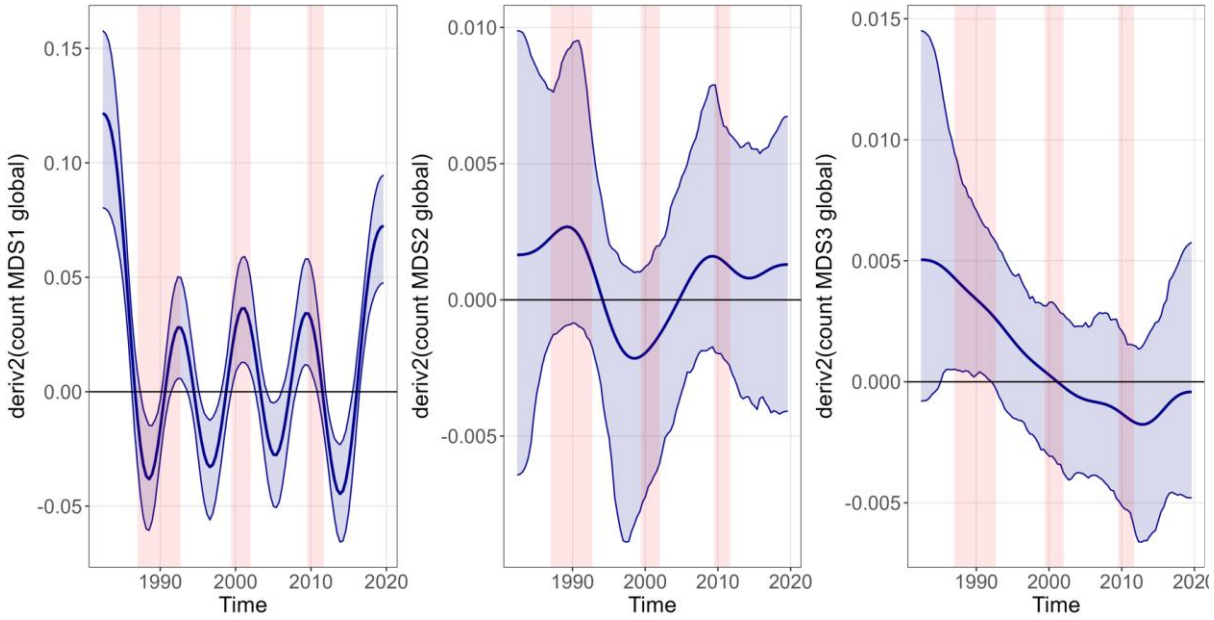


**Figure SM38**. Second derivative of the temporal trend in mobile invertebrates community at the island scale. The second derivative was calculated by central difference with 1000 draws. The blue shaded area represents the 95% credible interval of the second derivative, and the red shaded area represents the time of each regime shift.

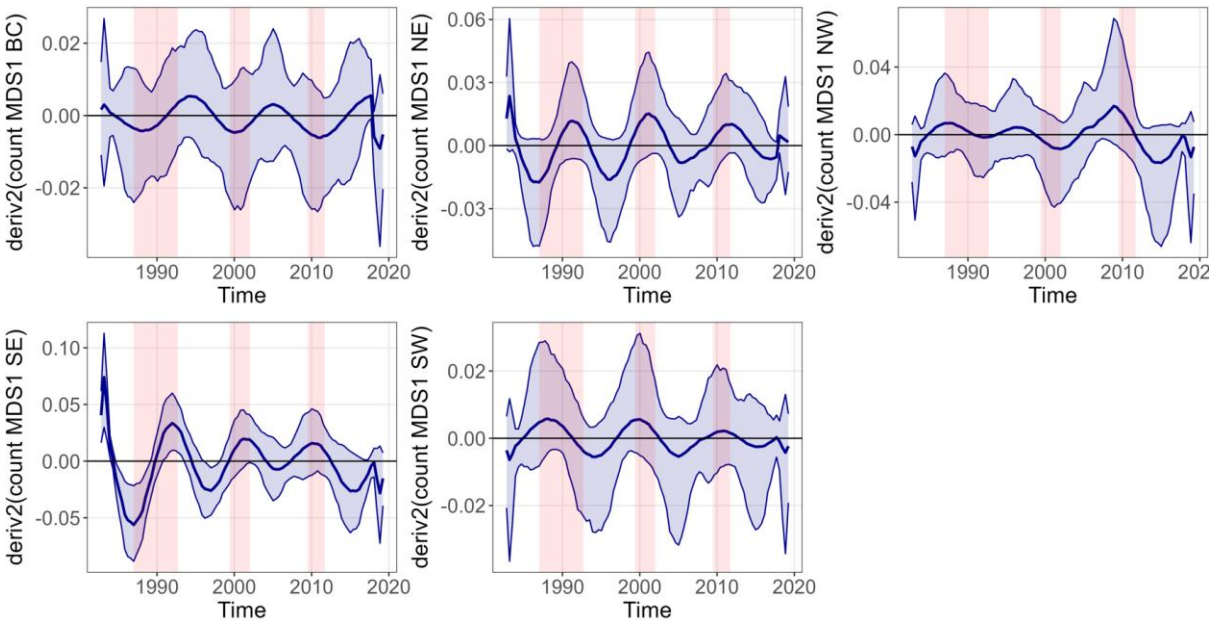


**Figure SM39**. Second derivative of the temporal trend in mobile organism community at the site scale for the first ordination axis. The second derivative was calculated by central difference with 1000 draws. The blue shaded area represents the 95% credible interval of the second derivative, and the red shaded area represents the time of each regime shift.

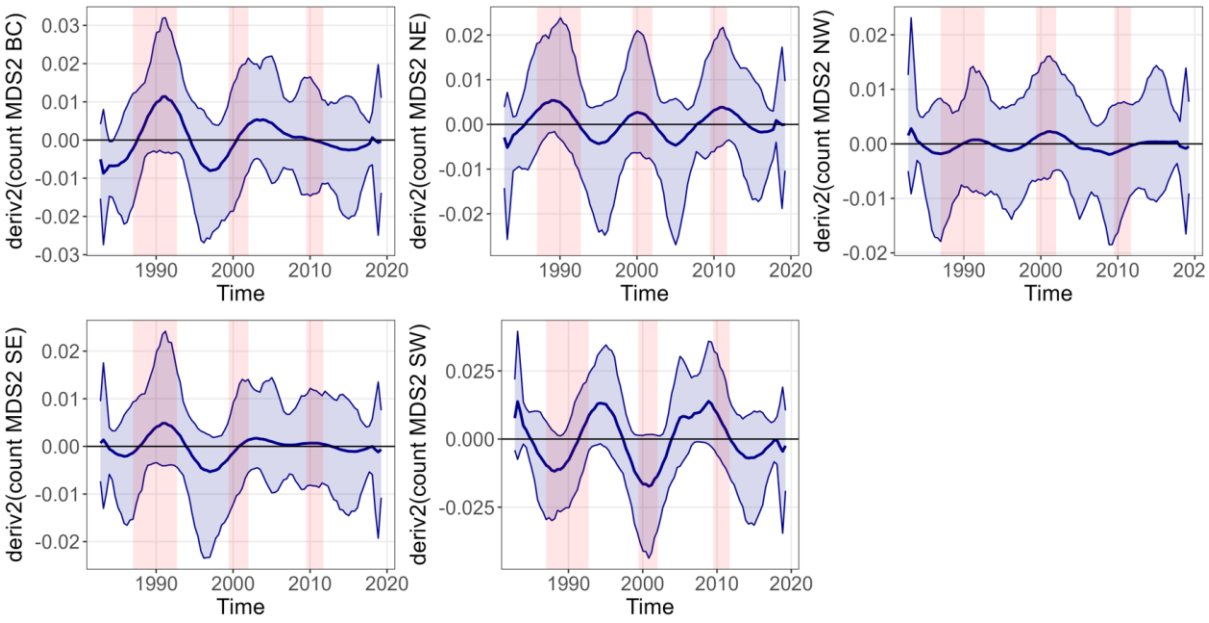


**Figure SM40**. Second derivative of the temporal trend in mobile organism community at the site scale for the second ordination axis. The second derivative was calculated by central difference with 1000 draws. The blue shaded area represents the 95% credible interval of the second derivative, and the red shaded area represents the time of each regime shift.

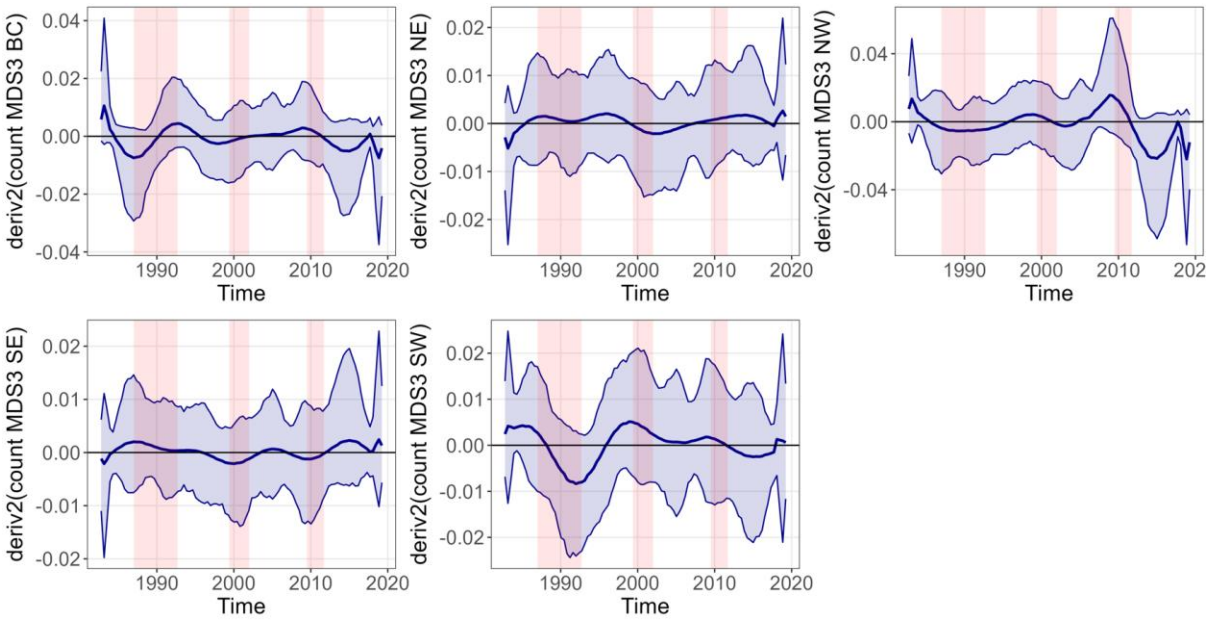


**Figure SM41**. Second derivative of the temporal trend in mobile organism community at the site scale for the third ordination axis. The second derivative was calculated by central difference with 1000 draws. The blue shaded area represents the 95% credible interval of the second derivative, and the red shaded area represents the time of each regime shift.

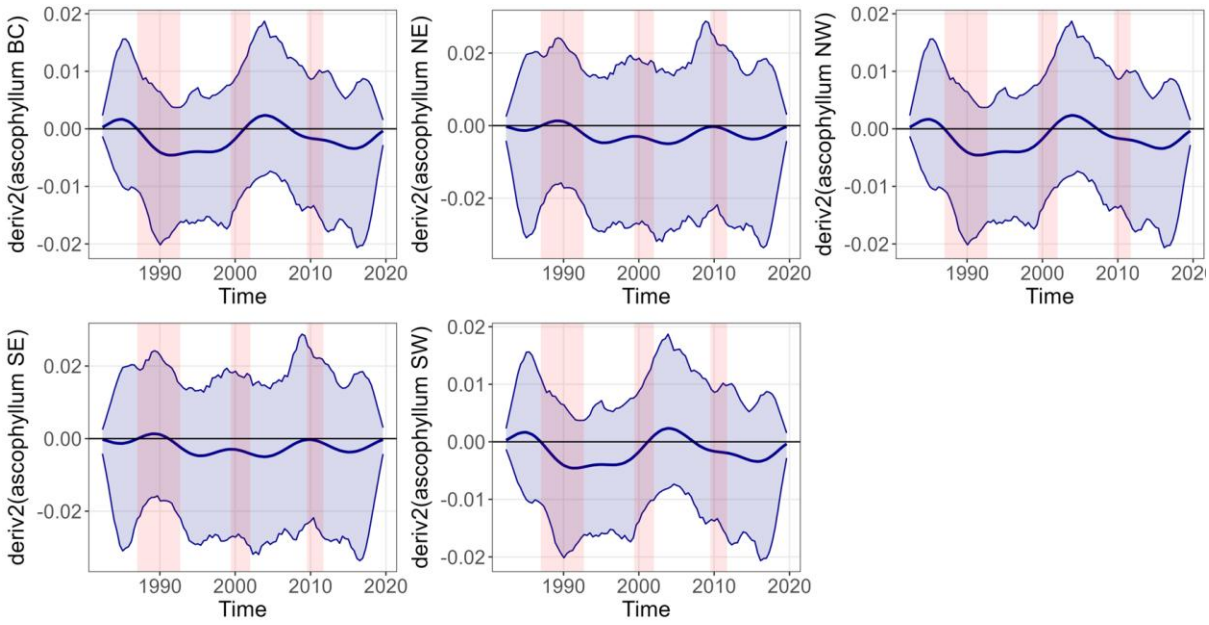


**Figure SM42**. Second derivative of the temporal trend in *Ascophyllum* abundance. The second derivative was calculated by central difference with 1000 draws. The blue shaded area represents the 95% credible interval of the second derivative, and the red shaded area represents the time of each regime shift.

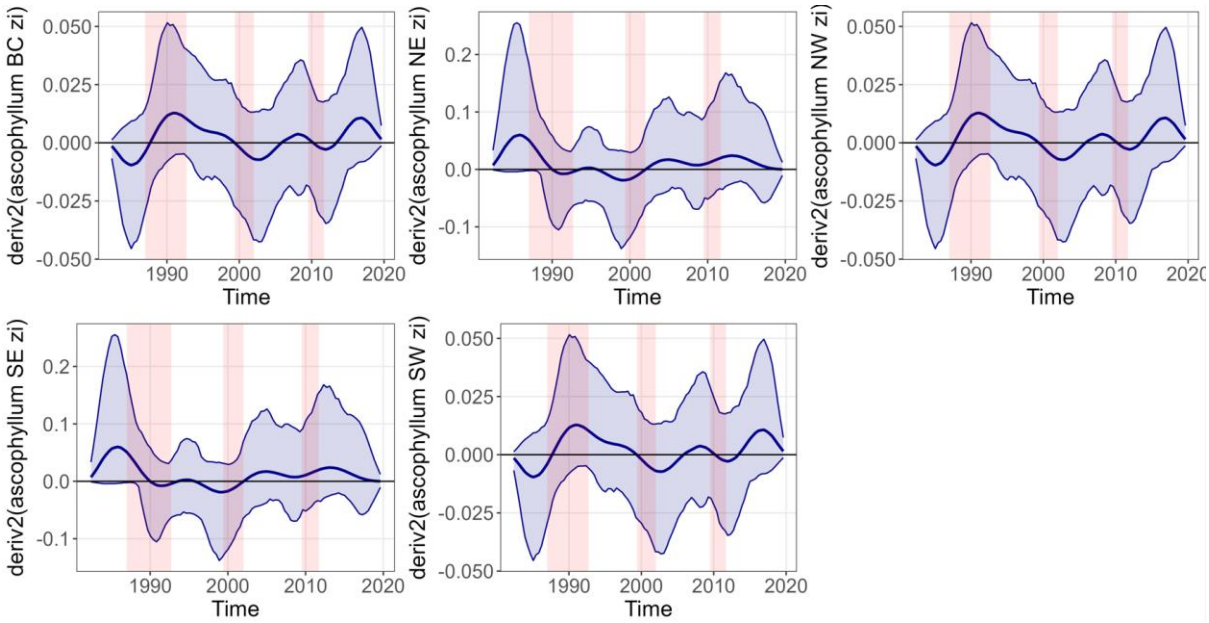


**Figure SM43**. Second derivative of the temporal trend in *Ascophyllum* presence. The presence is assessed by zero inflated part of the model. The second derivative was calculated by central difference with 1000 draws. The blue shaded area represents the 95% credible interval of the second derivative, and the red shaded area represents the time of each regime shift.

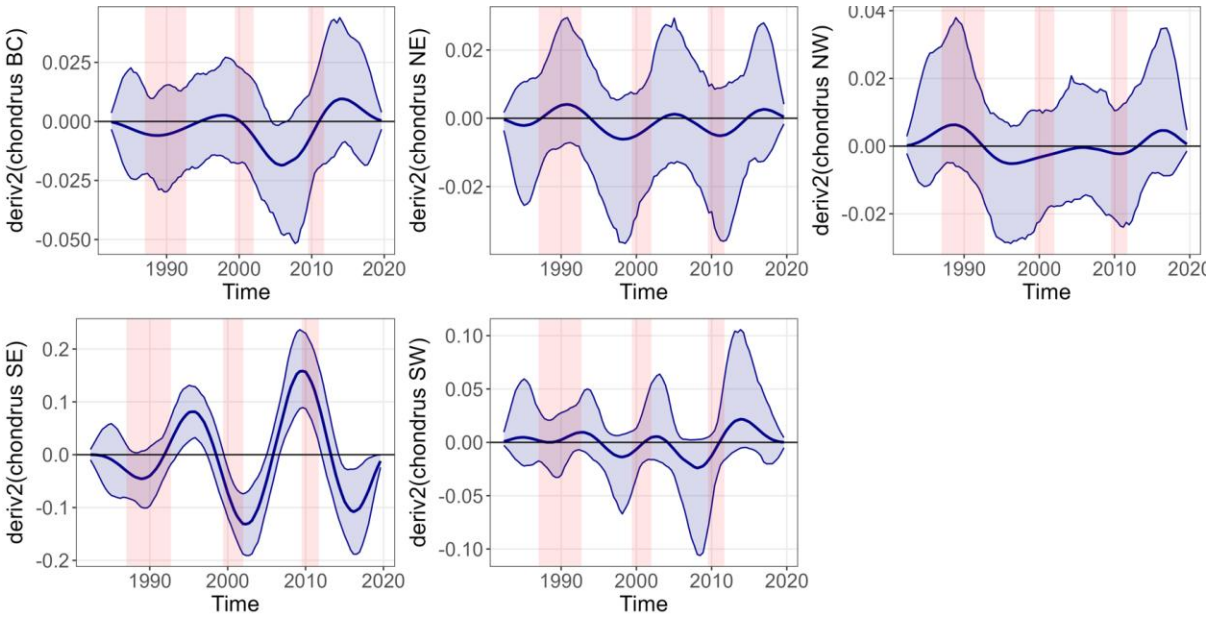


**Figure SM44**. Second derivative of the temporal trend in *Chondrus* abundance. The second derivative was calculated by central difference with 1000 draws. The blue shaded area represents the 95% credible interval of the second derivative, and the red shaded area represents the time of each regime shift.

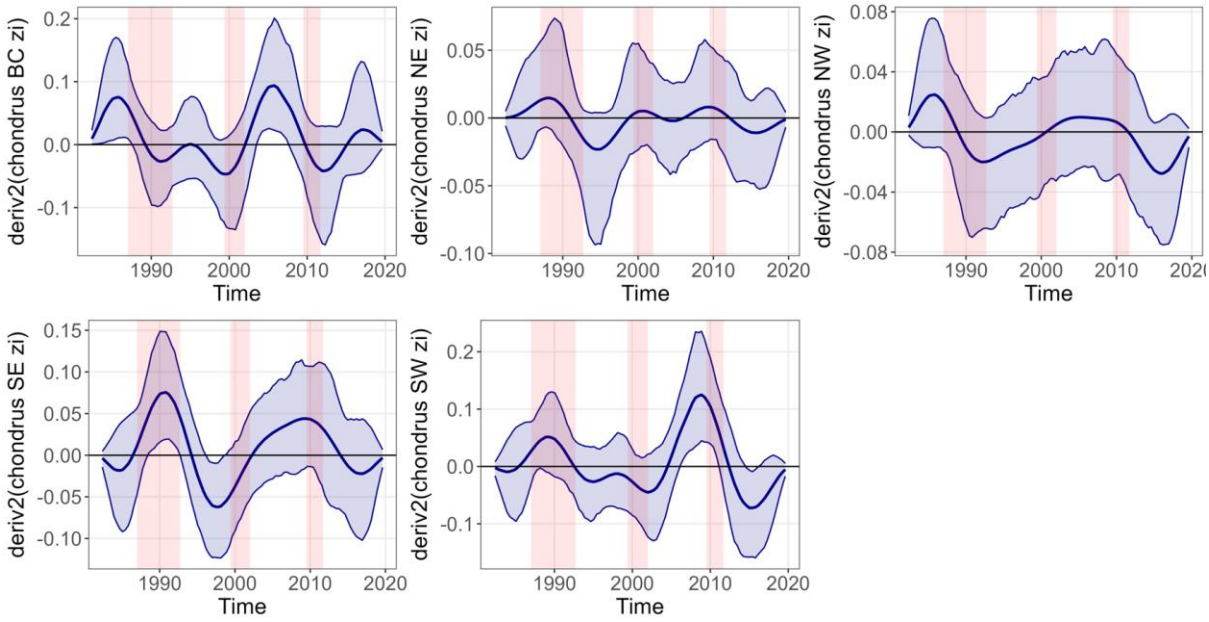


**Figure SM45**. Second derivative of the temporal trend in *Chondrus* presence. The presence is assessed by zero inflated part of the model. The second derivative was calculated by central difference with 1000 draws. The blue shaded area represents the 95% credible interval of the second derivative, and the red shaded area represents the time of each regime shift.

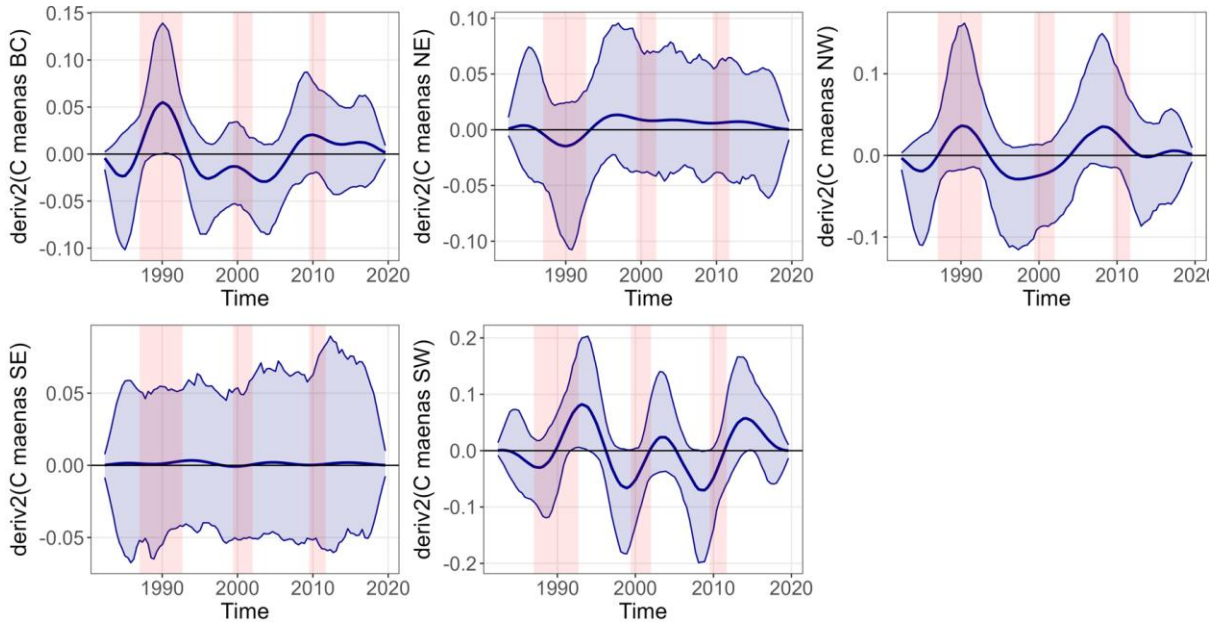


**Figure SM46**. Second derivative of the temporal trend in *C. maenas* abundance. The second derivative was calculated by central difference with 1000 draws. The blue shaded area represents the 95% credible interval of the second derivative, and the red shaded area represents the time of each regime shift.

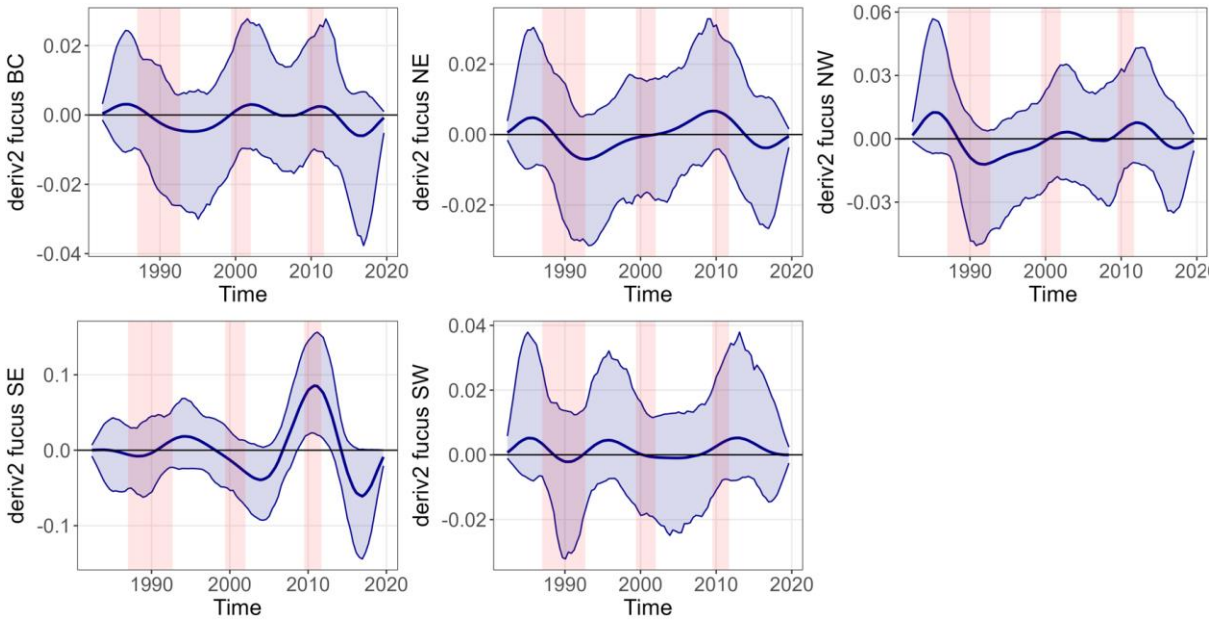


**Figure SM47**. Second derivative of the temporal trend in *Fucus* abundance. The second derivative was calculated by central difference with 1000 draws. The blue shaded area represents the 95% credible interval of the second derivative, and the red shaded area represents the time of each regime shift.

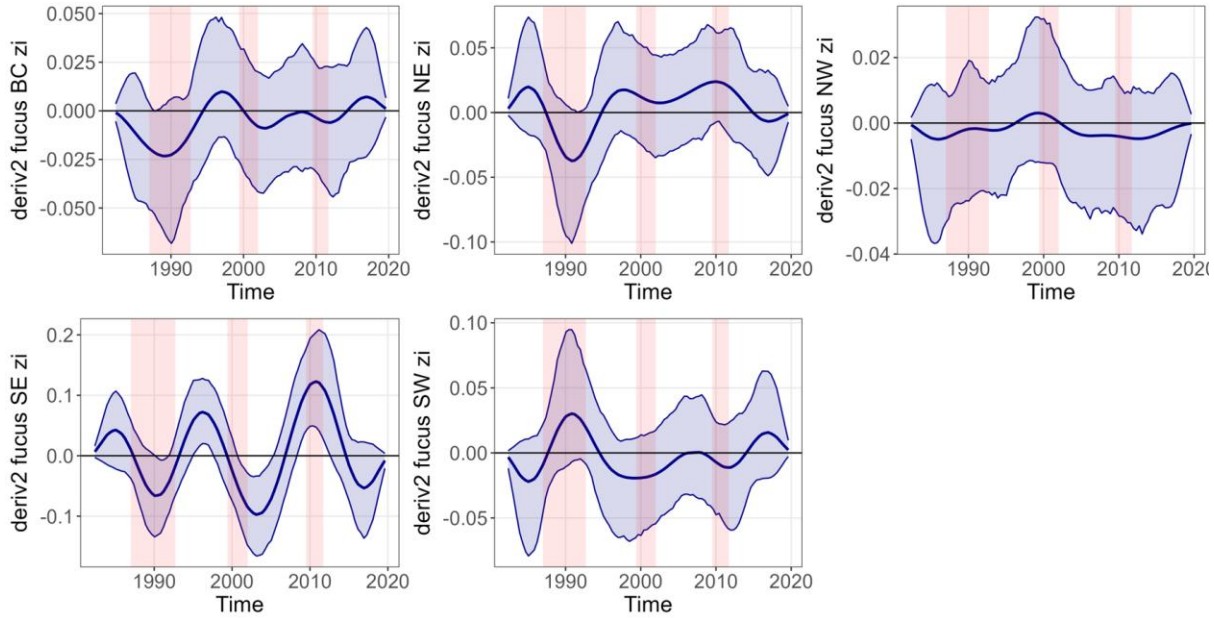


**Figure SM43**. Second derivative of the temporal trend in *Fucus* abundance. The second derivative was calculated by central difference with 1000 draws. The blue shaded area represents the 95% credible interval of the second derivative, and the red shaded area represents the time of each regime shift.

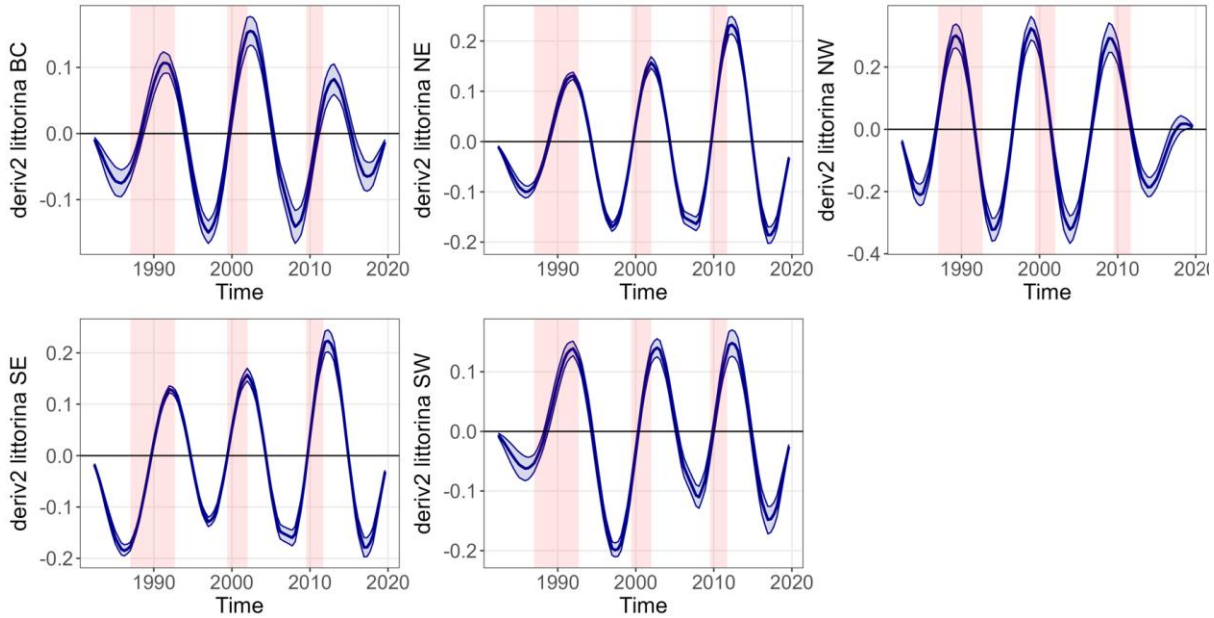


**Figure SM48**. Second derivative of the temporal trend in *Littorina* abundance. The second derivative was calculated by central difference with 1000 draws. The blue shaded area represents the 95% credible interval of the second derivative, and the red shaded area represents the time of each regime shift.

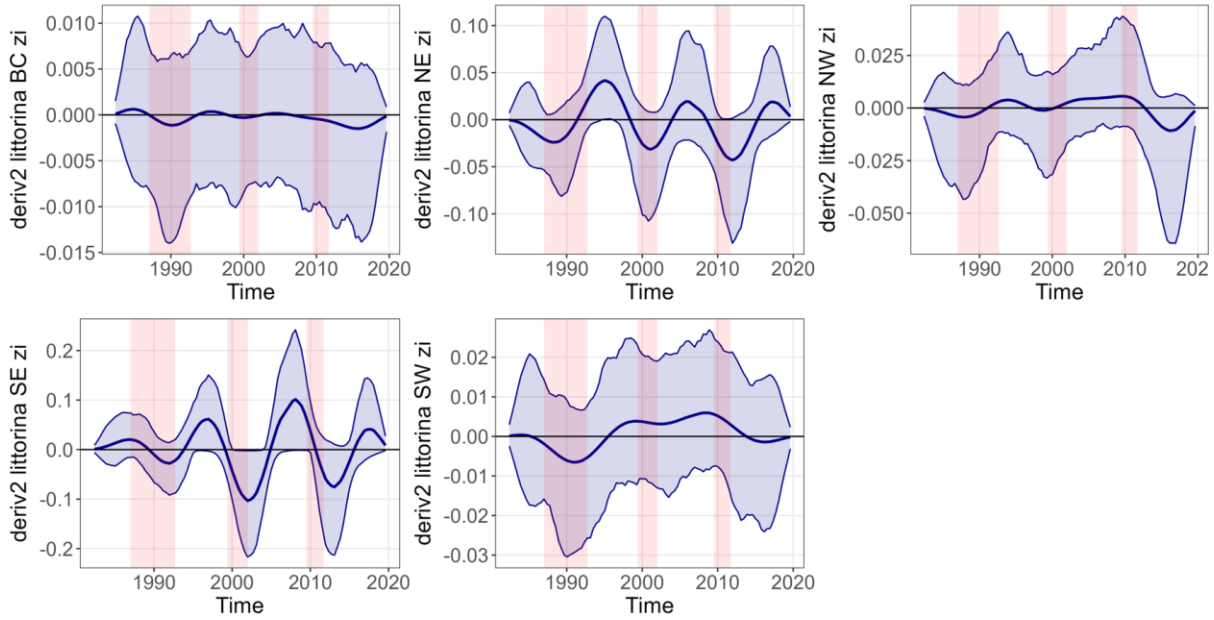


**Figure SM49**. Second derivative of the temporal trend in *Littorina* presence. The presence is assessed by zero inflated part of the model. The second derivative was calculated by central difference with 1000 draws. The blue shaded area represents the 95% credible interval of the second derivative, and the red shaded area represents the time of each regime shift.

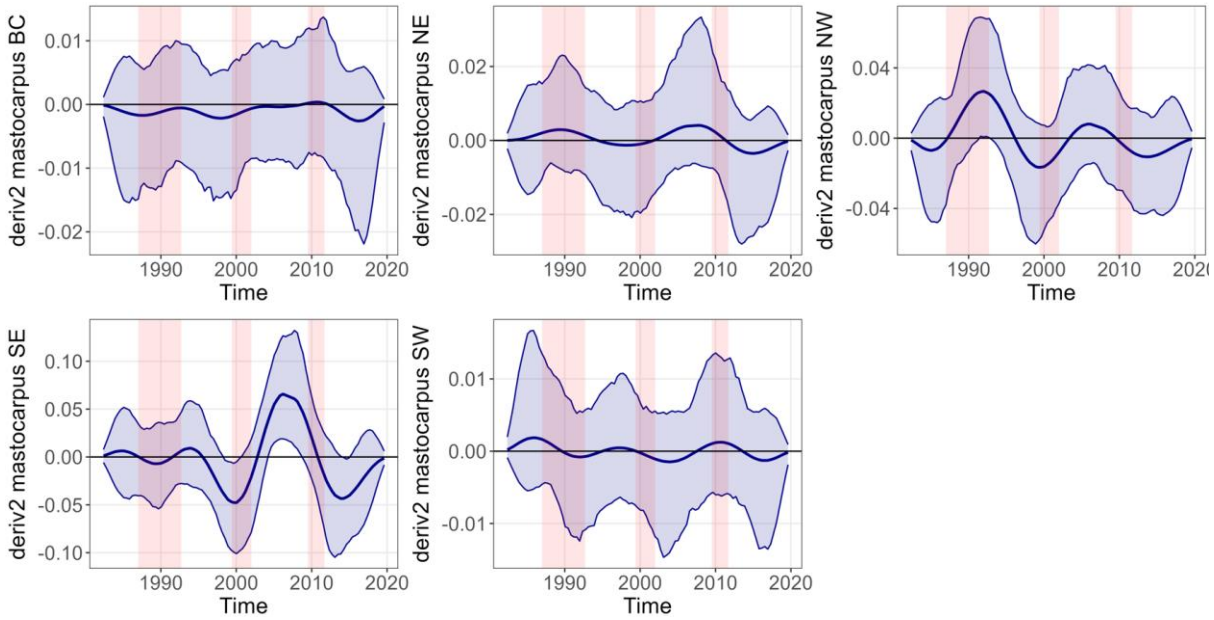


**Figure SM50**. Second derivative of the temporal trend in *Mastocarpus* abundance. The second derivative was calculated by central difference with 1000 draws. The blue shaded area represents the 95% credible interval of the second derivative, and the red shaded area represents the time of each regime shift.

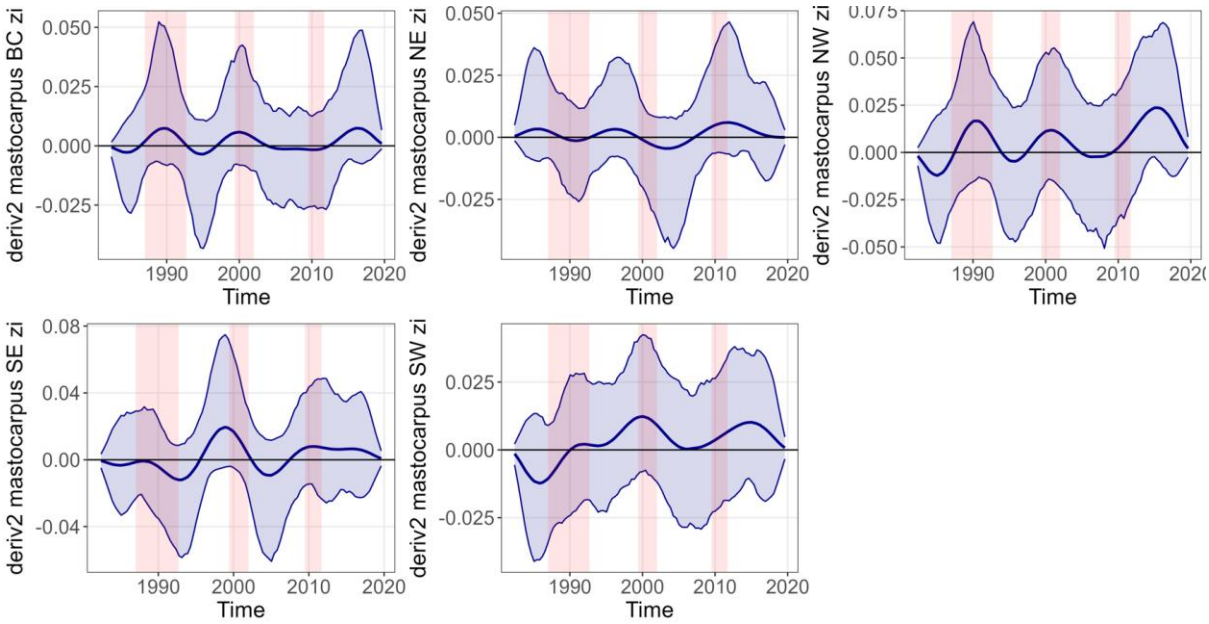


**Figure SM51**. Second derivative of the temporal trend in *Mastocarpus* presence. The presence is assessed by zero inflated part of the model. The second derivative was calculated by central difference with 1000 draws. The blue shaded area represents the 95% credible interval of the second derivative, and the red shaded area represents the time of each regime shift.

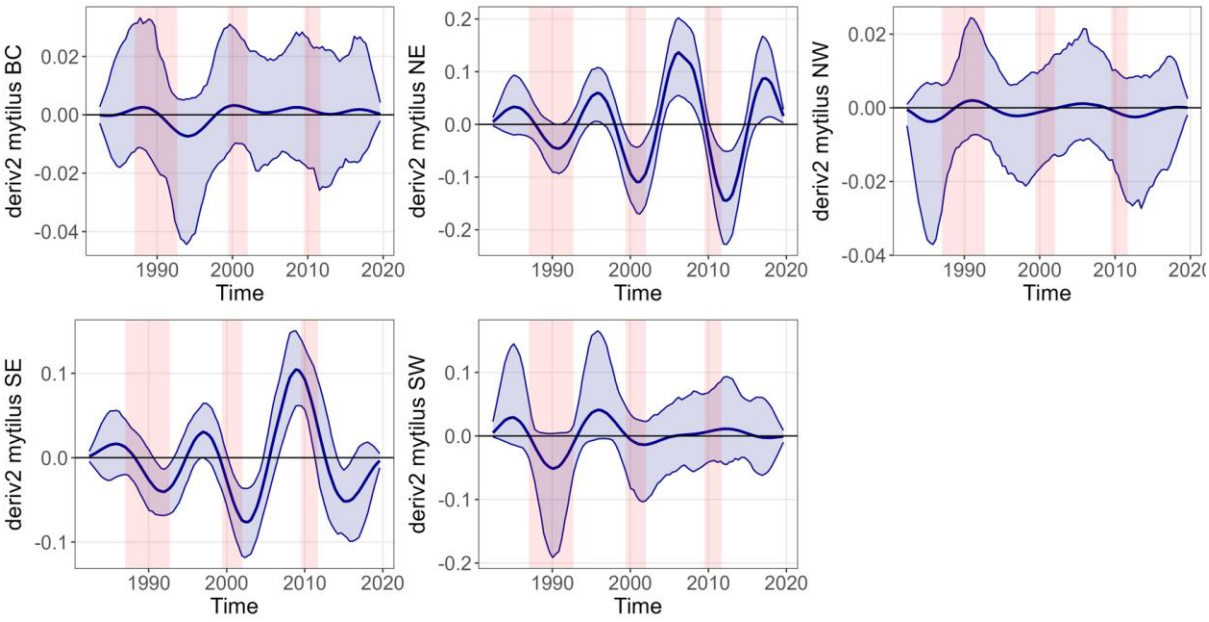


**Figure SM52**. Second derivative of the temporal trend in *Mytilus* abundance. The second derivative was calculated by central difference with 1000 draws. The blue shaded area represents the 95% credible interval of the second derivative, and the red shaded area represents the time of each regime shift.

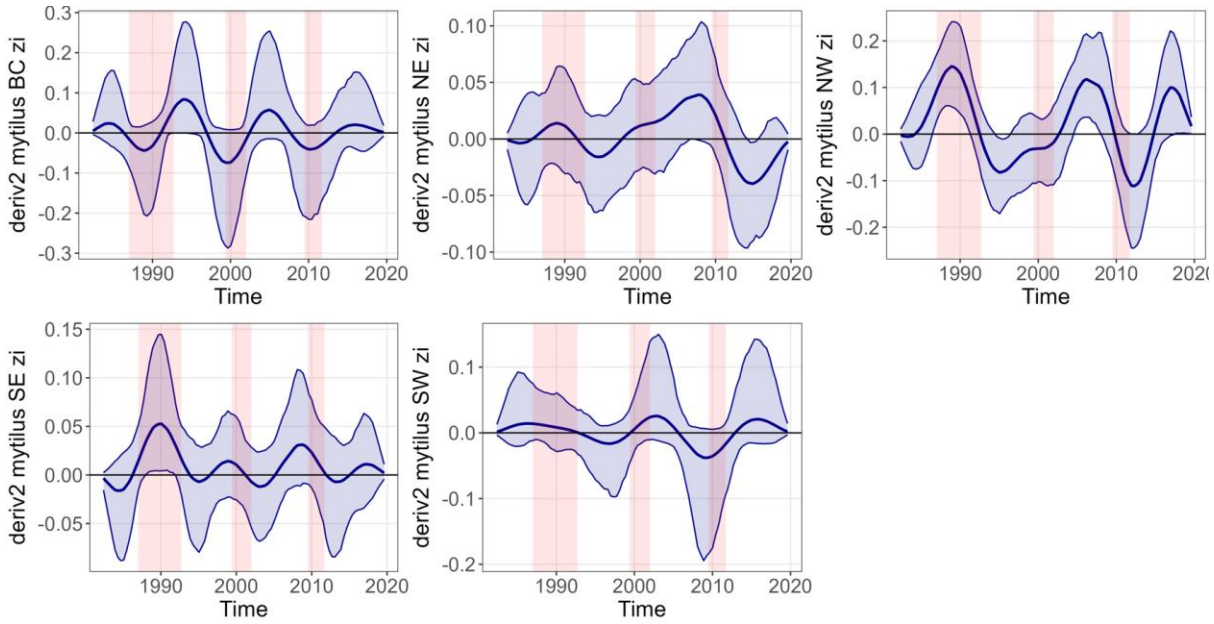


**Figure SM53**. Second derivative of the temporal trend in *Mytilus* presence. The presence is assessed by zero inflated part of the model. The second derivative was calculated by central difference with 1000 draws. The blue shaded area represents the 95% credible interval of the second derivative, and the red shaded area represents the time of each regime shift.

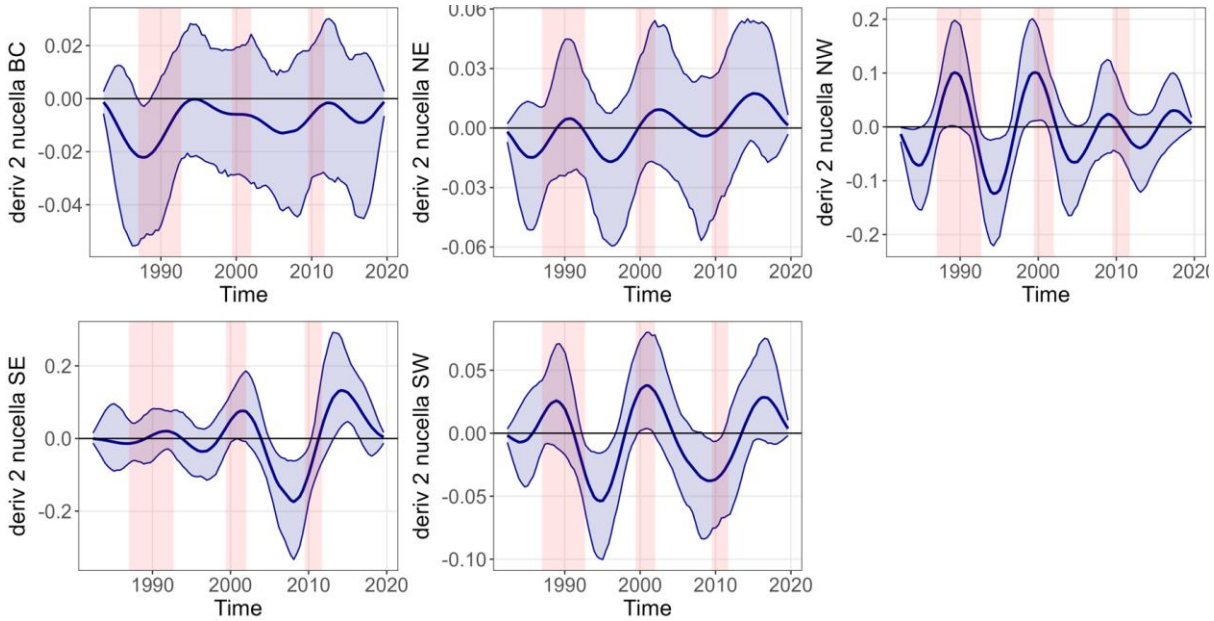


**Figure SM54**. Second derivative of the temporal trend in *Nucella* abundance. The second derivative was calculated by central difference with 1000 draws. The blue shaded area represents the 95% credible interval of the second derivative, and the red shaded area represents the time of each regime shift.

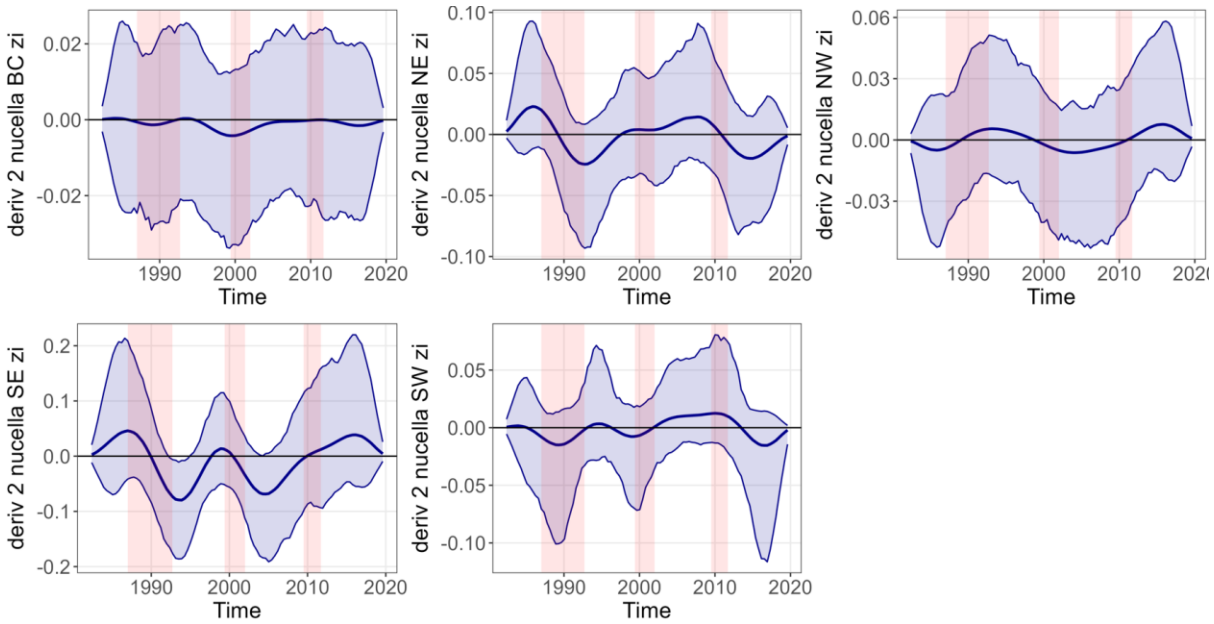


**Figure SM55**. Second derivative of the temporal trend in *Nucella* presence. The presence is assessed by zero inflated part of the model. The second derivative was calculated by central difference with 1000 draws. The blue shaded area represents the 95% credible interval of the second derivative, and the red shaded area represents the time of each regime shift.

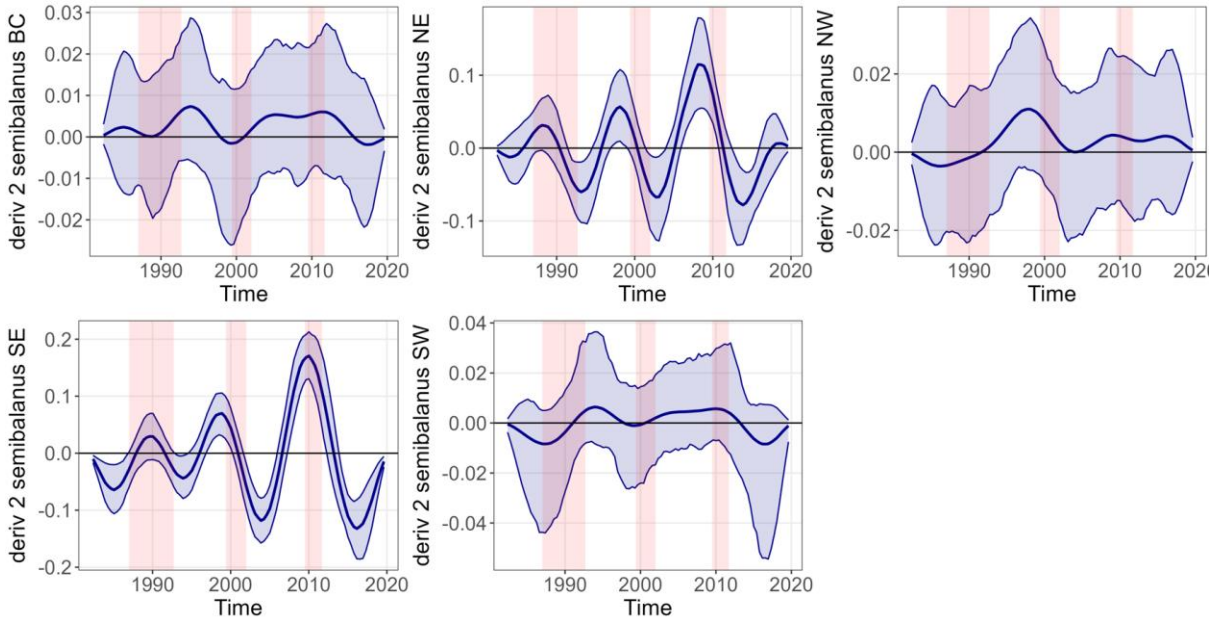


**Figure SM56**. Second derivative of the temporal trend in *Semibalanus* abundance. The second derivative was calculated by central difference with 1000 draws. The blue shaded area represents the 95% credible interval of the second derivative, and the red shaded area represents the time of each regime shift.

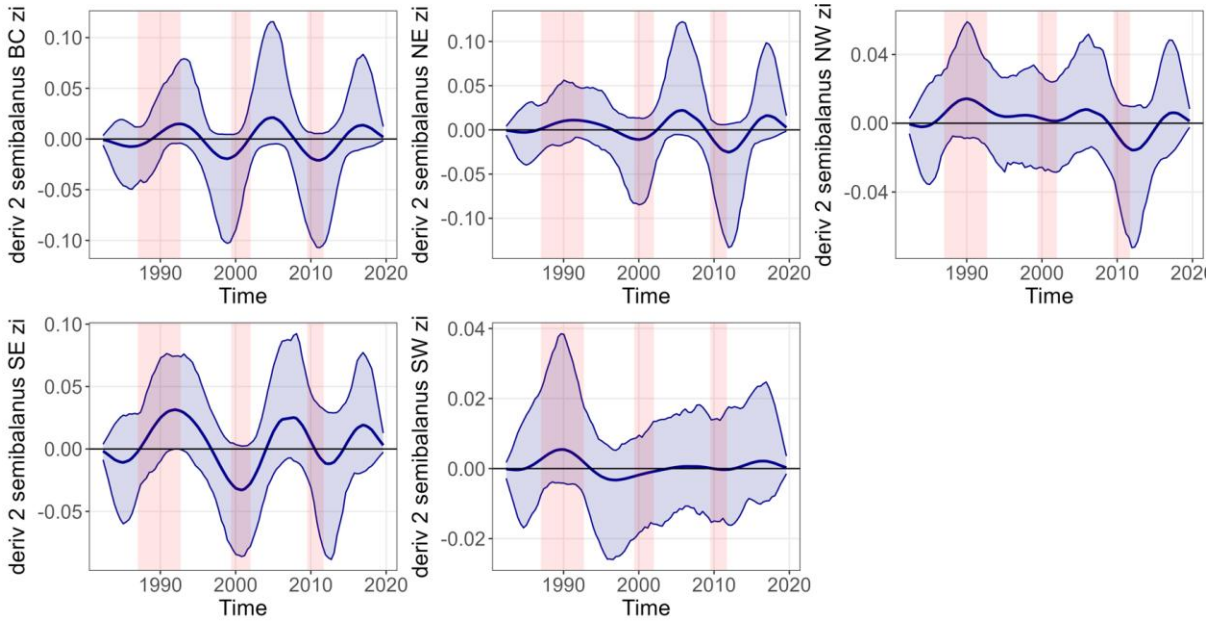


**Figure SM57**. Second derivative of the temporal trend in *Semibalanus* presence. The presence is assessed by zero inflated part of the model. The second derivative was calculated by central difference with 1000 draws. The blue shaded area represents the 95% credible interval of the second derivative, and the red shaded area represents the time of each regime shift.

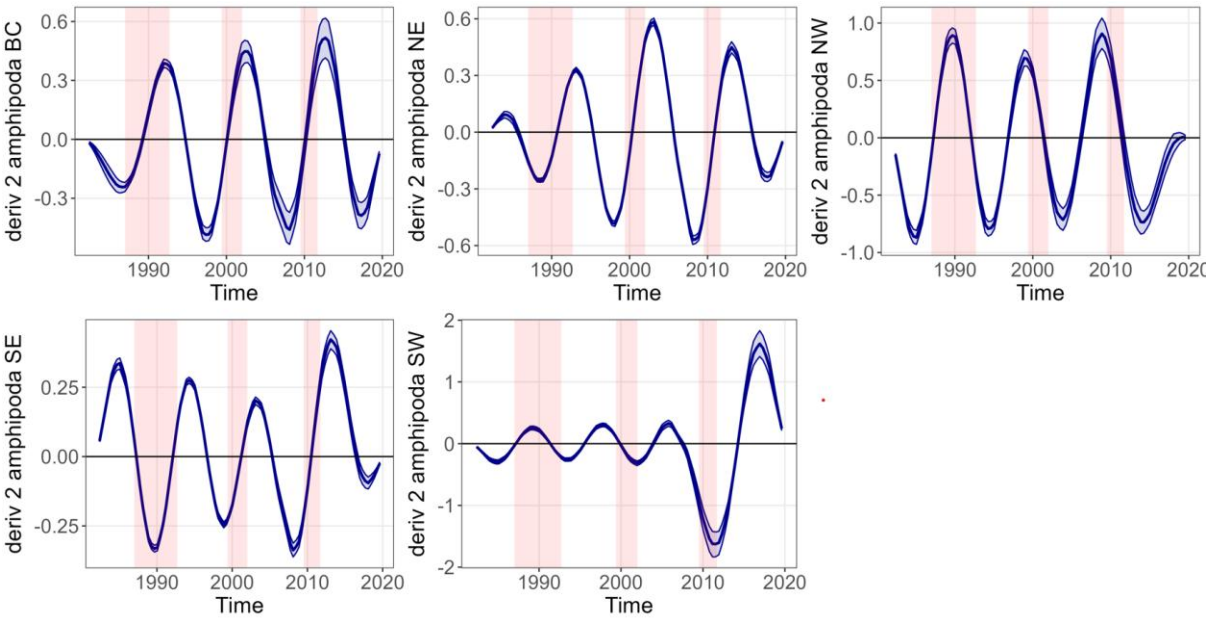


**Figure SM58**. Second derivative of the temporal trend in *Amphipoda* abundance. The second derivative was calculated by central difference with 1000 draws. The blue shaded area represents the 95% credible interval of the second derivative, and the red shaded area represents the time of each regime shift.

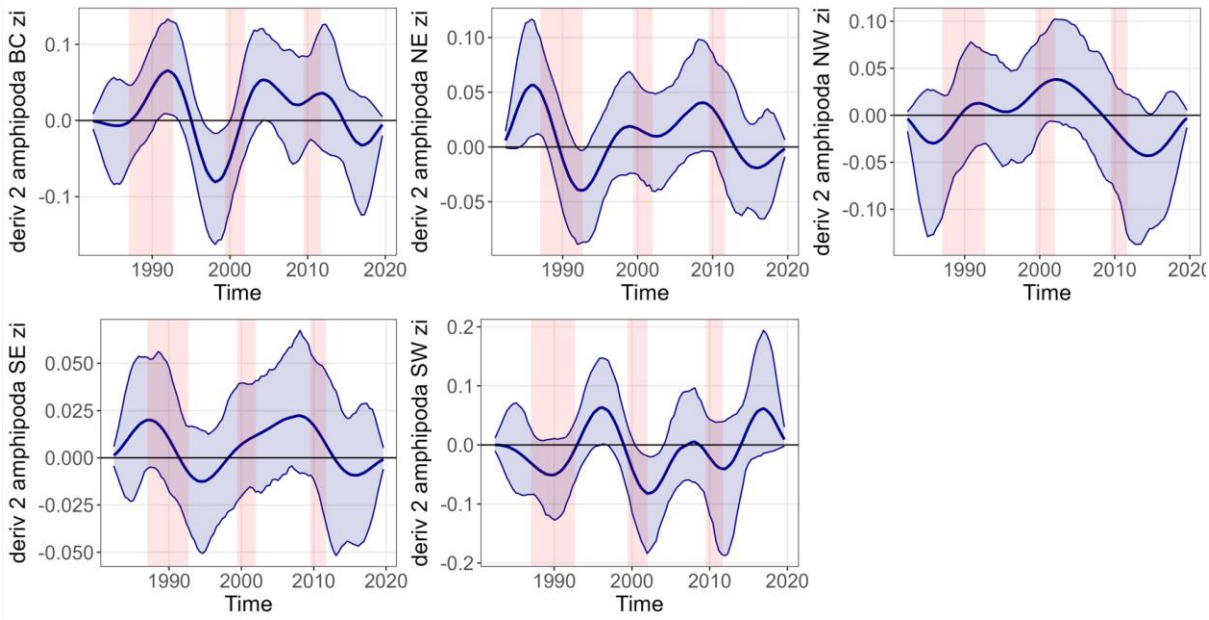


**Figure SM59**. Second derivative of the temporal trend in *Amphipoda* presence. The presence is assessed by zero inflated part of the model. The second derivative was calculated by central difference with 1000 draws. The blue shaded area represents the 95% credible interval of the second derivative, and the red shaded area represents the time of each regime shift.

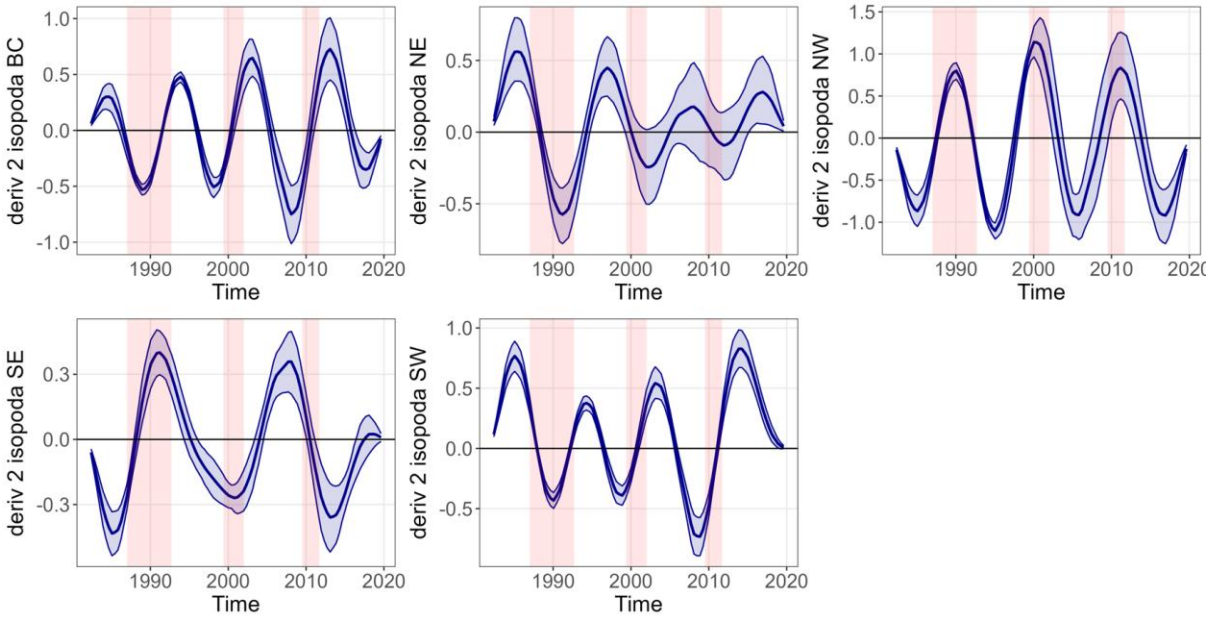


**Figure SM60**. Second derivative of the temporal trend in *Isopoda* abundance. The second derivative was calculated by central difference with 1000 draws. The blue shaded area represents the 95% credible interval of the second derivative, and the red shaded area represents the time of each regime shift.

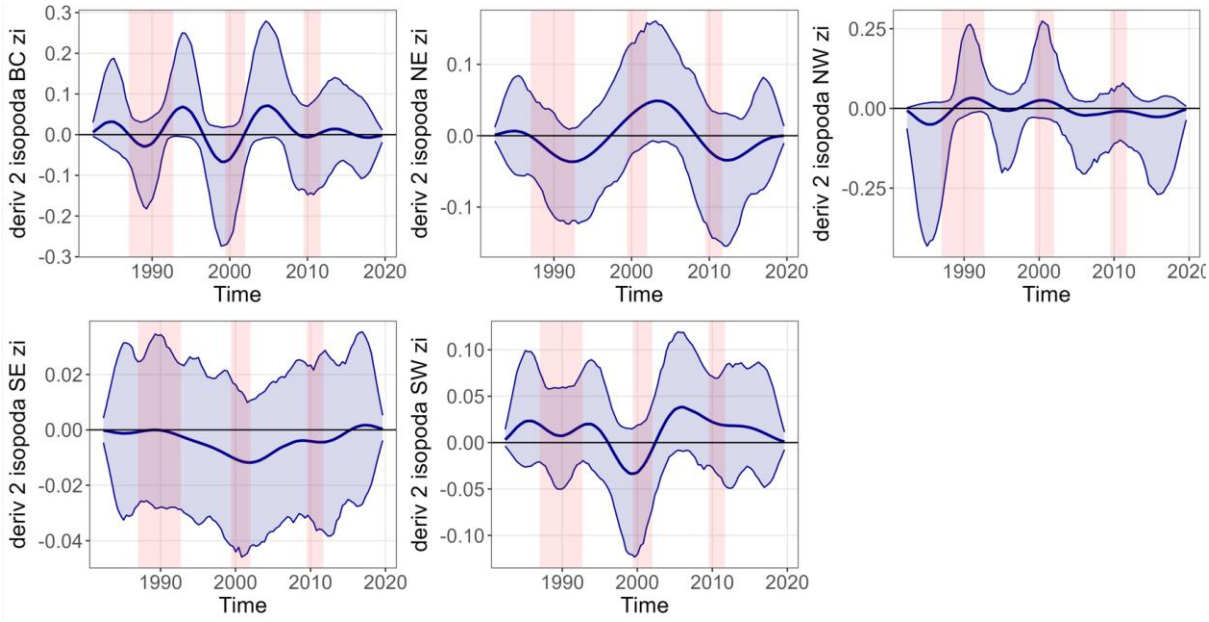


**Figure SM61**. Second derivative of the temporal trend in *Isopoda* presence. The presence is assessed by zero inflated part of the model. The second derivative was calculated by central difference with 1000 draws. The blue shaded area represents the 95% credible interval of the second derivative, and the red shaded area represents the time of each regime shift.

# Supplementary Material 7: Intertidal community composition and species specific trends' first derivative to assess a general shift starting in 2005.

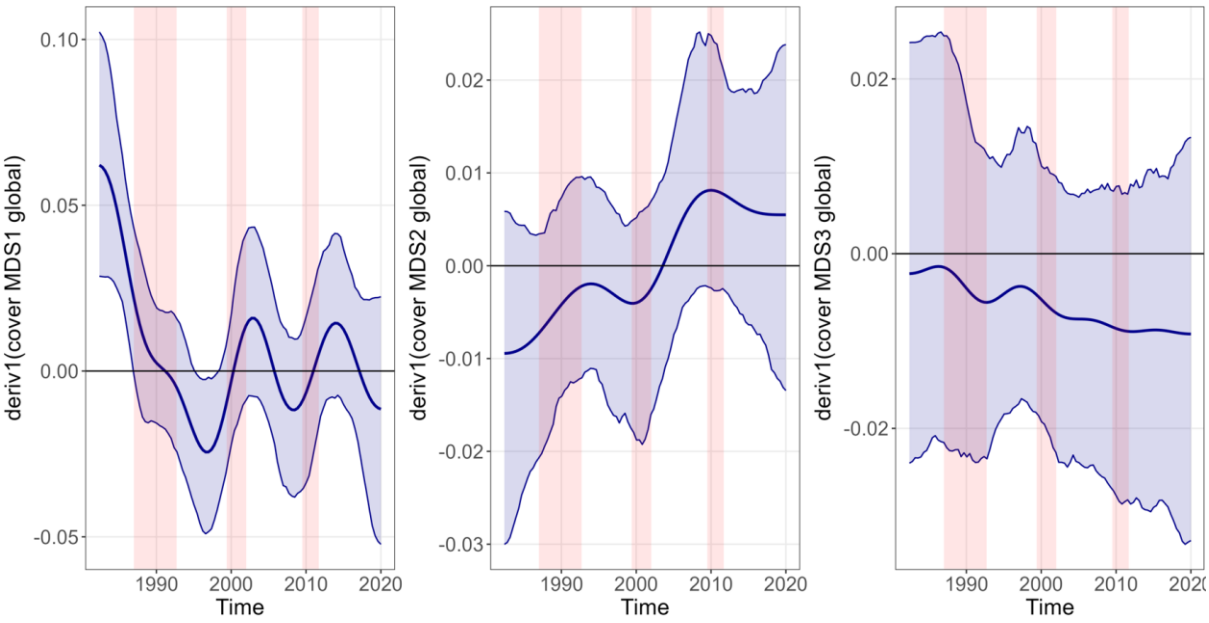

**Figure SM62**. First derivative of the temporal trend in sessile organism community composition at the island scale. The first derivative was calculated by forward difference with 1000 draws. The blue shaded area represents the 95% credible interval of the second derivative, and the red shaded area represents the time of each regime shift.

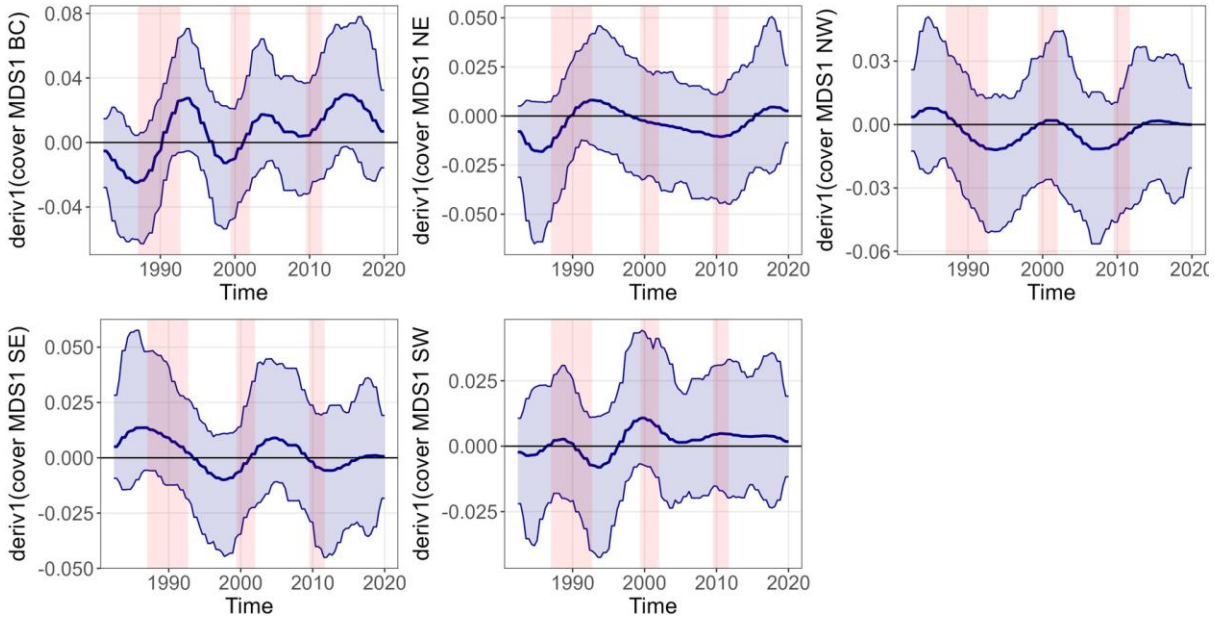


**Figure SM63**. First derivative of the temporal trend in sessile organism community composition at the site scale for the PCoA axis 1. The first derivative was calculated by forward difference with 1000 draws. The blue shaded area represents the 95% credible interval of the second derivative, and the red shaded area represents the time of each regime shift.

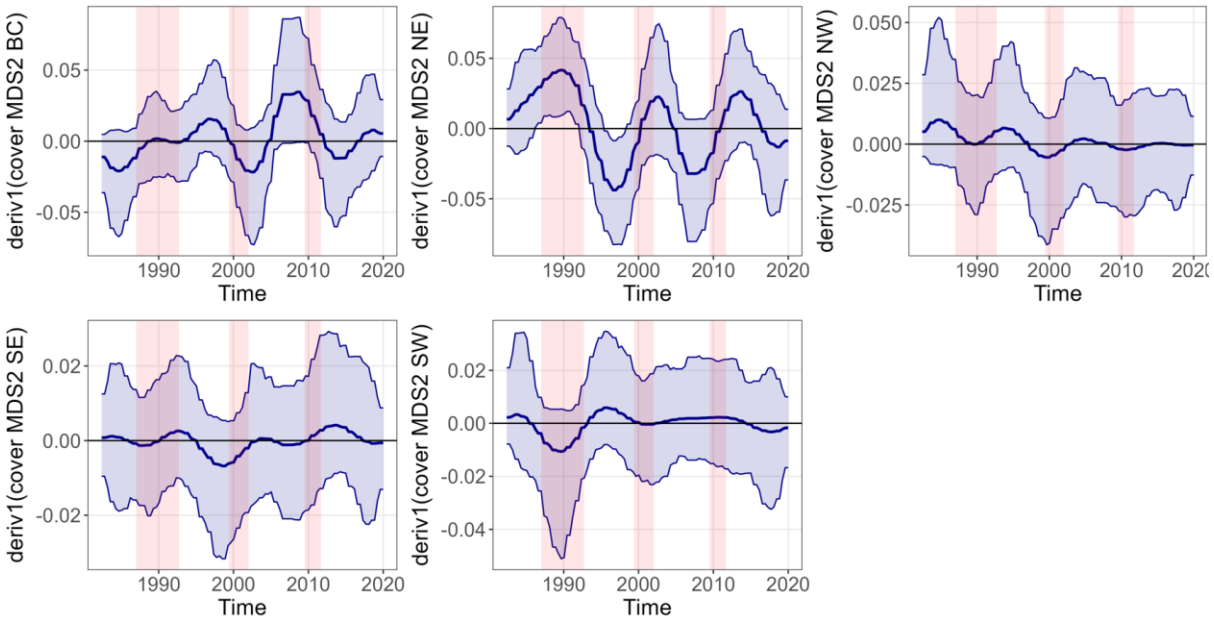

**Figure SM64**. First derivative of the temporal trend in sessile organism community composition at the site scale for the PCoA axis 2. The first derivative was calculated by forward difference with 1000 draws. The blue shaded area represents the 95% credible interval of the second derivative, and the red shaded area represents the time of each regime shift.

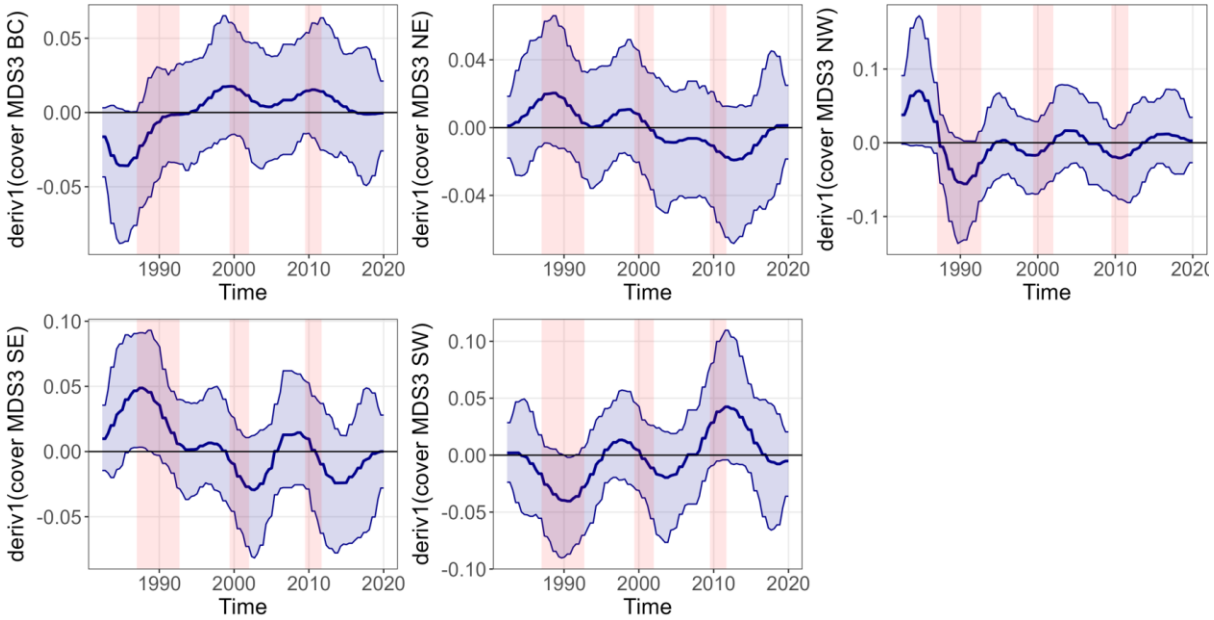


**Figure SM65**. First derivative of the temporal trend in sessile organism community composition at the site scale for the PCoA axis 3. The first derivative was calculated by forward difference with 1000 draws. The blue shaded area represents the 95% credible interval of the second derivative, and the red shaded area represents the time of each regime shift.

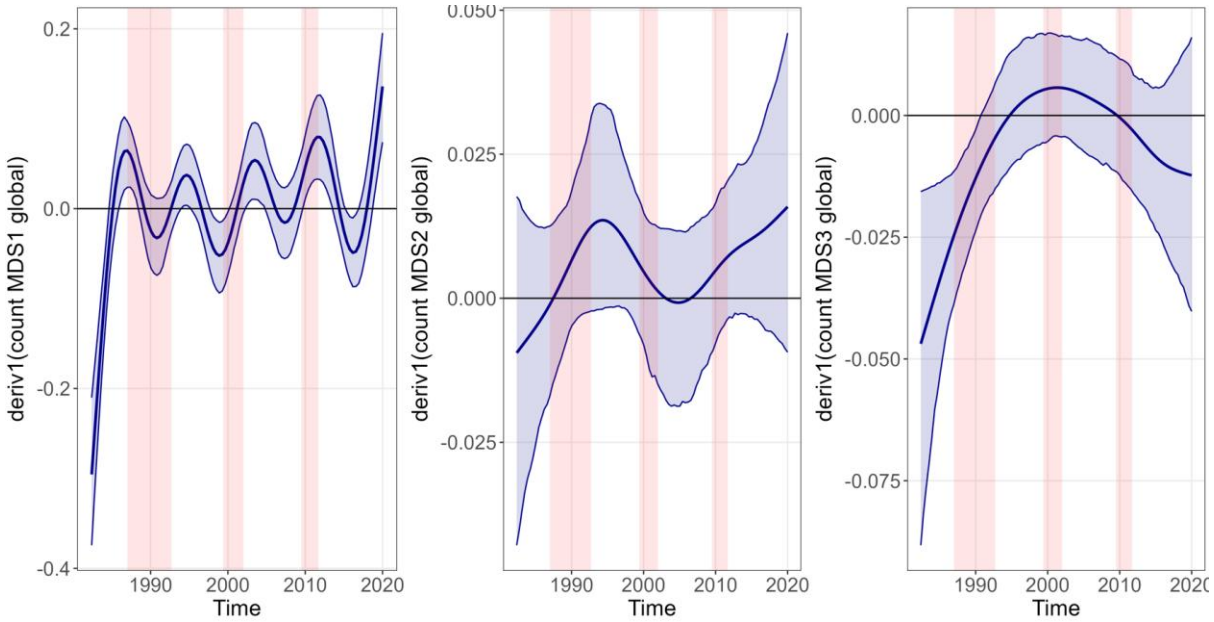


**Figure SM66**. First derivative of the temporal trend in mobile organism community composition at the island scale. The first derivative was calculated by forward difference with

1000 draws. The blue shaded area represents the 95% credible interval of the second derivative, and the red shaded area represents the time of each regime shift.

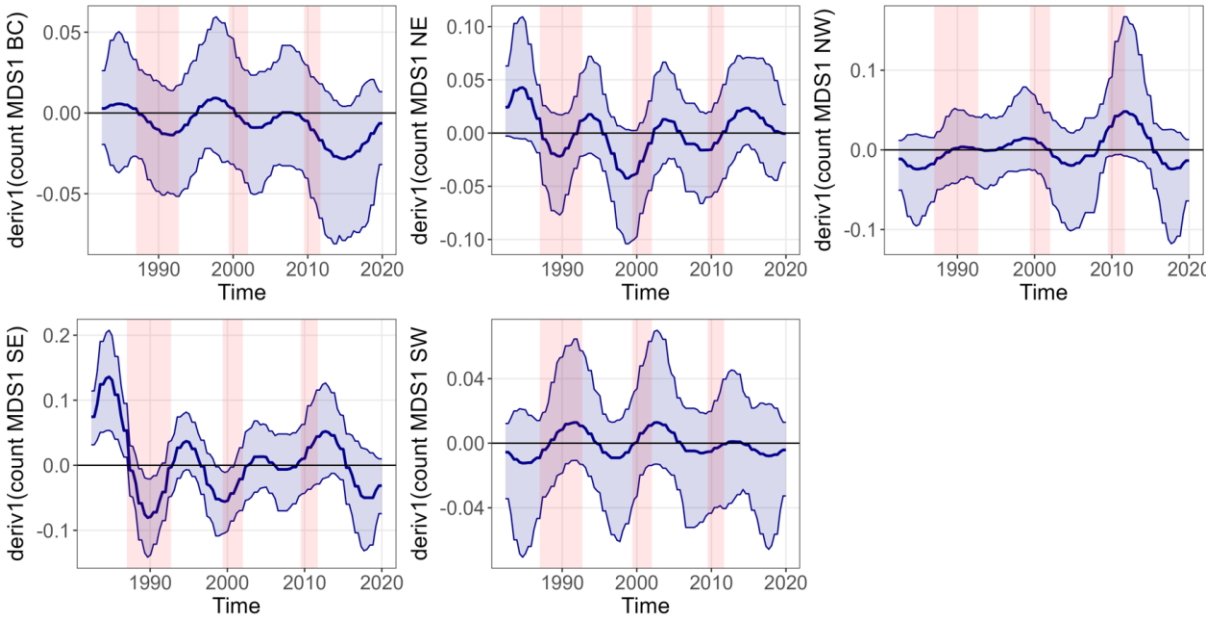


**Figure SM67**. First derivative of the temporal trend in mobile organism community composition at the site scale for the PCoA axis 1. The first derivative was calculated by forward difference with 1000 draws. The blue shaded area represents the 95% credible interval of the second derivative, and the red shaded area represents the time of each regime shift.

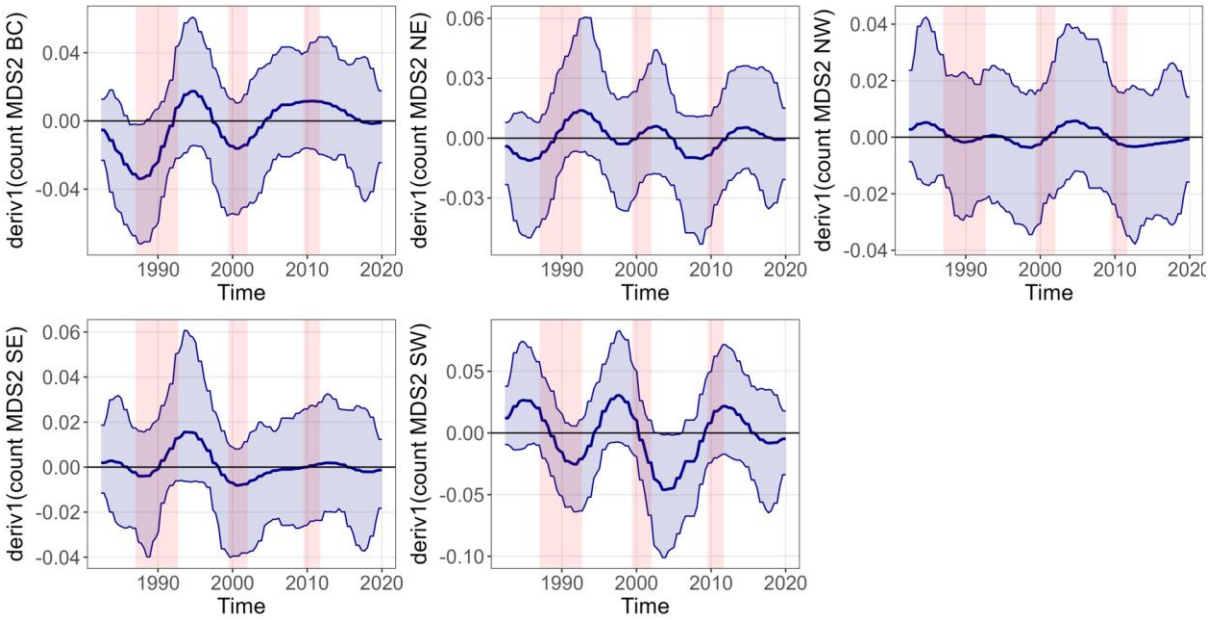


**Figure SM68**. First derivative of the temporal trend in mobile organism community composition at the site scale for the PCoA axis 2. The first derivative was calculated by forward difference with 1000 draws. The blue shaded area represents the 95% credible

interval of the second derivative, and the red shaded area represents the time of each regime shift.

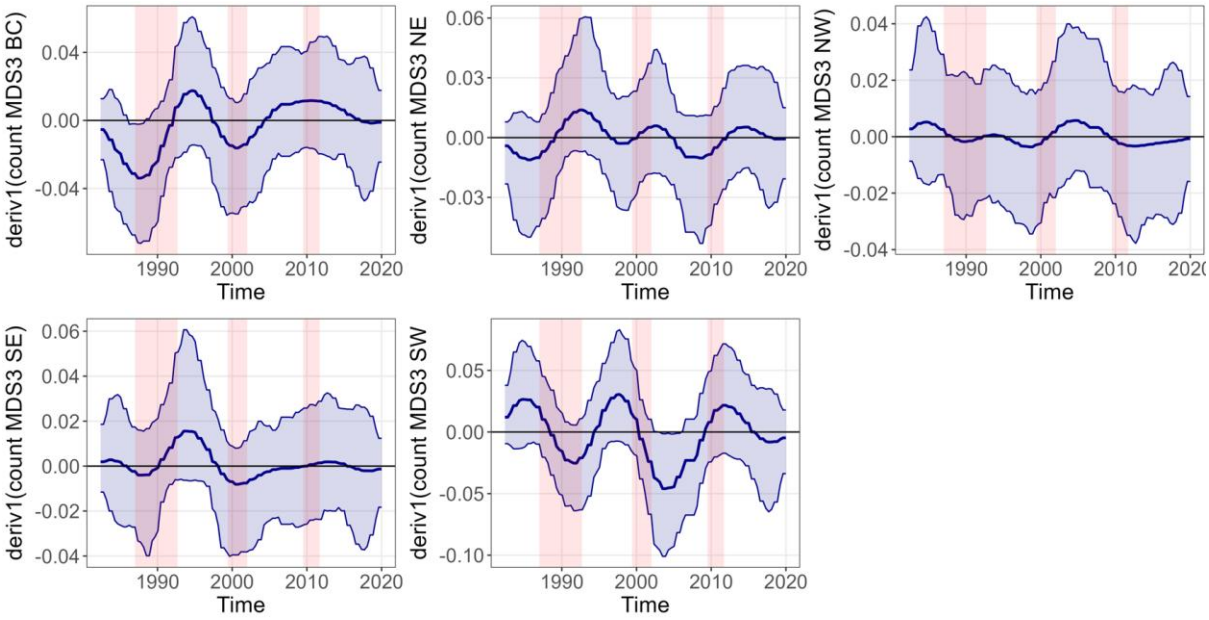


**Figure SM69**. First derivative of the temporal trend in mobile organism community composition at the site scale for the PCoA axis 3. The first derivative was calculated by forward difference with 1000 draws. The blue shaded area represents the 95% credible interval of the second derivative, and the red shaded area represents the time of each regime shift.

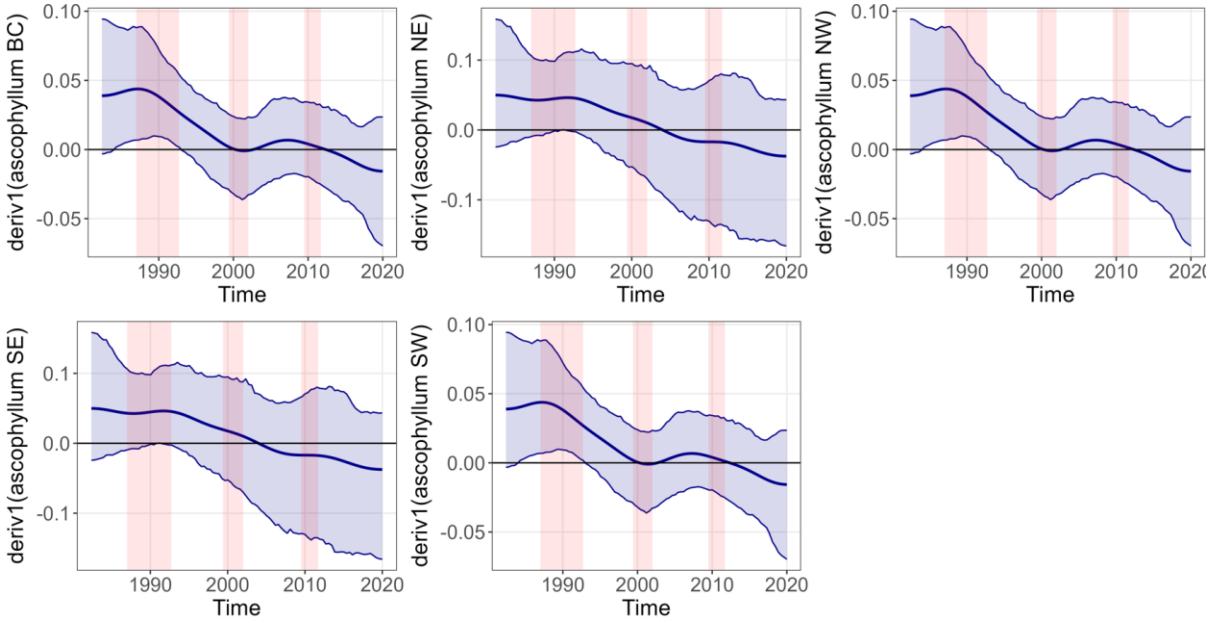


**Figure SM70**. First derivative of the temporal trend in *Ascophylum* presence. The first derivative was calculated by forward difference with 1000 draws. The blue shaded area

represents the 95% credible interval of the second derivative, and the red shaded area represents the time of each regime shift.

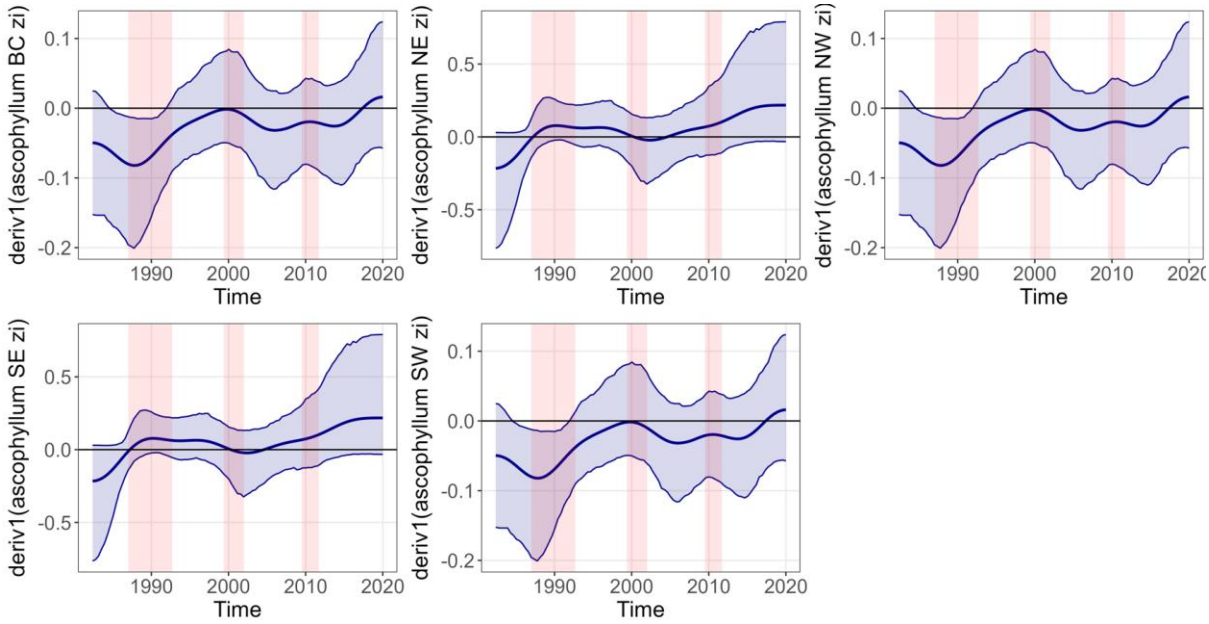


**Figure SM71**. First derivative of the temporal trend in *Ascophylum* presence. The presence is assessed by zero inflated part of the model. The first derivative was calculated by forward difference with 1000 draws. The blue shaded area represents the 95% credible interval of the second derivative, and the red shaded area represents the time of each regime shift.

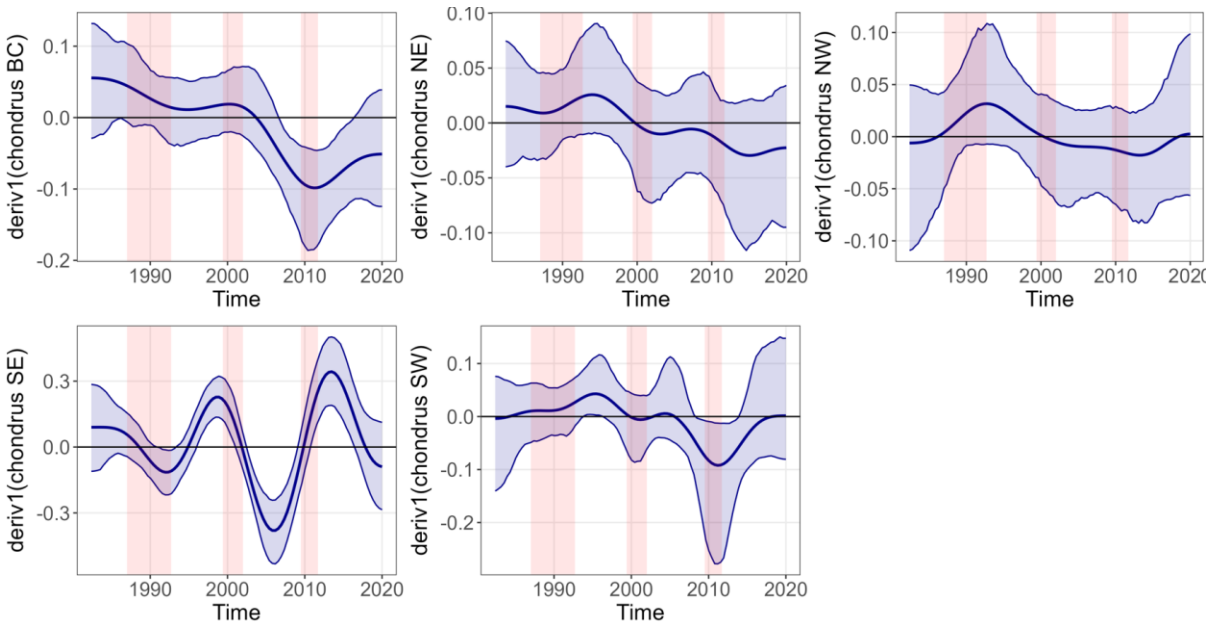


**Figure SM72**. First derivative of the temporal trend in *Chondrus* abundance. The first derivative was calculated by forward difference with 1000 draws. The blue shaded area

represents the 95% credible interval of the second derivative, and the red shaded area represents the time of each regime shift.

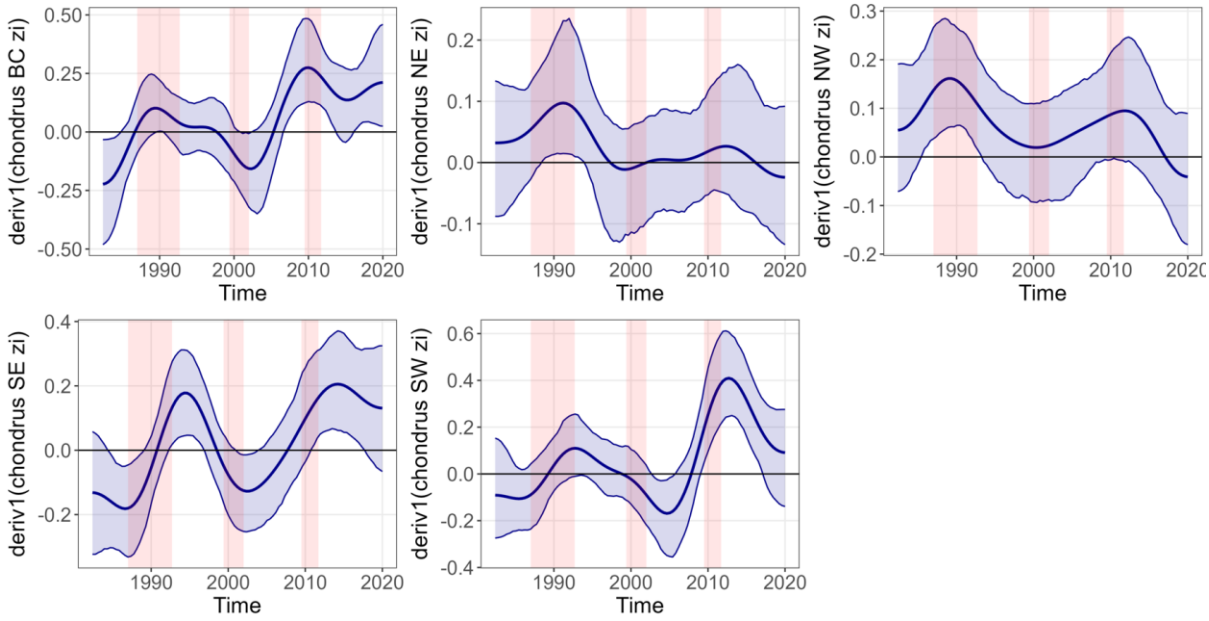


**Figure SM73**. First derivative of the temporal trend in *Chondrus* presence. The presence is assessed by zero inflated part of the model. The first derivative was calculated by forward difference with 1000 draws. The blue shaded area represents the 95% credible interval of the second derivative, and the red shaded area represents the time of each regime shift.

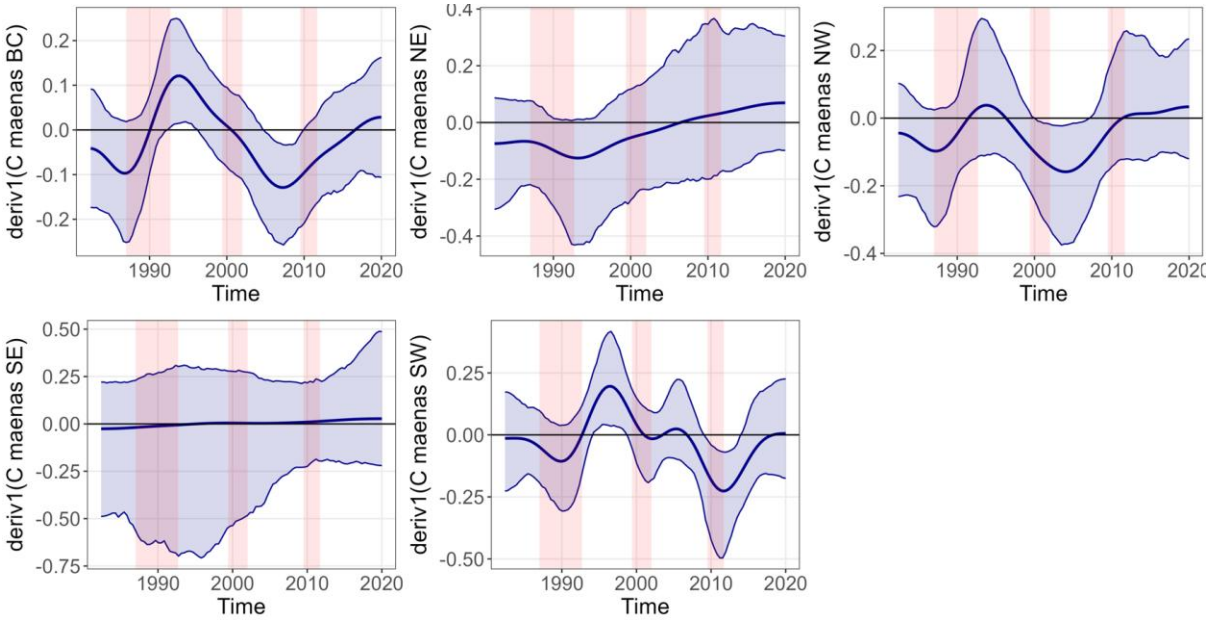


**Figure SM74**. First derivative of the temporal trend in *C. maenas* abundance. The first derivative was calculated by forward difference with 1000 draws. The blue shaded area

represents the 95% credible interval of the second derivative, and the red shaded area represents the time of each regime shift.

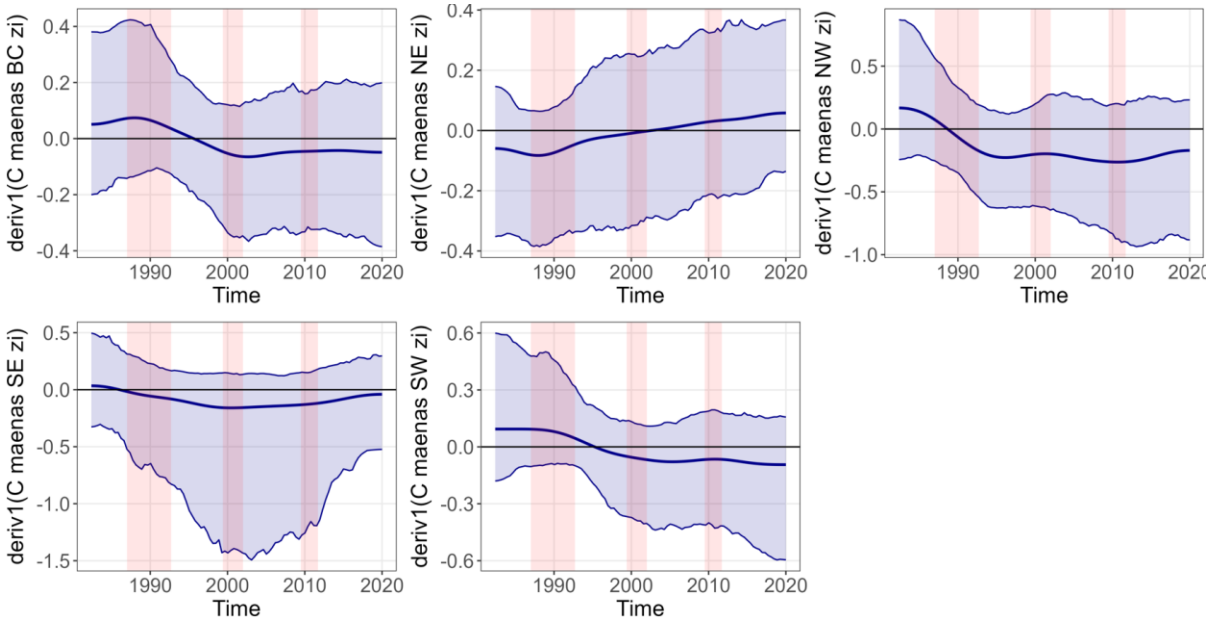


**Figure SM75**. First derivative of the temporal trend in *C. maenas* presence. The presence is assessed by zero inflated part of the model. The first derivative was calculated by forward difference with 1000 draws. The blue shaded area represents the 95% credible interval of the second derivative, and the red shaded area represents the time of each regime shift.

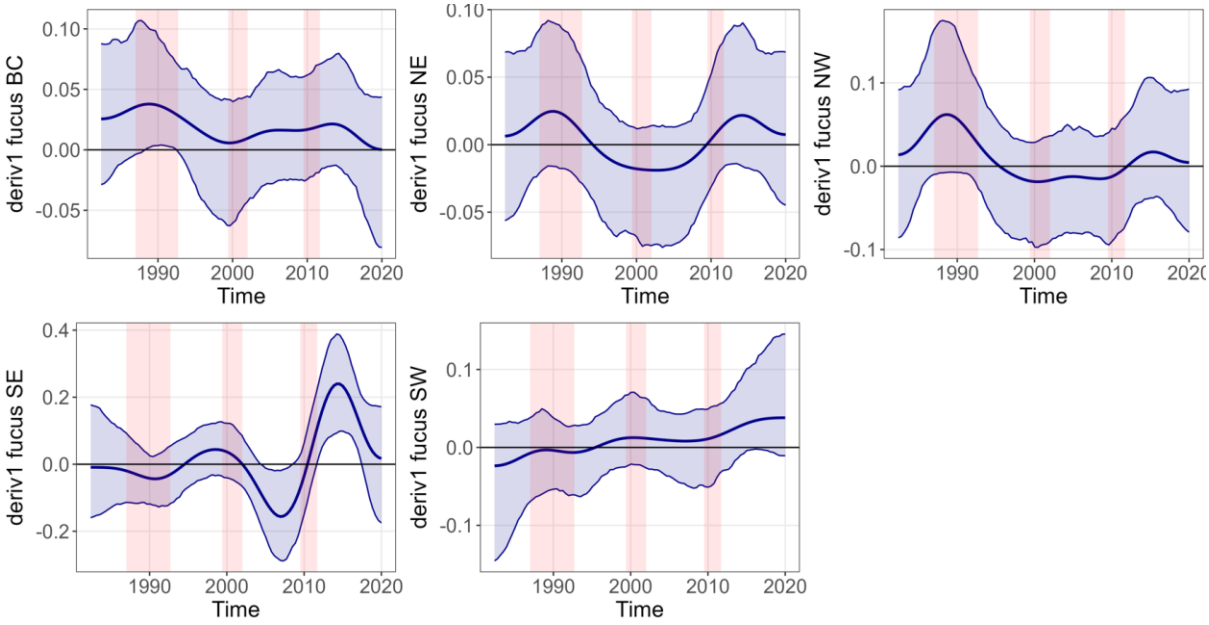


**Figure SM76**. First derivative of the temporal trend in *Fucus* abundance. The first derivative was calculated by forward difference with 1000 draws. The blue shaded area represents the

95% credible interval of the second derivative, and the red shaded area represents the time of each regime shift.

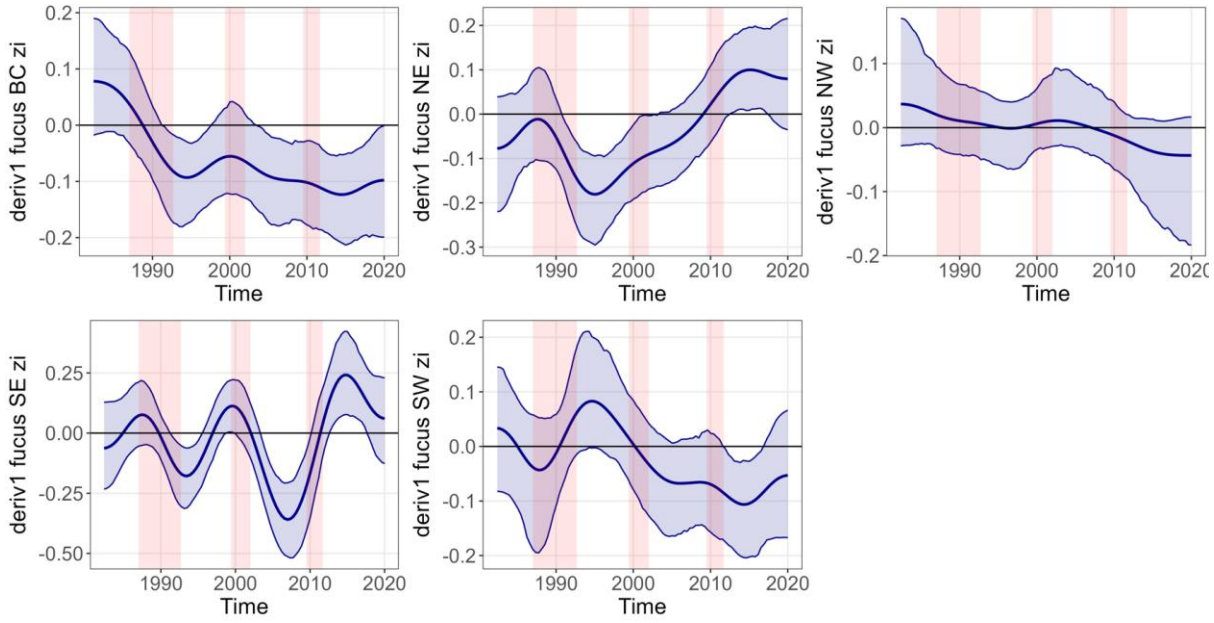


**Figure SM77**. First derivative of the temporal trend in *Fucus* presence. The presence is assessed by zero inflated part of the model. The first derivative was calculated by forward difference with 1000 draws. The blue shaded area represents the 95% credible interval of the second derivative, and the red shaded area represents the time of each regime shift.

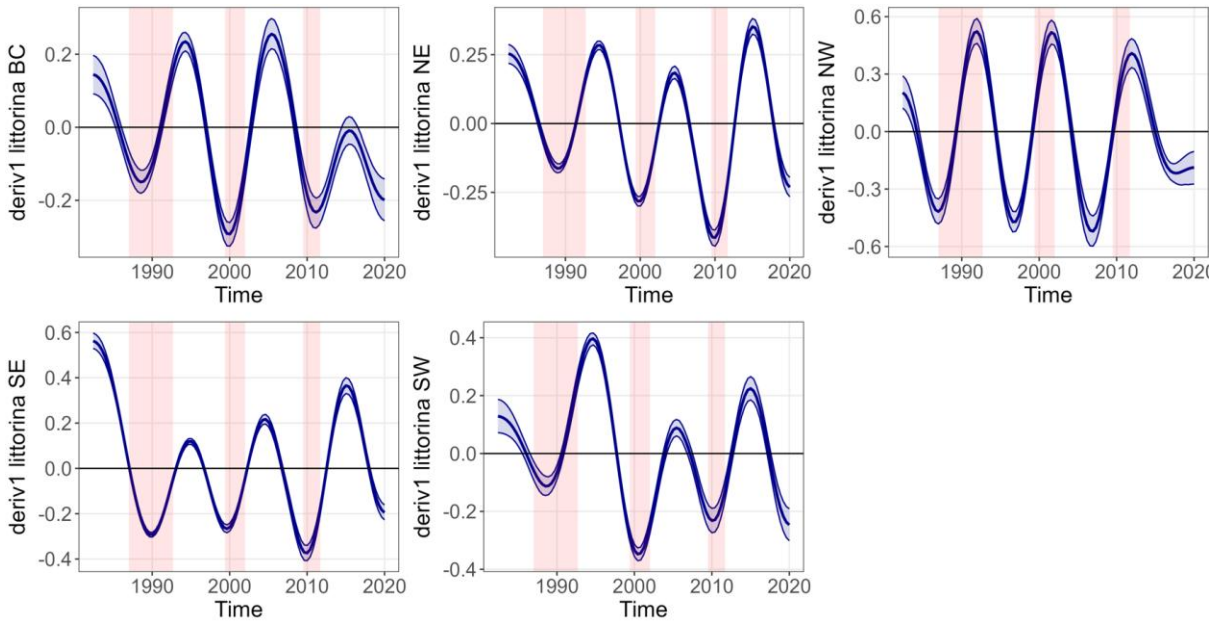


**Figure SM78**. First derivative of the temporal trend in *Littorina* abundance. The first derivative was calculated by forward difference with 1000 draws. The blue shaded area

represents the 95% credible interval of the second derivative, and the red shaded area represents the time of each regime shift.

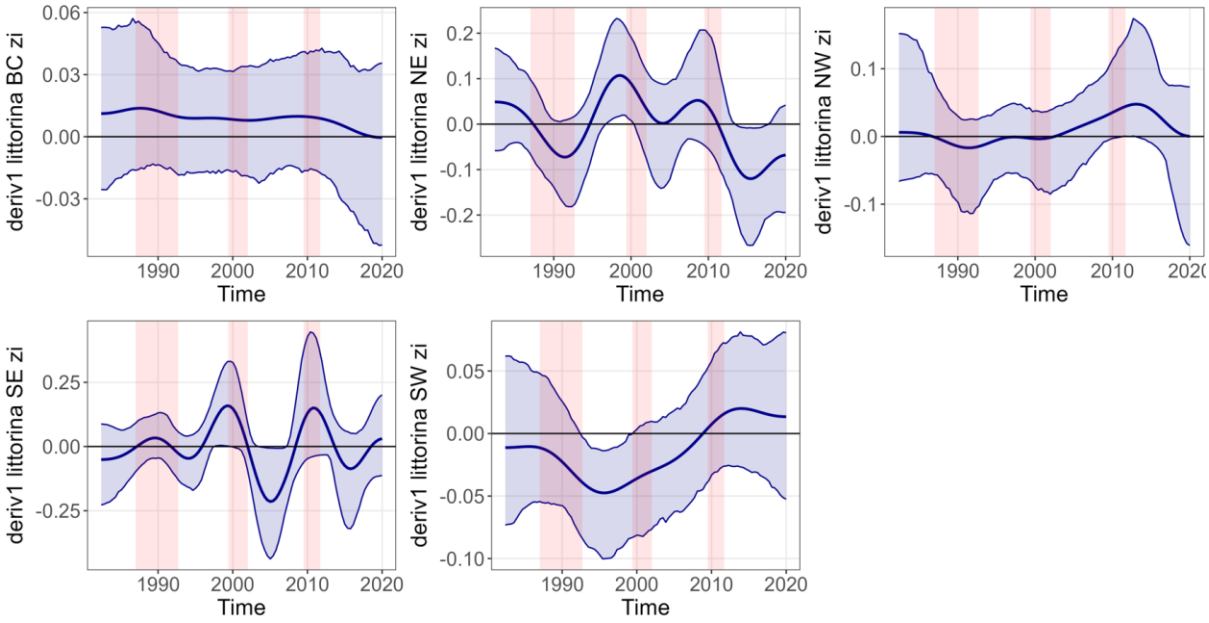


**Figure SM79**. First derivative of the temporal trend in *Littorina* presence. The presence is assessed by zero inflated part of the model. The first derivative was calculated by forward difference with 1000 draws. The blue shaded area represents the 95% credible interval of the second derivative, and the red shaded area represents the time of each regime shift.

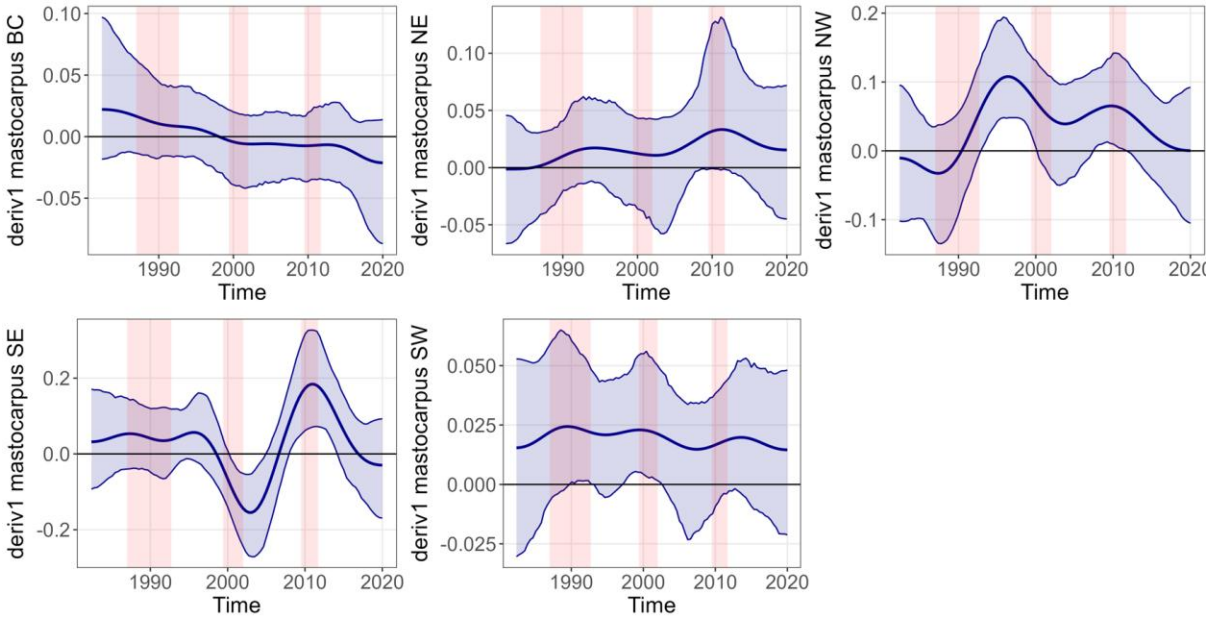


**Figure SM80**. First derivative of the temporal trend in *Mastocarpus* abundance. The first derivative was calculated by forward difference with 1000 draws. The blue shaded area

represents the 95% credible interval of the second derivative, and the red shaded area represents the time of each regime shift.

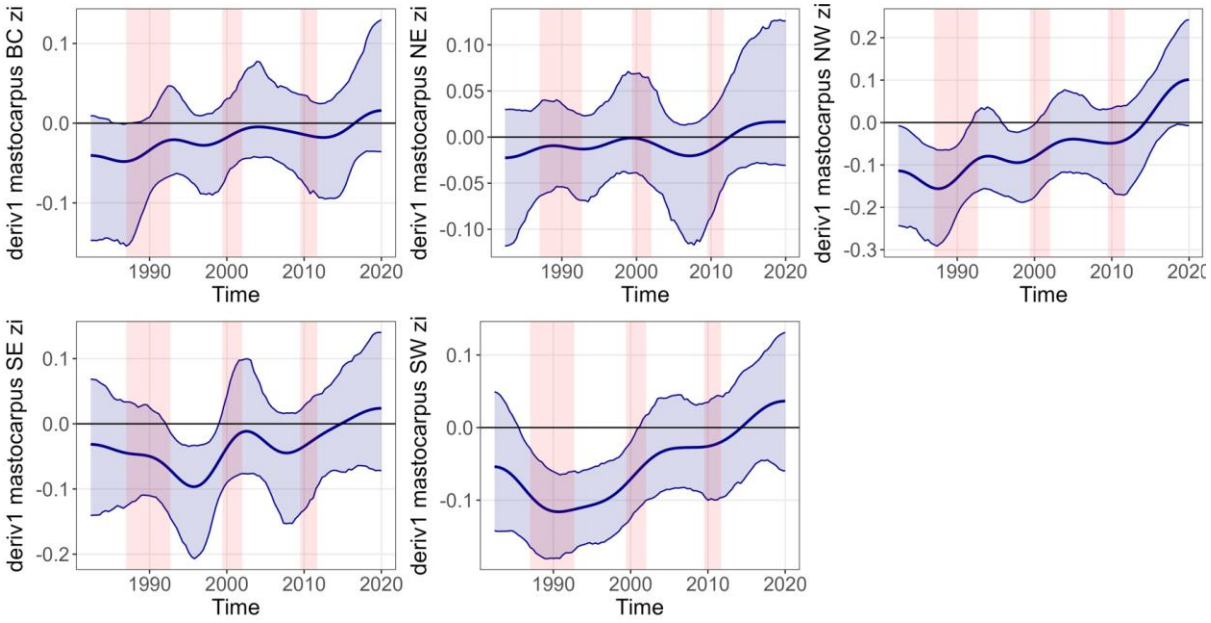


**Figure SM81**. First derivative of the temporal trend in *Mastocarpus* presence. The presence is assessed by zero inflated part of the model. The first derivative was calculated by forward difference with 1000 draws. The blue shaded area represents the 95% credible interval of the second derivative, and the red shaded area represents the time of each regime shift.

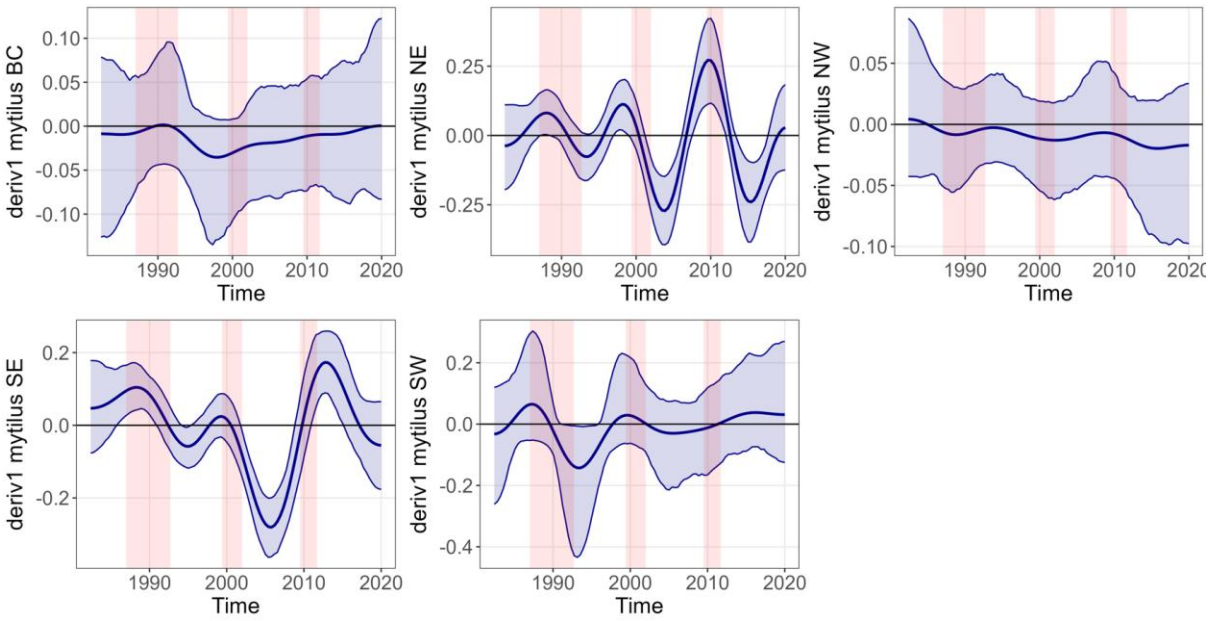


**Figure SM82**. First derivative of the temporal trend in *Mytilus* abundance. The first derivative was calculated by forward difference with 1000 draws. The blue shaded area represents the

95% credible interval of the second derivative, and the red shaded area represents the time of each regime shift.

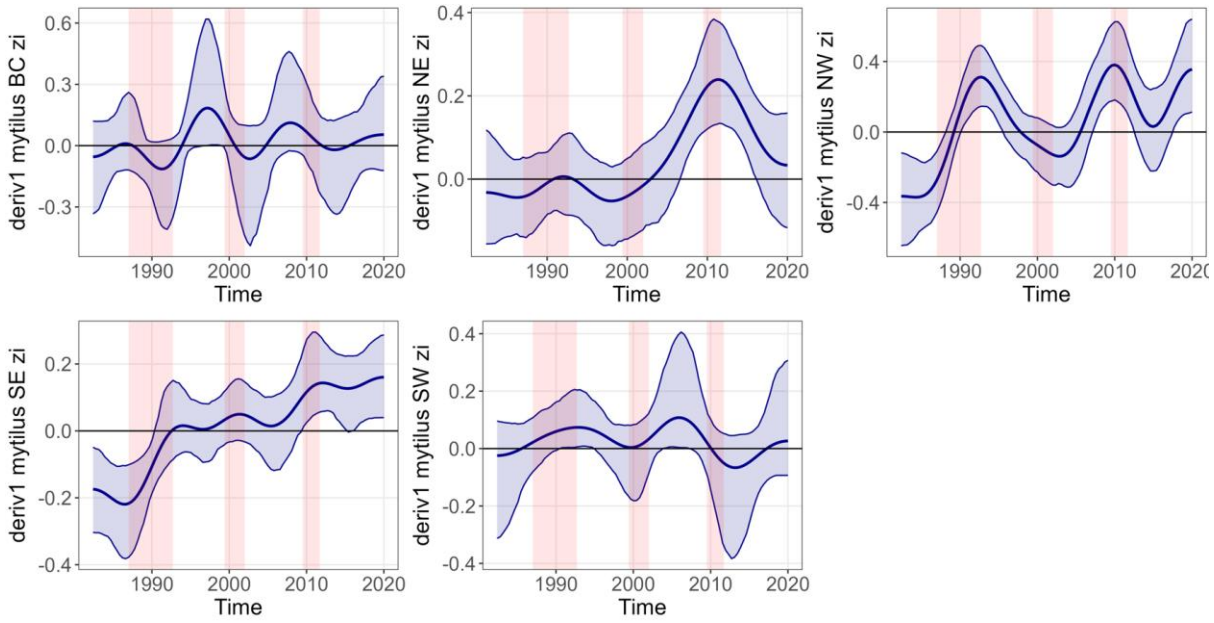


**Figure SM83**. First derivative of the temporal trend in *Mytilus* presence. The presence is assessed by zero inflated part of the model. The first derivative was calculated by forward difference with 1000 draws. The blue shaded area represents the 95% credible interval of the second derivative, and the red shaded area represents the time of each regime shift.

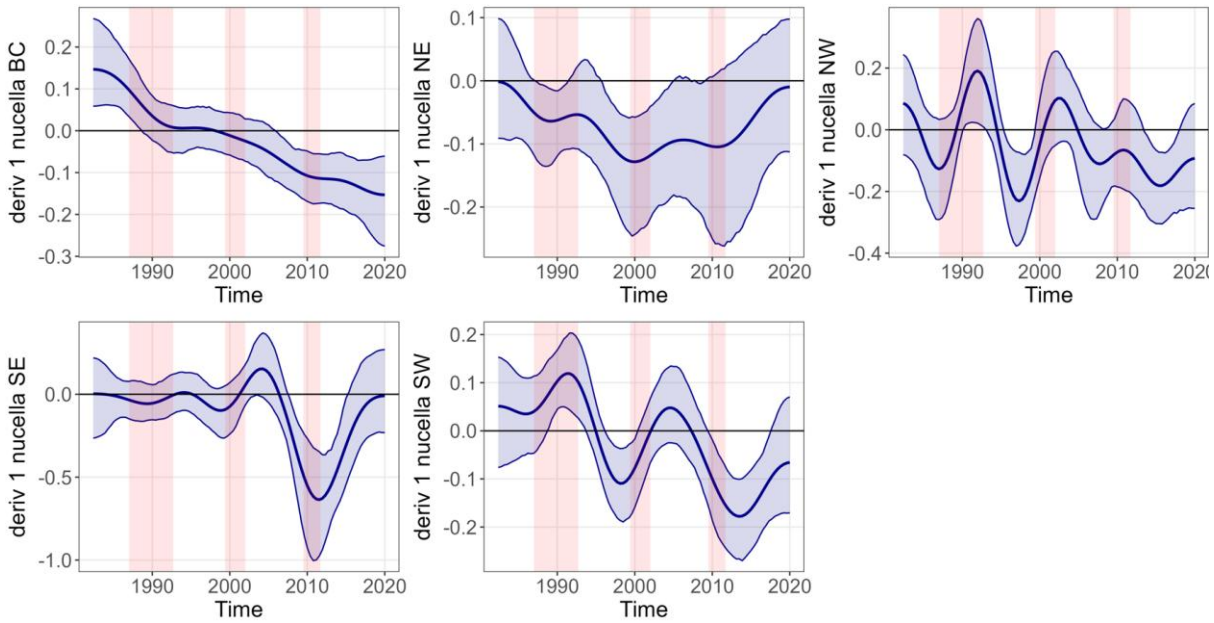


**Figure SM84**. First derivative of the temporal trend in *Nucella* abundance. The first derivative was calculated by forward difference with 1000 draws. The blue shaded area

represents the 95% credible interval of the second derivative, and the red shaded area represents the time of each regime shift.

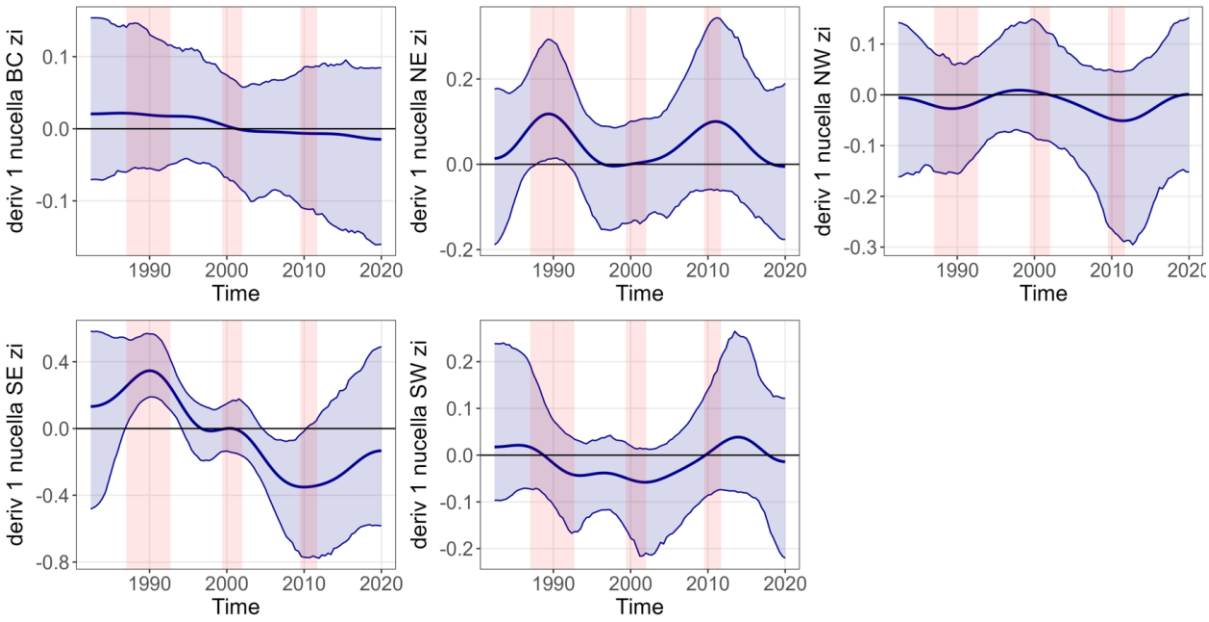


**Figure SM85**. First derivative of the temporal trend in *Nucella* presence. The presence is assessed by zero inflated part of the model. The first derivative was calculated by forward difference with 1000 draws. The blue shaded area represents the 95% credible interval of the second derivative, and the red shaded area represents the time of each regime shift.

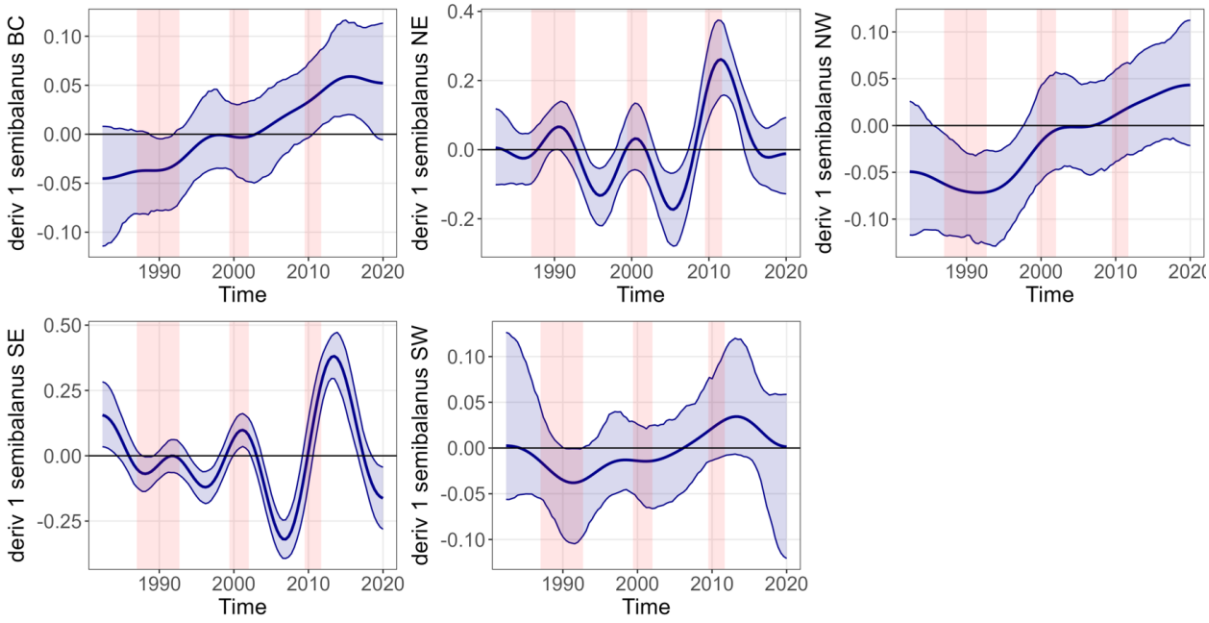

**Figure SM86**. First derivative of the temporal trend in *Semibalanus* abundance. The first derivative was calculated by forward difference with 1000 draws. The blue shaded area represents the 95% credible interval of the second derivative, and the red shaded area represents the time of each regime shift.

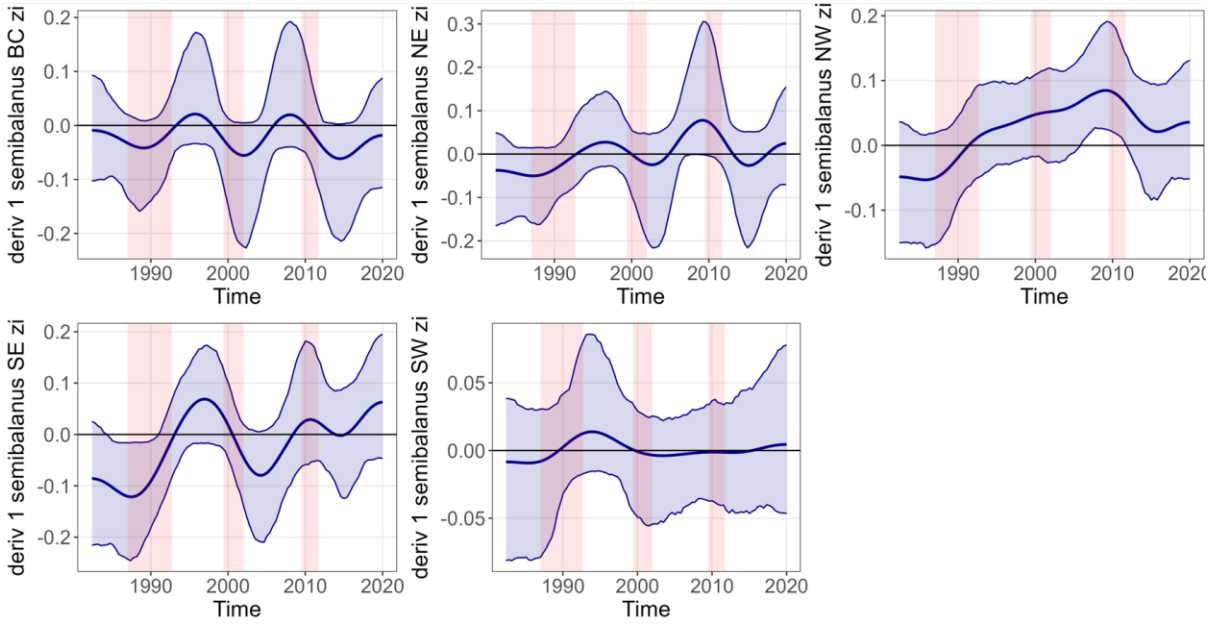


**Figure SM87**. First derivative of the temporal trend in *Semibalanus* presence. The presence is assessed by zero inflated part of the model. The first derivative was calculated by forward difference with 1000 draws. The blue shaded area represents the 95% credible interval of the second derivative, and the red shaded area represents the time of each regime shift.

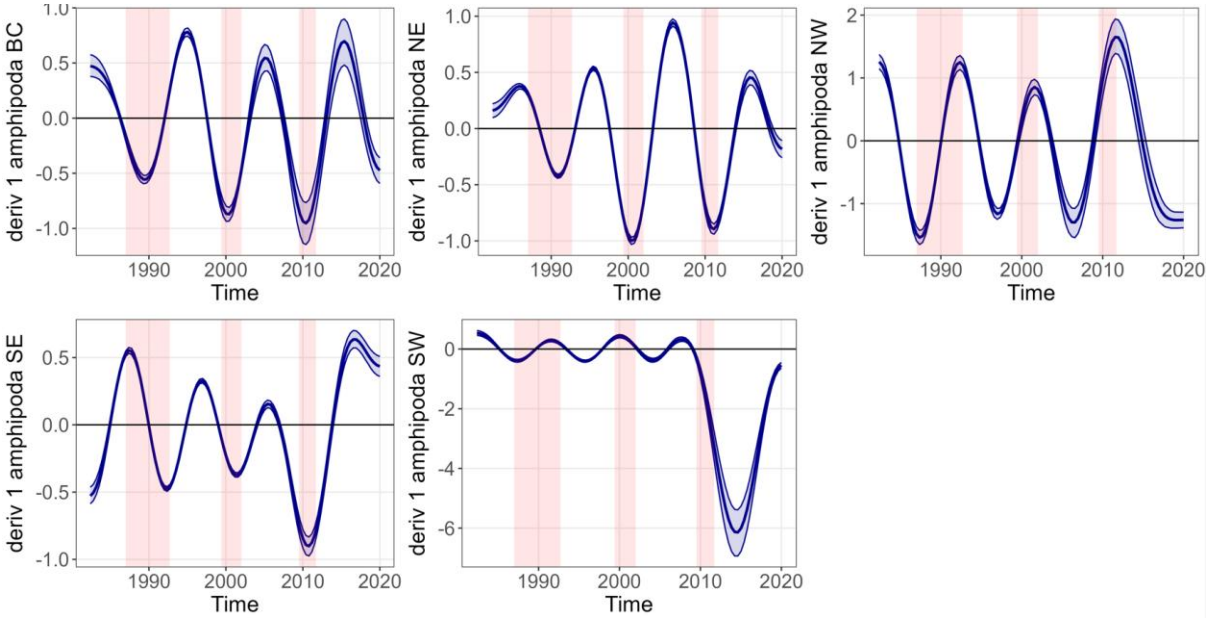


**Figure SM88**. First derivative of the temporal trend in *Amphipoda* abundance. The first derivative was calculated by forward difference with 1000 draws. The blue shaded area

represents the 95% credible interval of the second derivative, and the red shaded area represents the time of each regime shift.

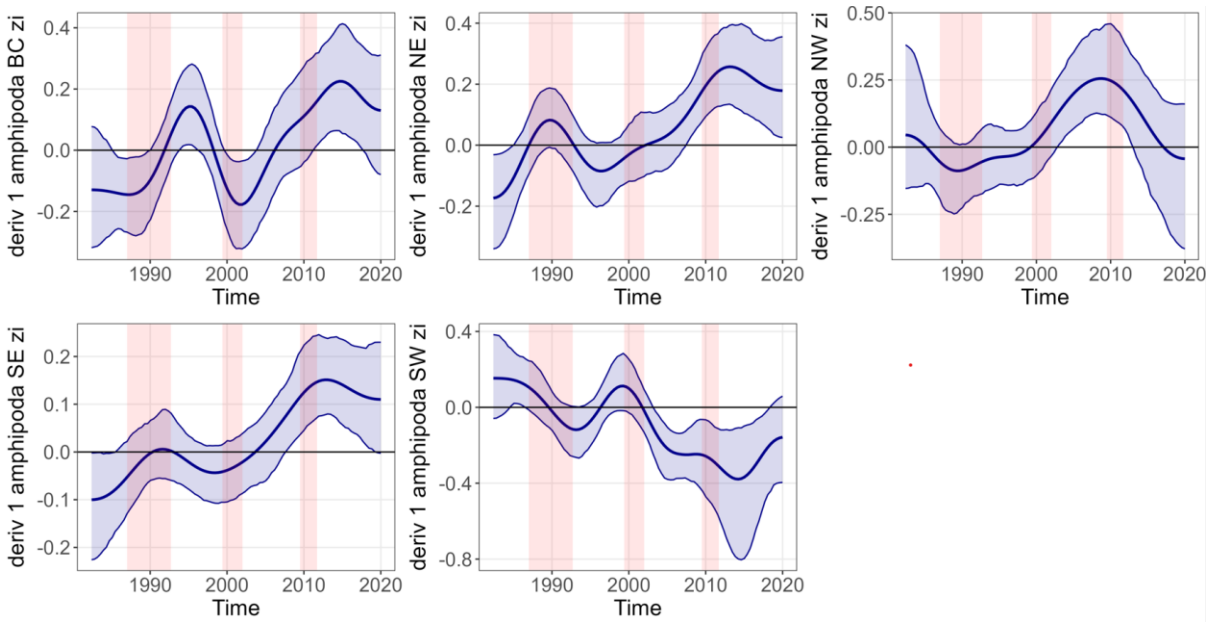


**Figure SM89.** First derivative of the temporal trend in *Amphipoda* presence. The presence is assessed by zero inflated part of the model. The first derivative was calculated by forward difference with 1000 draws. The blue shaded area represents the 95% credible interval of the second derivative, and the red shaded area represents the time of each regime shift.

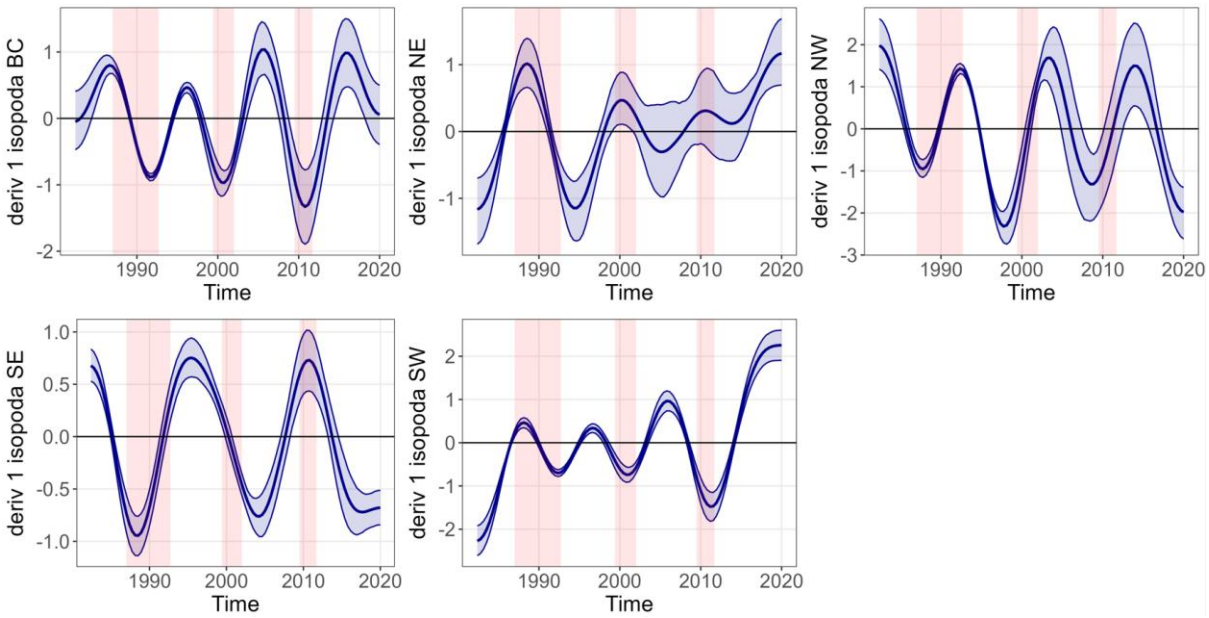


**Figure SM90**. First derivative of the temporal trend in *Isopoda* abundance. The first derivative was calculated by forward difference with 1000 draws. The blue shaded area represents the 95% credible interval of the second derivative, and the red shaded area represents the time of each regime shift.

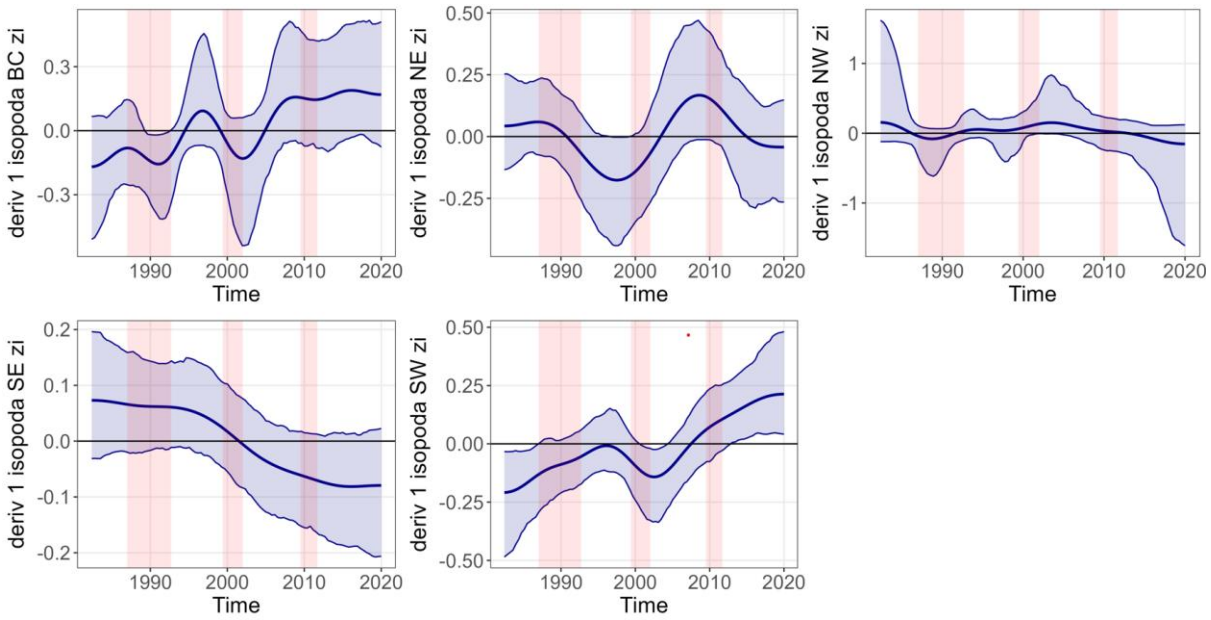


**Figure SM91**. First derivative of the temporal trend in *Isopoda* presence. The presence is assessed by zero inflated part of the model. The first derivative was calculated by forward difference with 1000 draws. The blue shaded area represents the 95% credible interval of the second derivative, and the red shaded area represents the time of each regime shift.

# Supplementary Material 8: Priors used for time series fit

```
prior_mytilus <- c(prior(student_t(3, 0, 2.5), class = "Intercept"),
                   prior(normal(0, 1), class = "b"),
                   prior(gamma(0.01, 0.01), class = "phi"),
                   prior(student_t(3,0,2.5), class = "sd"),
                   prior(student_t(3,0,2.5), class = "sds"),
                   prior(student_t(3,0,2.5), class = "sd", dpar = "zi"),
                   prior(student_t(3,0,2.5), class = "sds", dpar = "zi"),
                   prior(logistic(0,1), class = "Intercept", dpar = "zi"),
                   prior(normal(0, 1), class = "b", dpar = "zi")
)



prior_semibalanus <- c(prior(student_t(3, 0, 2.5), class = "Intercept"),
                       prior(normal(0, 1), class = "b"),
                       prior(gamma(0.01, 0.01), class = "phi"),
                       prior(student_t(3,0,2.5), class = "sd"),
                       prior(student_t(3,0,2.5), class = "sds"),
                       prior(student_t(3,0,2.5), class = "sd", dpar = "zi"),
                       prior(student_t(3,0,2.5), class = "sds", dpar = "zi"),
                       prior(logistic(0,1), class = "Intercept", dpar = "zi"),
                       prior(normal(0, 1), class = "b", dpar = "zi")
)



prior_fucus <- c(prior(student_t(3, -2.3, 2.5), class = "Intercept"),
                 prior(normal(0, 1), class = "b"),
                 prior(gamma(0.01, 0.01), class = "shape"),
                 prior(student_t(3,0,2.5), class = "sd"),
                 prior(student_t(3,0,2.5), class = "sds"),
                  prior(student_t(3,0,2.5), class = "sd", dpar = "hu"),
                  prior(student_t(3,0,2.5), class = "sds", dpar = "hu"),
                 prior(logistic(0,1), class = "Intercept", dpar = "hu"),
                 prior(normal(0, 1), class = "b", dpar = "hu")
)



prior_ascophyllum <- c(prior(student_t(3, -2.3, 2.5), class = "Intercept"),
                       prior(normal(0, 1), class = "b"),
```

```
                    prior(gamma(0.01, 0.01), class = "shape"),
                    prior(student_t(3,0,2.5), class = "sd"),
                   prior(student_t(3,0,2.5), class = "sds"),
                    prior(student_t(3,0,2.5), class = "sd", dpar = "hu"),
                    prior(student_t(3,0,2.5), class = "sds", dpar = "hu"),
                   prior(logistic(0,1), class = "Intercept", dpar = "hu"),
                   prior(normal(0, 1), class = "b", dpar = "hu")
)



prior_chondrus <- c(prior(student_t(3, -2.3, 2.5), class = "Intercept"),
                    prior(normal(0, 1), class = "b"),
                    prior(gamma(0.01, 0.01), class = "shape"),
                    prior(student_t(3,0,2.5), class = "sd"),
                    prior(student_t(3,0,2.5), class = "sds"),
                    prior(student_t(3,0,2.5), class = "sd", dpar = "hu"),
                    prior(student_t(3,0,2.5), class = "sds", dpar = "hu"),
                    prior(logistic(0,1), class = "Intercept", dpar = "hu"),
                    prior(normal(0, 1), class = "b", dpar = "hu")
)



prior_littorina <- c(prior(student_t(3, -2.3, 2.5), class = "Intercept"),
                   prior(normal(0,1), class = "b"),
                   prior(student_t(3,0,2.5), class = "sd"),
                   prior(student_t(3,0,2.5), class = "sds"),
                   prior(student_t(3,0,2.5), class = "sd", dpar = "zi"),
                   prior(student_t(3,0,2.5), class = "sds", dpar = "zi"),
                   prior(logistic(0,1), class = "Intercept", dpar = "zi"),
                   prior(normal(0, 1), class = "b", dpar = "zi")
)


prior_mastocarpus <- c(prior(student_t(3, -2.3, 2.5), class = "Intercept"),
                   prior(normal(0, 1), class = "b"),
                   prior(gamma(0.01, 0.01), class = "shape"),
                   prior(student_t(3,0,2.5), class = "sd"),
                   prior(student_t(3,0,2.5), class = "sds"),
                   prior(student_t(3,0,2.5), class = "sd", dpar = "hu"),
                   prior(student_t(3,0,2.5), class = "sds", dpar = "hu"),
                   prior(logistic(0,1), class = "Intercept", dpar = "hu"),
                   prior(normal(0, 1), class = "b", dpar = "hu")
)
prior_cmenas <- c(prior(student_t(3, -2.3, 2.5), class = "Intercept"),
```

```
                prior(normal(0, 1), class = "b"),
                prior(student_t(3,0,2.5), class = "sd"),
                prior(student_t(3,0,2.5), class = "sds"),
                prior(student_t(3,0,2.5), class = "sd", dpar = "zi"),
                prior(student_t(3,0,2.5), class = "sds", dpar = "zi"),
                prior(logistic(0,1), class = "Intercept", dpar = "zi"),
                prior(normal(0, 1), class = "b", dpar = "zi")
)



prior_nucella <- c(prior(student_t(3, -2.3, 2.5), class = "Intercept"),
                prior(normal(0, 1), class = "b"),
                prior(gamma(0.01, 0.01), class = "shape"),
                prior(student_t(3,0,2.5), class = "sd"),
                prior(student_t(3,0,2.5), class = "sds"),
                prior(student_t(3,0,2.5), class = "sd", dpar = "zi"),
                prior(student_t(3,0,2.5), class = "sds", dpar = "zi"),
                prior(logistic(0,1), class = "Intercept", dpar = "zi"),
                prior(normal(0, 1), class = "b", dpar = "zi")
)


prior_amphipoda <- c(prior(student_t(3, -2.3, 2.5), class = "Intercept"),
                prior(normal(0, 1), class = "b"),
                prior(student_t(3,0,2.5), class = "sd"),
                prior(student_t(3,0,2.5), class = "sds"),
                prior(student_t(3,0,2.5), class = "sd", dpar = "zi"),
                prior(student_t(3,0,2.5), class = "sds", dpar = "zi"),
                prior(logistic(0,1), class = "Intercept", dpar = "zi"),
                prior(normal(0, 1), class = "b", dpar = "zi")
)

prior_Isopoda <- c(prior(student_t(3, -2.3, 2.5), class = "Intercept"),
                prior(normal(0, 1), class = "b"),
                prior(student_t(3,0,2.5), class = "sd"),
                prior(student_t(3,0,2.5), class = "sds"),
                prior(student_t(3,0,2.5), class = "sd", dpar = "zi"),
                prior(student_t(3,0,2.5), class = "sds", dpar = "zi"),
                prior(logistic(0,1), class = "Intercept", dpar = "zi"),
                prior(normal(0, 1), class = "b", dpar = "zi")
)

prior_noaa_pcoa_mod <- c(prior(normal(0,1), class = "b", resp = ""),
                    prior(normal(0,1), class = "b", resp ="MDS1"),
                    prior(normal(0,1), class = "b", resp = "MDS2"),
                    prior(normal(0,1), class = "b", resp = "MDS3"),
                    prior(normal(0,1), class = "Intercept", resp = ""),
```

```
                  prior(student_t(3,0,2.5), class = "Intercept", resp = "MDS1"),
                  prior(student_t(3,0,2.5), class = "Intercept", resp = "MDS2"),
                  prior(student_t(3,0,2.5), class = "Intercept", resp = "MDS3"),
                  prior(student_t(3,0,2.5), class = "sds", resp = "MDS1"),
                  prior(student_t(3,0,2.5), class = "sds", resp = "MDS2"),
                  prior(student_t(3,0,2.5), class = "sds", resp = "MDS3"),
                  prior(student_t(3,0,2.5), class = "sigma", resp = "MDS1"),
                  prior(student_t(3,0,2.5), class = "sigma", resp = "MDS2"),
                  prior(student_t(3,0,2.5), class = "sigma", resp = "MDS3")
)


prior_pcoa_count_GS_GI <- c(prior(normal(0,1), class = "b", resp = ""),
                  prior(normal(0,1), class = "b", resp ="MDS1"),
                  prior(normal(0,1), class = "b", resp = "MDS2"),
                  prior(normal(0,1), class = "b", resp = "MDS3"),
                  prior(normal(0,1), class = "Intercept", resp = ""),
                  prior(student_t(3,-0.6,2.5), class = "Intercept", resp = "MDS1"),
                  prior(student_t(3,0.2,2.5), class = "Intercept", resp = "MDS2"),
                  prior(student_t(3,0.3,2.5), class = "Intercept", resp = "MDS3"),
                  prior(student_t(3,0,2.5), class = "sds", resp = "MDS1"),
                  prior(student_t(3,0,2.5), class = "sds", resp = "MDS2"),
                  prior(student_t(3,0,2.5), class = "sds", resp = "MDS3"),
                  prior(student_t(3,0,2.5), class = "sigma", resp = "MDS1"),
                  prior(student_t(3,0,2.5), class = "sigma", resp = "MDS2"),
                  prior(student_t(3,0,2.5), class = "sigma", resp = "MDS3"))


prior_pcoa_count_I <- c(prior(normal(0,1), class = "b", resp = ""),
                  prior(normal(0,1), class = "b", resp ="MDS1"),
                  prior(normal(0,1), class = "b", resp = "MDS2"),
                  prior(normal(0,1), class = "b", resp = "MDS3"),
                  prior(normal(0,1), class = "Intercept", resp = ""),
                  prior(student_t(3,-0.3,2.5), class = "Intercept", resp = "MDS1"),
                  prior(student_t(3,0.2,2.5), class = "Intercept", resp = "MDS2"),
                  prior(student_t(3,0.3,2.5), class = "Intercept", resp = "MDS3"),
                  prior(student_t(3,0,2.5), class = "sds", resp = "MDS1"),
                  prior(student_t(3,0,2.5), class = "sds", resp = "MDS2"),
                  prior(student_t(3,0,2.5), class = "sds", resp = "MDS3"),
                  prior(student_t(3,0,2.5), class = "sd", resp = "MDS1"),
                  prior(student_t(3,0,2.5), class = "sd", resp = "MDS2"),
                  prior(student_t(3,0,2.5), class = "sd", resp = "MDS3"),
                  prior(student_t(3,0,2.5), class = "sigma", resp = "MDS1"),
                  prior(student_t(3,0,2.5), class = "sigma", resp = "MDS2"),
                  prior(student_t(3,0,2.5), class = "sigma", resp = "MDS3"))


prior_pcoa_cover_GS_GI <- c(prior(normal(0,1), class = "b", resp = ""),
```

```
prior(normal(0,1), class = "b", resp ="MDS1"),
prior(normal(0,1), class = "b", resp = "MDS2"),
prior(normal(0,1), class = "b", resp = "MDS3"),
prior(normal(0,1), class = "Intercept", resp = ""),
prior(student_t(3,0.4,2.5), class = "Intercept", resp = "MDS1"),
prior(student_t(3,0.1,2.5), class = "Intercept", resp = "MDS2"),
prior(student_t(3,0,2.5), class = "Intercept", resp = "MDS3"),
prior(student_t(3,0,2.5), class = "sds", resp = "MDS1"),
prior(student_t(3,0,2.5), class = "sds", resp = "MDS2"),
prior(student_t(3,0,2.5), class = "sds", resp = "MDS3"),
prior(student_t(3,0,2.5), class = "sigma", resp = "MDS1"),
prior(student_t(3,0,2.5), class = "sigma", resp = "MDS2"),
prior(student_t(3,0,2.5), class = "sigma", resp = "MDS3"))
```

# Supplementary Material 8: Potential top-down pressure from the subtidal to the intertidal

## Assessing Subtidal - Intertidal Interactions

To assess the presence of trophic interactions between the subtidal and intertidal communities and determine which subtidal species are potentially coupling these habitats via predation, we obtained data from the GLOBI database (https://www.globalbioticinteractions.org/) for the intertidal species present in more than 2.5% of the quadrats, and for subtidal species present in more than 10 years. GLOBI interactions were complemented with an exhaustive literature review following recommended GLOBI protocol. Among the subtidal predators identified to feed on species present in the intertidal, we identified predators that were impacted by at least one subtidal regime shift by looking at each species' temporal trend. To do so, we started by modeling time series using GAMs for each of these subtidal predators with effort-corrected biomass as the dependent variable and a smoothing term of year as the predictor.

To test whether intertidal species were regulated by top-down effects, we calculated the cross-correlation in abundance between subtidal predator species and focal intertidal prey species at each site, for pairs identified to interact based on the information pulled from the GLOBI database. We calculated the cross-correlation between the mean posterior prediction of the subtidal predator biomass over time and the mean posterior predictions of the abundances over time of their intertidal prey at each site. We used 100 points and 16 lags, retaining the lags with the maximum absolute value of the correlation.

To propose the most likely linking mechanism explaining the responses of key intertidal species, the species present in NOAA bottom trawl survey were compared to near shore subtidal visual surveys around Appledore Island that started in 2014 by the Kelp Ecosystem Ecology Network. Proposed "linkers" were species impacted by a regime shift, negatively cross-correlated with their intertidal prey that responded in delayed synchrony with the same

regime shift coherently with altered top-down pressure and that were detected at least once in the near shore intertidal.

## Subtidal - Intertidal Interactions

Using GLOBI interactions databases, we identified 60 consumer species present in the subtidal around Appledore Island that feed on taxa identified in the intertidal zone of the island (Fig. SM92). Among those 60 consumers, 39 were identified to be impacted by one or two subtidal regime shifts based on the ordinations and subtidal time series (Fig. SM92). Of those 39 species' biomass, 31 were negatively cross-correlated with the abundance of some of their intertidal prey and impacted by the same regime shift in at least one site. Among those 31 species, six were detected in the nearshore subtidal (*C. borealis, H. americanus, P. virens, P. americanus, T. adspersus* and *U. regia*).

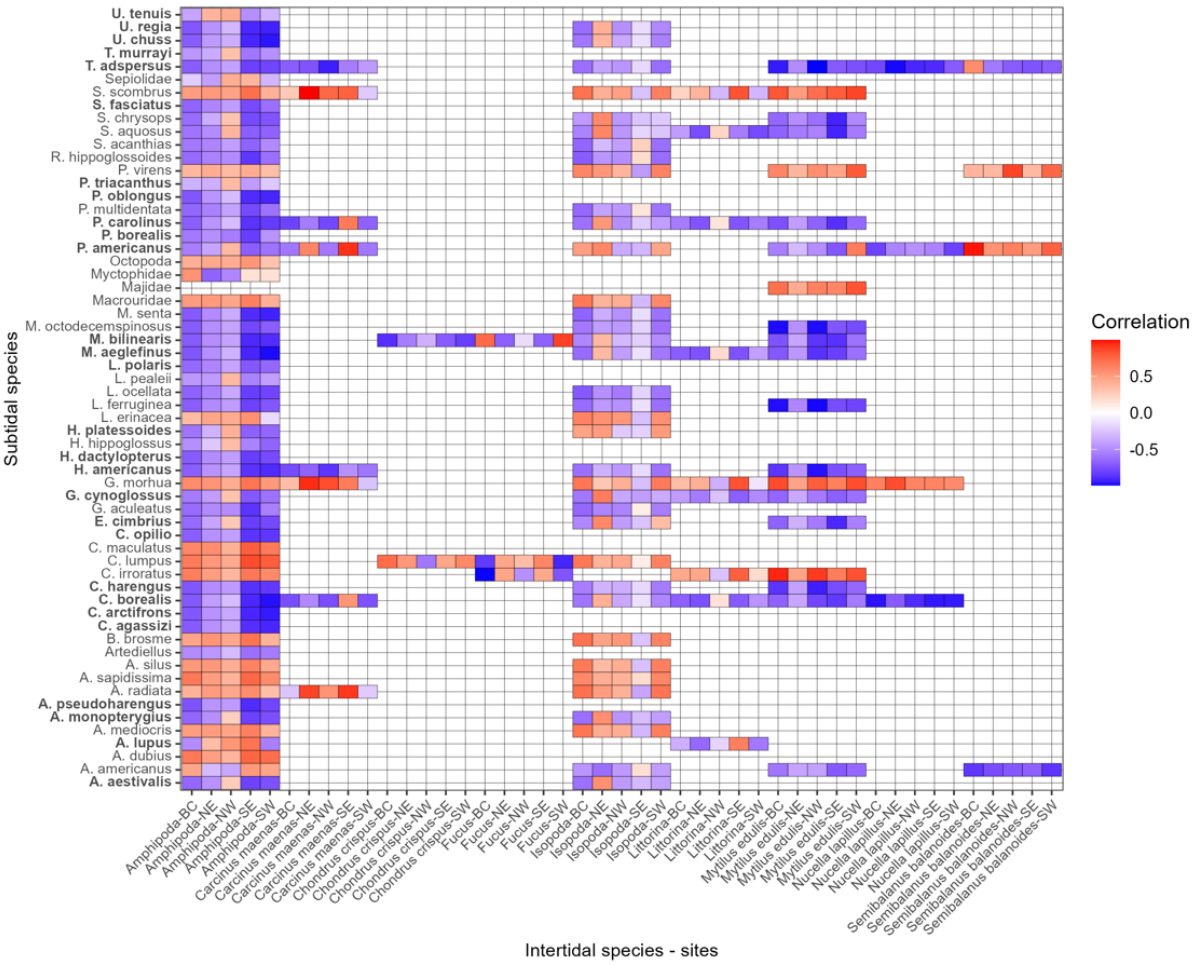


**Figure SM92.** Cross-boundary interactions between subtidal predators and intertidal organisms. Cross-correlation between the subtidal predators identified to feed on organisms present in the intertidal and focal intertidal taxa's abundance in each site. Subtidal taxa in bold are the 23 taxa impacted by regime shifts that were negatively cross-correlated with their intertidal preys. Lags with the maximal cross-correlation absolute value were selected. The cross-correlation was calculated from the mean posterior prediction of each taxa with 100 points and 16 lags.

**Table SM2**: Subtidal taxa impacted by each regime shifts. A "0" indicates no detected changes in abundance and no strong association with PCoA axis one or two. A "+" and a "-" indicate a positive and negative effect of the regime shift on the taxon abundance and/or relative abundances (i.e. strong association with the PCoA axis 1 or 2).

| Taxa | Regime shift 1990 | Regime shift 2000 | Regime shift 2010 |
|---|---|---|---|
| amblyraja_radiata | - | 0 | 0 |
| anarhichas_lupus | 0 | - | 0 |

| | | | |
|---|---|---|---|
| aspidophoroides_monopterygius | - | 0 | 0 |
| bathypolypus_arcticus | 0 | + | 0 |
| brosme_brosme | - | 0 | 0 |
| chionoecetes_opilio | 0 | 0 | + |
| chlorophthalmus_agassizi | 0 | 0 | + |
| citharichthys_arctifrons | 0 | 0 | + |
| clupea_harengus | 0 | 0 | + |
| crangon_septemspinosa | 0 | 0 | 0 |
| crustacea_shrimp | 0 | + | 0 |
| cryptacanthodes_maculatus | 0 | - | 0 |
| cyclopterus_lumpus | 0 | - | 0 |
| dichelopandalus_leptocerus | 0 | 0 | 0 |
| dipturus_laevis | 0 | + | 0 |
| enchelyopus_cimbrius | 0 | 0 | + |
| gadus_morhua | - | 0 | 0 |
| gasterosteus_aculeatus | 0 | + | 0 |
| geryon_quinquedens | 0 | - | 0 |
| glyptocephalus_cynoglossus | - | 0 | + |
| helicolenus_dactylopterus | 0 | + | 0 |
| hemitripterus_americanus | 0 | 0 | 0 |
| hippoglossoides_platessoides | - | 0 | 0 |
| hippoglossus_hippoglossus | 0 | 0 | 0 |
| homarus_americanus | 0 | 0 | + |
| illex_illecebrosus | 0 | 0 | 0 |
| lebbeus_polaris | 0 | + | 0 |
| leucoraja_erinacea | 0 | 0 | 0 |
| leucoraja_ocellata | 0 | 0 | 0 |

| | | | |
|---|---|---|---|
| limanda_ferruginea | 0 | + | 0 |
| lithodes_maja | 0 | 0 | 0 |
| loligo_pealeii | 0 | 0 | 0 |
| lophius_americanus | 0 | 0 | 0 |
| lumpenus_lumpretaeformis | 0 | - | 0 |
| lumpenus_maculatus | 0 | 0 | 0 |
| lycenchelys_verrilli | 0 | + | 0 |
| macrouridae | 0 | 0 | 0 |
| macrozoarces_americanus | 0 | - | 0 |
| majidae | 0 | 0 | 0 |
| malacoraja_senta | 0 | 0 | 0 |
| maurolicus_weitzmani | 0 | + | 0 |
| melanogrammus_aeglefinus | 0 | 0 | + |
| melanostigma_atlanticum | 0 | + | 0 |
| merluccius_bilinearis | 0 | + | + |
| myctophidae | 0 | 0 | 0 |
| myoxocephalus_octodecemspinosus | 0 | 0 | 0 |
| myxine_glutinosa | 0 | 0 | 0 |
| octopoda | + | 0 | - |
| pandalus_borealis | 0 | + | 0 |
| pandalus_montagui | + | 0 | - |
| pandalus_propinquus | + | 0 | - |
| paralepidae | 0 | 0 | 0 |
| paralichthys_oblongus | 0 | 0 | + |
| pasiphaea_multidentata | 0 | 0 | 0 |
| peprilus_triacanthus | 0 | 0 | + |
| petromyzon_marinus | 0 | 0 | 0 |

| | | | |
|---|---|---|---|
| placopecten_magellanicus | 0 | 0 | 0 |
| pollachius_virens | - | 0 | 0 |
| pontophilus_norvegicus | 0 | + | 0 |
| prionotus_carolinus | 0 | 0 | + |
| pseudopleuronectes_americanus | - | 0 | 0 |
| reinhardtius_hippoglossoides | 0 | 0 | 0 |
| scomber_scombrus | 0 | - | 0 |
| scomberesox_saurus | - | 0 | + |
| scophthalmus_aquosus | - | 0 | + |
| sebastes_fasciatus | 0 | + | 0 |
| sepiolidae | 0 | 0 | 0 |
| spirontocaris_liljeborgii | 0 | + | 0 |
| squalus_acanthias | 0 | 0 | 0 |
| stenotomus_chrysops | - | 0 | + |
| stoloteuthis_leucoptera | 0 | 0 | 0 |
| tautogolabrus_adspersus | 0 | 0 | + |
| triglops_murrayi | - | 0 | 0 |
| sum_alosa | - | 0 | + |
| sum_ammodytes | 0 | 0 | 0 |
| sum_argentina | 0 | 0 | 0 |
| sum_cancer | 0 | - | + |
| sum_ urophycis | - | 0 | + |

## Potential mechanism for regime shift propagation in the intertidal

We identified offset synchrony between the intertidal and the subtidal communities for all three subtidal regime shifts, although the sites and species impacted differed. We

attributed the first subtidal regime shift (~1990) to fisheries collapse and detected reductions in harvested bottom fish based on other observations of the Gulf of Maine (Jackson et al., 2001; Myers & Worm, 2003). There was offset synchrony in the changes in intertidal sessile and mobile communities at the whole island and community scale. While our data does not address specific interactions that would cause the shifts *per se*, based on the natural history of the system and cross-correlations in species abundances, we draw some reasonable hypotheses. Among the subtidal species negatively impacted by the first regime shift, eight were identified to feed on intertidal key species among which *P. americanus* and *P. virens* were also detected in the nearshore subtidal. *C. maenas,* Amphipoda*, Isopoda* (although the opposite trend was also observed) and *Littorina* spp. increased in abundance slightly after the subtidal regime shifts (offset synchrony), coherent with a relaxed top-down pressure from decreased subtidal predator populations. This explanation is also supported by a negative cross-correlation between impacted subtidal predators (i.e. *P. americanus* and *P. virens*) and their intertidal prey *C. maenas, Amphipoda* and *Littorina sp*. As *C. maenas* increased, *M. edulis* and *S. balanoides* decreased in abundance, consistent with a trophic cascade (Ellis et al 2007). The increase in *Fucus* spp. abundance, still in offset synchrony with the first subtidal regime shift, could be the result of an increased substrate availability resulting from *M. edulis* and *S. balanoides* reductions.

The second subtidal regime shift (~2000) lines up with urchins' collapse due to overharvesting and mesopredator release (Steneck et al., 2013). Among the taxa negatively impacted by the second regime shift and detected in the near shore intertidal, Cancer crabs are known predators of *Littorina* spp. and negatively cross-correlated with their abundance in most sites. The reduced abundance of Cancer

crabs could explain the changes toward a higher abundance of *Littorina* spp. in offset synchrony with this second subtidal regime shift. *Nucella lapillus* abundance also increased in offset synchrony with the second subtidal regime shift. The only identified subtidal predator of *N. lapillus* within these trawl data is *Cancer borealis*. *C. borealis* abundance was negatively cross-correlated with *N. lapillus*, suggesting top-down regulation, coherently with previous research on Appledore Island (Ellis et al., 2007). There was also a directional change toward a smaller *M. edulis* abundance which could be due to increased top-down pressure from *N. lapillus (Ellis et al., 2007)*. The third subtidal regime shift (~2010) lines up with the combined impacts of climate change, exotic species introduction and changes in management strategies seen in the Gulf of Maine (Dijkstra et al., 2017; Jackson et al., 2001; Myers & Worm, 2003; Pershing et al., 2015). Among the subtidal taxa impacted by this regime shift, 15 were positively impacted and predators of intertidal organisms. Two of these were *Cancer borealis* and *Homarus americanus*, which feed on *Nucella*. C. borealis has even been found to regulate Nucella populations on Appledore Island (Ellis et al., 2007), which is also sustained by a negative cross-correlation between the two species. Top-down regulation could explain the decreased abundance of *N. lapillus* and corresponding increased abundance of its prey, *S. balanoides* (Ellis et al., 2007). Amphipod abundance decreased in offset synchrony with this third regime shift, which may be linked to increases in predation pressure from subtidal predator fish, 15 of which were negatively cross-correlated with amphipods. Another intertidal species that showed offset synchrony with the third subtidal regime shift is *Littorina littorea*, which became more abundant. Yet, only three of the subtidal predators impacted by this regime shift feed on *L. littorea*, and none of them were negatively cross-correlated with *L. littorea*, suggesting no changes in top-down regulation with changes in subtidal predator

populations. The change in *L. littorea* direction toward a higher abundance could be the result of changes in biological conditions, especially if competitors or other intertidal predators that we did not focus on were impacted.

Overall, for each of the three subtidal regime shifts, there are potential pathways by which altered cross-boundary interactions with subtidal species may impact intertidal communities. We acknowledge that these mechanisms are speculative and should be tested and that some intertidal community change could result from confounding effects, qualities inherent to time series analysis. Yet, we think the impact of confounding effects were reduced to the minimum by quantitatively looking at specific patterns in time (i.e. offset synchrony). However, as the communities from near shore subtidal and deeper subtidal are different, other species not present in the NOAA bottom trawl surveys, but present in the near shore intertidal could have been impacted by the subtidal regime shifts and in turn change intertidal communities.